AFOSR 67-0979

AD651595

RESEARCH ON ELECTROMAGNETIC PLASMA ACCELERATION

VOLUME I

THE DEVELOPMENT OF A CW TRAVELING WAVE ACCELERATOR FOR THE PRODUCTION OF PINCHED PLASMA TOROIDS

Final Report: Contract AF 49(638)-1251

Submitted to

United States Air Force
Office of Scientific Research
Office of Aerospace Research
Washington D. C.

D D C
MAY 17 1967

January, 1967

ARCHIVE COPY

SPACE SCIENCES LABORATORIES
Litton Systems, Inc.
336 North Foothill Road, Beverly Hills, California

(A. S. Penfold and R. M. Rosen: authors)

Distribution of this
document is unlimited

RESEARCH ON ELECTROMAGNETIC PLASMA ACCELERATION

VOLUME I

THE DEVELOPMENT OF A CW TRAVELING WAVE ACCELERATOR FOR THE PRODUCTION OF PINCHED PLASMA TOROIDS

Final Report: Contract AF 49(638)-1251

Submitted to

United States Air Force
Office of Scientific Research
Office of Aerospace Research
Washington D. C.

January, 1967

SPACE SCIENCES LABORATORIES
Litton Systems, Inc.
336 North Foothill Road, Beverly Hills, California

(A. S. Penfold and R. M. Rosen: authors)

CONTENTS

1. INTRODUCTION 1-1

2. EXPERIMENTAL INVESTIGATIONS 2-1

2.1 Apparatus Development 2-1
2.1.1 Electrical Circuit Development 2-1
2.1.2 The Mercury Feed System 2-11
2.1.3 Special Modifications 2-21
2.1.4 Diagnostic Apparatus 2-32
2.2 Experiments with the Plasma Discharge 2-40
2.2.1 Operation of the Accelerator 2-40
2.2.2 Operation of the Accelerator with Plasma 2-41
2.2.3 Experimental Results and Interpretations 2-44

3. SUMMARY AND CONCLUSIONS 3-1

APPENDIX A — Fringe Field Investigation

APPENDIX B — Additional Investigations

REFERENCES

LIST OF ILLUSTRATIONS

Figure		Page
1-1	Mark II Accelerator	1-4
2-1	Field Coil Winding	2-3
2-2	General Schematic Electrical Network	2-4
2-3	Simplified Scheme for Providing Neutralizing Voltages	2-7
2-4	Photograph of Neutralizing Transformers	2-8
2-5	Inner Coil Drive Circuit Schematic	2-10
2-6	Inner Coil Coupling Circuit	2-12
2-7	Mercury Feed System	2-14
2-8	Mercury System	2-15
2-9	Liquid Pump	2-18
2-10	Detail of Mercury Feed System	2-19
2-11	Liquid Pump Calibration	2-20
2-12	Apparatus for Symmetry Test	2-22
2-13	Test of Azimuthal Symmetry	2-23
2-14	Photograph of Discharge and Nozzles	2-24
2-15	Arc Strike Puncture	2-27
2-16	Voltage Isolation	2-28
2-17	Isolating Transformers	2-29
2-18	DC Probe	2-30
2-19	DC Probe Schematic	2-31
2-20	Blown Field Coil	2-33
2-21	Flux Probe in Accelerator	2-35
2-22a	Schematic of Search Coil	2-37
2-22b	Search Coil and Blocking Probe	2-38
2-23	Position of Optical Apparatus	2-39
2-24	Broken Ceramic Vacuum Channels	2-43
2-25	Ring Current Model	2-45
2-26	Resultant Search Coil Signals	2-46
2-27	Oscilloscope Display	2-48
2-28	Probe Trace, Mercury	2-49
2-29	Probe Trace, Mercury	2-50
2-30	Probe Trace, Mercury	2-51
2-31	Probe Trace, Argon	2-52
2-32	Probe Trace, Argon	2-53
2-33	Probe Trace, Mercury-Argon	2-54
2-34	Probe Trace, Mercury-Argon	2-55

LIST OF ILLUSTRATIONS (cont)

Figure		Page
2-35	Probe Trace, Mercury-Argon	2-56
2-36	Probe Trace, Mercury-Argon	2-57
2-37	Probe Trace, Mercury-Argon	2-58
2-38	Effect of Blocker on Probe Signal	2-59
2-39	Electrostatic Probe Traces	2-62
2-40	Relation of DC Voltage to Coil Current	2-63
2-41	Spectrogram of Mark II Discharge	2-64

APPENDIX A

A-1	Coordinate System	A-3
A-2	ζ versus $\beta - \beta_o$	A-5
A-3	S versus $\beta - \beta_o$	A-6
A-4	C_S Dependence	A-10
A-5	S_S Dependence	A-11
A-6	Amplitude Function, $\bar{A}_o$	A-12
A-7	End Field Effects	A-17
A-8	Reduction of End Field Effects	A-20

APPENDIX B

B-1	Probe Traces, Argon	B-4
B-2	Probe Traces, Argon and Mercury	B-5
B-3	Probe Traces, Mercury	B-6
B-4	Probe Traces, Mercury	B-7
B-5	Probe Traces, Mercury	B-8

PREFACE

This is Volume I of two volumes, together comprising the Final Report of Contract AF 49(638)-1251, entitled "Research on Electromagnetic Plasma Acceleration." The report covers the period from November 1963 through December 1966. The work was performed in the Space Sciences Laboratories of Litton Systems, Inc., located in Beverly Hills, California. Dr. Alan S. Penfold was the Principal Investigator. The document bears the Litton Publication number 6126.

ACKNOWLEDGEMENTS

The authors wish to express their appreciation to Dr. G. R. Seemann of this laboratory for his assistance in operating the accelerator and his contribution to the writing of Appendix A of this volume. They also wish to thank Mr. R. de Craene for the unending patience and meticulous care he exercised on behalf of the Mark II.

ABSTRACT

The development of a CW traveling wave accelerator for the production and acceleration of high-speed pinched plasma toroids is described. The accelerator is a polyphase-driven electrical system. Mercury and argon-seeded mercury were used as test gases. A comprehensive technology was developed to compensate for the inductive back-reaction of the plasma discharge on the coils producing the traveling wave field. Severe and rapid thermal overloading of the walls of the plasma channel limited the run times to a few seconds. Several types of ceramic channels were tired but the problem remained. The short run times made proper utilization of the back-reaction compensating circuits an impossibility. However, evidence of plasma acceleration was obtained and microscopic discrete ring-currents were observed in the plasma efflux. The axial Hall voltage was monitored and a maximum value of 1000 volts was recorded.

1. INTRODUCTION

The work reported in Volume I of this Final Report is a direct extension and continuation of the work reported in AFOSR Sci. Doc. 64-1340, Final Report, Contract AF 49(638)-759, entitled "Research on Electromagnetic Plasma Acceleration". Many references will be made in this document to that report and it will hereinafter be referred to as 64-1340.

This continuing research program has been directed toward the production of a continuous stream of high-speed, pinched plasma toroids and the study of their physical properties. The theory upon which this research is based is given in detail in 64-1340. In summary, the theory predicts that in the presence of a cylindrically-symmetric, CW traveling magnetic field of sufficiently high field strength the following sequence of events will occur.

1. Any electrons present will be accelerated by the azimuthal electric field and will initiate an avalanche.
2. The resulting current will build up until a pinch force develops.
3. The current ring will be accelerated by the traveling wave field, bringing about a charge separation axial electric field since the heavy positive ions will tend to remain stationary. This axial field will then accelerate the ions
4. The resultant plasma toroid will then be accelerated and carried out through the fringe field.

The traveling field is produced by a traveling sinusoidal sheet current and thus will reverse polarity every half cycle. Therefore alternate plasma toroids will have reversed currents every half cycle. The picture of the ring-current acceleration process indicates that the toroids may exit the accelerator with a maximum speed of twice the traveling field speed.

Two previous contracts had supported the design and operation of a "single-shot" plasma accelerator (Mark I), which produced a traveling wave by means of a time-sequential firing of a set of linearly arrayed capacitors. The succeeding CW accelerator, designated Mark II, was designed to produce a traveling wave by means of a polyphase excited field coil, driven by a set of power amplifiers.

The present effort can be divided into two parts:

1. The development of the polyphase accelerator.
2. The study of the properties of the plasma toroids.

The development of the accelerator was largely dependent on what could be predicted about the interaction between the plasma and the electrical circuitry of the device. The plasma was low in density with strong circulating currents, so it was predicted that the interaction would be primarily inductively dominated (rather than, say, resistively dominated as would be the case at high density). The following problem is immediately presented. The externally applied traveling wave is produced by a set of coils whose amplitudes and phases must be held in a fixed relation. The phases must interact with one another in order to produce the desired wave. The interaction among the coils is a mutual inductance. One of the first considerations then is the adjusting of many circuits to obtain the correct electrical relationships when all the circuits are interacting with all other circuits and secondly, to hold these relationships in the presence of an inductive plasma which will change the coupling among the circuits. A phase-servo system was developed in order to automatically hold the correct phase relations and this has proven to be both successful and necessary.

The general electrical circuit design was dictated by the type of power supplies available. These supplies are a group of five highly modified surplus Navy rf transmitters; the modifications for operations in the regime of interest were accomplished under the previous contract and are described in 64-1340. The circuits are parallel resonant networks with the field coils in the inductive branch.

Since the Mark II accelerator is electrodeless, and since it was specifically designed to prevent the toroids from expanding and impacting with the walls of the accelerating channel, it was felt that the walls would not present problems of major consequence. In practice, this

has not proven to be the case. Severe thermal overloading of the walls has been repeatedly observed, the load being severe enough to crack the wall of the plasma channel even though the channel was made of a ceramic. It has not been possible to operate the Mark II for more than a few seconds at a time. This length of time, while more than sufficient to gather data since $\sim 10^6$ toroids should be produced in a few seconds, is not sufficient to make tuning adjustments in the presence of the plasma.

A photograph of the accelerator is shown in Figure 1-1.

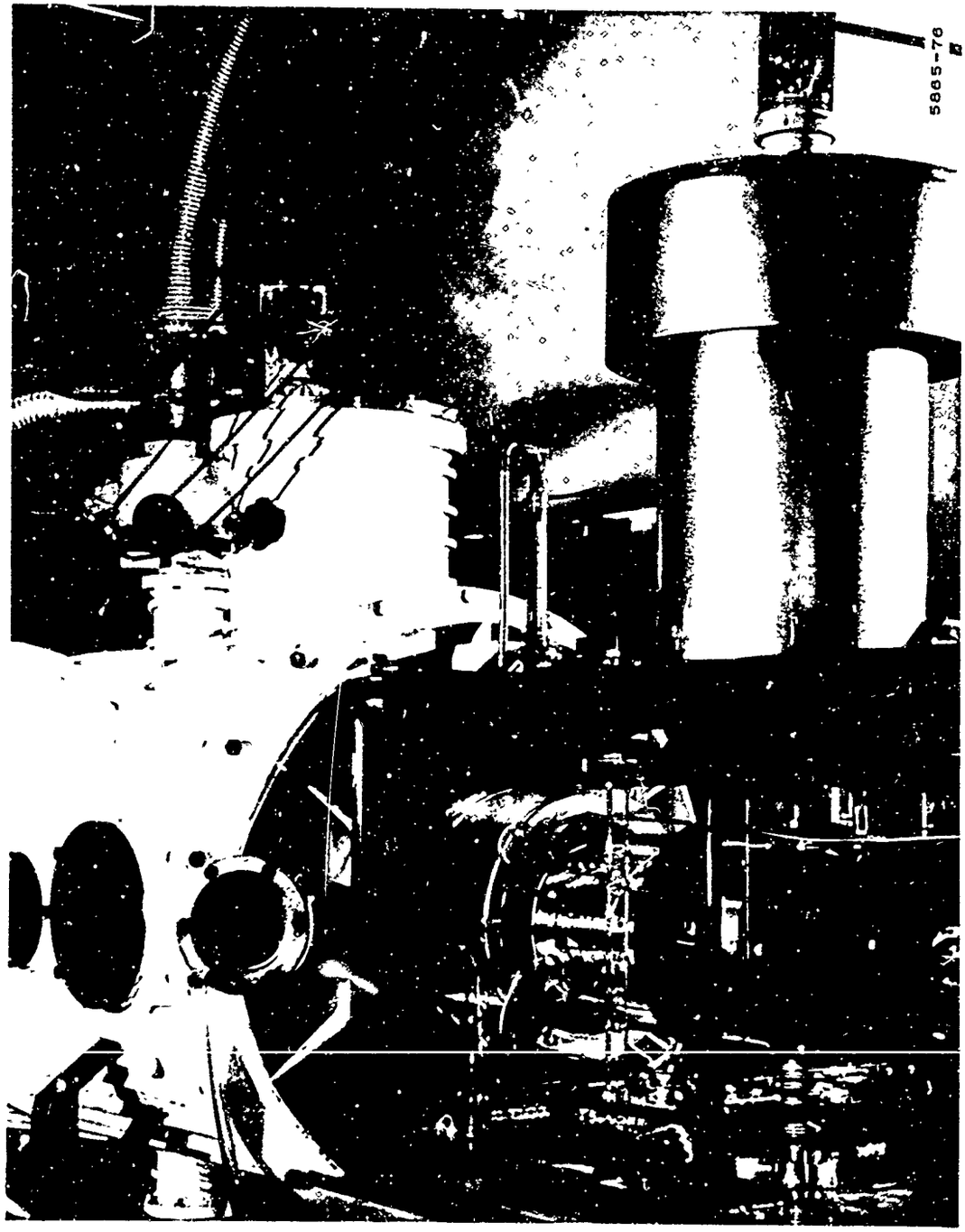

Figure 1-1. Mark II Accelerator

2. EXPERIMENTAL INVESTIGATIONS

This section is divided into two parts. The first part describes the development of the apparatus of the traveling wave accelerator. The second deals with the use of the accelerator as an experimental device and discusses the results of the plasma experiments as they relate to the predictions of the theory.

2.1 APPARATUS DEVELOPMENT

This section discusses the continued development of the accelerator electrical and mechanical hardware.

2.1.1 Electrical Circuit Development

Introduction

We shall first describe the high voltage electrical networks in the Mark II accelerator with particular emphasis on the changes in design which have been found necessary since the publication of 64-1340.

General

The basic electrical parameters which were chosen for the accelerator are the following (see section 4 of 64-1340 for details):

Number of phases	5
Field frequency	240,000 cps
Field speed	5.4×10^4 m/sec
Number of wavelengths	1
Power level	50 kw

The main field coil of the Mark II consists of five separate sections. Each section consists of two coils in series connection in such a way that the currents in the two sections are 180° out of phase (see Figure 2-1). The five sections are physically interleaved in such a way that the current running in the coil approximates a traveling wave sheet current when the five coils are polyphase excited. The "quality" of the traveling wave depends on the realization of correct phase and amplitude relations in the five phases. In addition to the main field coil there is a secondary coil of smaller diameter but the same length, co-axial with the main coil. The main coil is called the "outer" coil and the smaller coil is called the "inner" coil. The purpose of the inner coil is to provide a perturbation of the main field in order to tilt the field lines so as to counteract the tendency of a toroid to expand radially outward (see section 3 of 64-1340). The inner coil is electrically phase shifted with respect to the outer coil and carries 1/5 the outer coil current.

The circuits are excited by five power supplies operated as Class C power amplifiers, each capable of delivering 50 kw (a power in excess of that required). Because of the Class C operation each main circuit is a parallel resonant network with the field coil as part of the inductive branch.

2.1.1.1. System Electrical Network

A schematic of the total electrical network of one of the five phases of the accelerator is shown in Figure 2-2.

The details of the block labelled "Control Circuits", as well as the details of the power supply are given in Appendices I and J of 64-1340. Details of the components labelled "Neutralizing Transformers" and "Inner Coil Drive" are given in this section. A general description of the system is also given here.

The signal from the master oscillator and frequency servo is split into five equally spaced phases 72 electrical degrees apart and each is fed into a phase servo. The phase servo controls the phase of the output of the power supply. The high voltage signal from the supply is the source of the circulating current in the parallel tank circuit. The current in the field coil is sensed by the pickup loop and the pickup signal is fed back to the phase servo and compared to the standard. If these signals do not have the correct phase relation, an error signal is generated which changes the phase of the output from the supply until the correct relation is established.

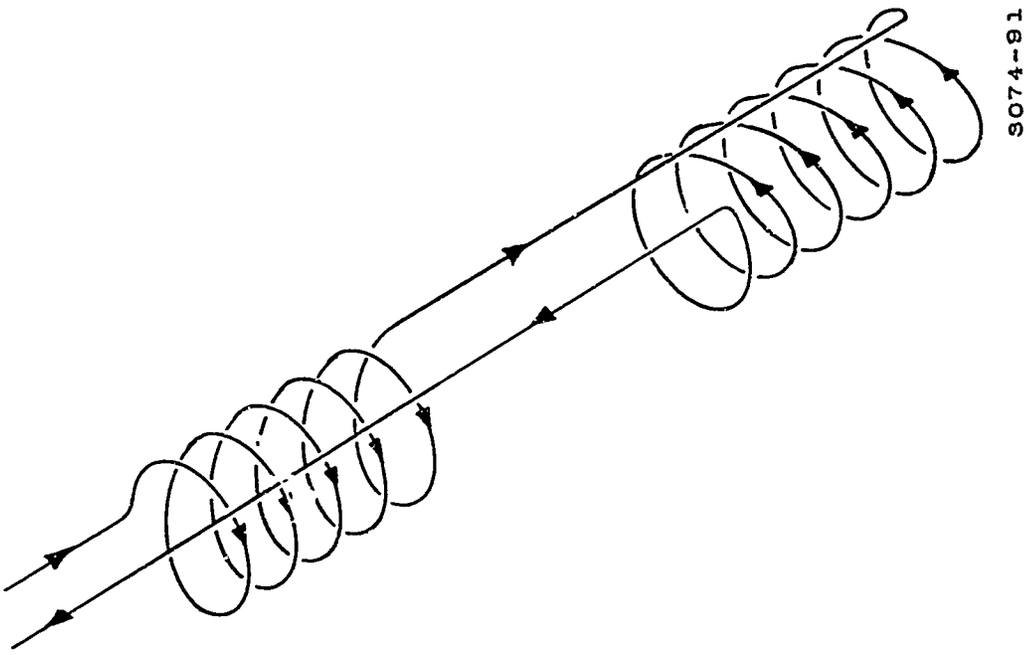

Figure 2-1. Field Coil Winding

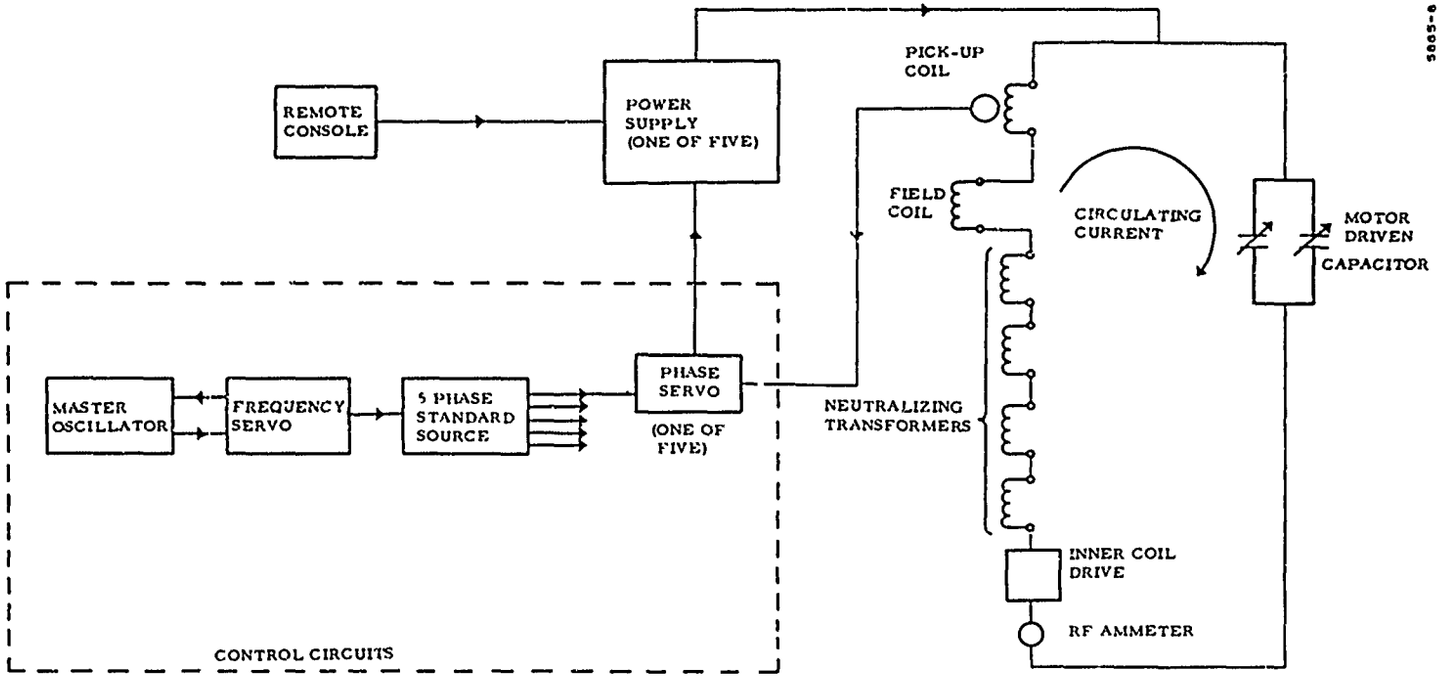

Figure 2-2. General Schematic of Electrical Network

The motor driven capacitor serves to provide tuning adjustments for the tank circuit.

The remote console has the triggering keys for the power supplies, the bias controls for the final power amplifiers, and meters for the measurement of power amplifier dc plate current and grid current. In addition, it contains the read-out meters for five specially calibrated 0-50 amp Weston Thermocouple-type rf ammeters. The remote sensing heads of these meters are in the inductive branch of the resonant circuits.

The total electrical power delivered to the Mark II is calculated according to the relation

$$W = \alpha E_{pp} I_p$$

where

W = power to a load

E_{pp} = peak-to-peak voltage output of the power supply

I_p = dc plate current

Each supply has been calibrated at 240 kc and the α's are determined as functions of plate current. The theoretical maximum for α is 0.5 and it is only weakly dependent on I_p. The calibration does not extend to the very low I_p's but can be extrapolated down to an I_p of one ampere.

2.1.1.2 Decoupling Network Development

One of the major problems anticipated in the development of the Mark II circuitry was that of the mutual interactions among the various electrical phases, as mentioned in the Introduction. There were several alternatives available during the design phase and the one that was chosen was the ring-coupling network discussed in detail in Appendix L of 64-1340. The analysis showed that the mutual effects could be compensated by this capacitance-coupled network, and the proper distribution of loading, amplitudes and phases achieved. This network was built and it exhibited the required electrical properties. One disadvantage of this scheme is that it tightly coupled the supplies to one another and eventually this proved to be a major problem.

In practice the time required to make the adjustments in the network was found to be prohibitively long and a decision was made to abandon this design and employ an alternative method which required more construction but was less sophisticated and possessed the primary advantage of de-coupling the power supplies from one another. The idea is quite straightforward. If one phase of the accelerator is excited, voltages appear in the other circuits because of the mutual inductances among the five primary coils in the accelerator. If, external to the accelerator, one were to somehow provide equal and opposite voltages, there would be no net effect and the power supplies could be adjusted independently.

Figure 2-3 is a simplified schematic of a two-phase system showing the method of providing the neutralizing voltages. The driving voltage is V_o and the induced voltage is V_i. V_i can be cancelled out by a suitable adjustment of the variable transformer. In the case of the Mark II the induced voltages are both in phase and 180° out of phase with the driving voltage, depending on the particular circuits chosen. The transformers can be connected in such a way to provide either in or out of phase neutralizing voltages. Since mutual coupling effects exist among all of the phases of the Mark II, each circuit must be coupled to every other circuit. This means that 10 variable transformers had to be built. Figure 2-4 is a photograph of this transformer array. The transformers had to be adjustable since the presence of the plasma would change the couplings. Each side of each transformer consists of four turns, made up by properly connecting, in series, the braid and inner conductor of RG-17/U coaxial cable; large conductors are necessary because the transformers carry the primary circulating currents. Each transformer consists of a stationary side and a moveable side with motor drive. The transformers have maximum coupling coefficients of about 85 percent.

The transformers reduced the induced voltage to negligible proportions in the absence of any plasma (for example, 25,000 p-p volts primary voltage would produce only 500 p-p volts secondary voltage). The residual voltage was the result of capacitive coupling among the coils which cannot be neutralized by this method. However this residual voltage is negligible.

It should be pointed out here that a high order of neutralization is necessary. The main circuits while appearing as a high impedance to the power supplies when adjusted to parallel resonance, present at the same time, a low impedance, series resonant circuit to an equivalent generator in series with the secondary circuit. This generator is the mutual voltage. Thus

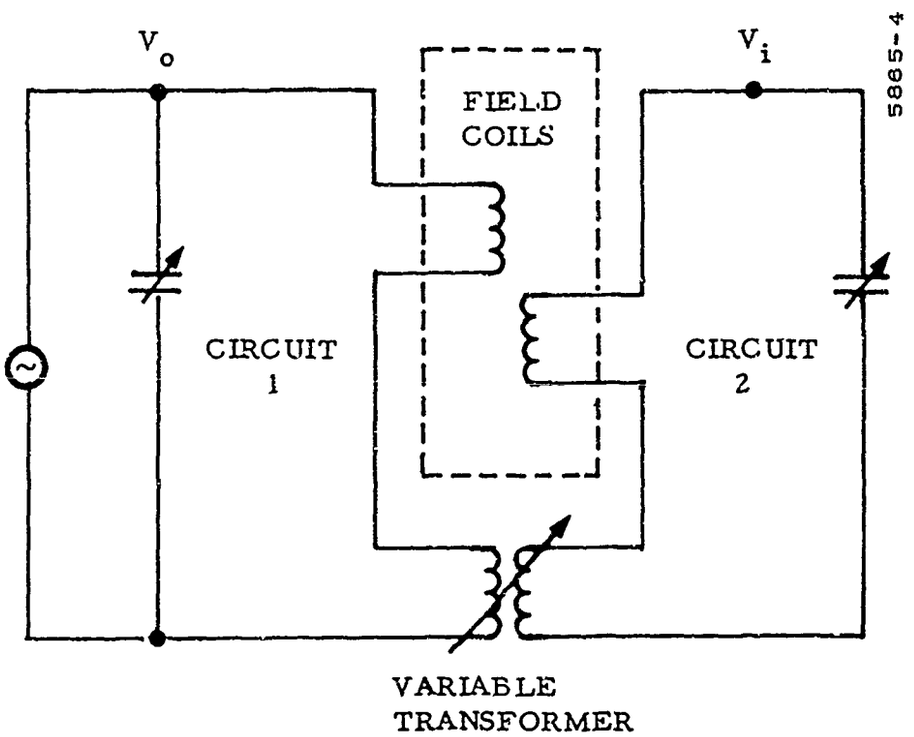

Figure 2-3. Simplified Scheme for Providing Neutralizing Voltages

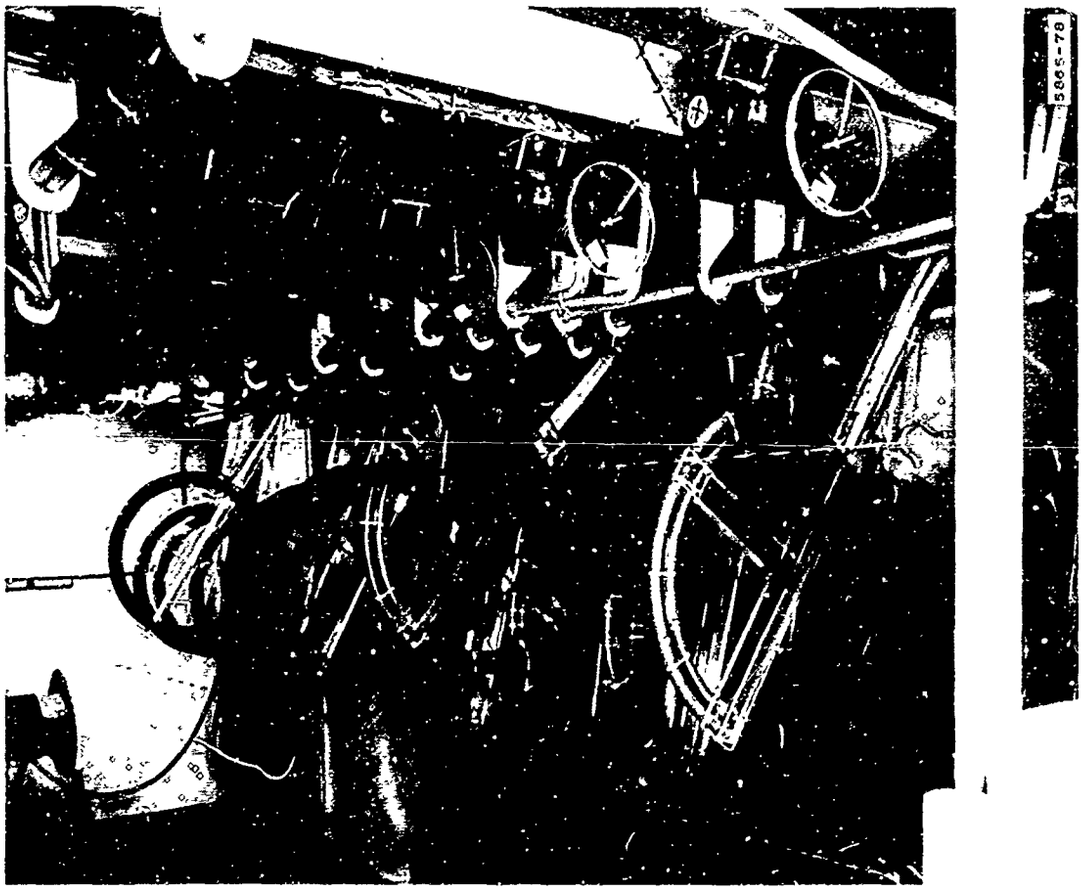

Figure 2-4. Photograph of Neutralizing Transformers

even small voltages from the equivalent generator can produce large circulating currents. The induced voltage V_i actually measured is not the voltage of the equivalent generator but rather the voltage drop developed by the induced current.

The experimentally observed effects of the plasma on this circuit are discussed in section 2.2.2.

2.1.1.3 Inner Coil Network

As mentioned previously, the purpose of the inner set of coils is to provide a perturbation on the main field and to tilt the flux lines in order to minimize the radial expansion of the plasmoids. The tilt provides a force directed radially inward. The amount of tilt is determined by the phase shift and amplitude ratio between the outer and inner current sheets. The phase shift is provided by the method in section 4.2.3 of 64-1340. As shown therein a set of coaxial cable transformers was built which allowed the inner set to be driven by the main circulating currents of the outer coils. Measurements made at that time with rf ammeters showed that the transformers were operating properly, that is, they were providing the correct inner coil currents. After the publication of 64-1340 an error in the Mark II wiring was discovered and, when corrected, measurements were again taken to check the inner coil currents; they were found to be incorrect. The reason for this discrepancy could not be found. The coaxial transformers are rather difficult to analyze due to their large capacities and the complicated distribution of these capacities. It was decided that, rather than spend the time trying to correct the transformers, it would be preferable to replace them by a simpler circuit with the same desirable physical properties.

The schematic shown in Figure 2-5 is the circuit chosen to replace the coaxial transformers. The requirements of the circuit are two-fold:

1. A correct (5:1) current transform
2. A reasonably small impedance reflected into the primary circuit.

The relation between the main current (I_i) and the current through the load (the inner coils) of the circuit of Figure 2-5 is as follows:

$$\frac{I_i}{I_\ell} = \omega^2 LC_2 + \left(1 + \frac{L_\ell}{L}\right)\left(1 + \frac{C_1}{C_2}\right)\left(1 - \omega^2 L\left(\frac{C_1 C_2}{C_1 + C_2}\right)\right)$$

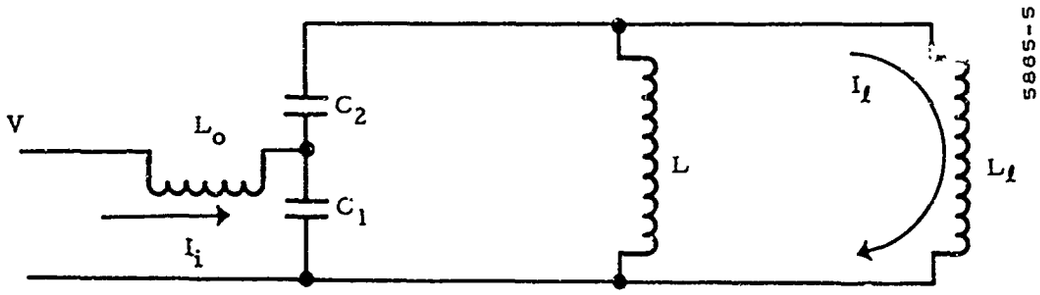

Figure 2-5. Inner Coil Drive Circuit Schematic

If L is chosen so that

$$\omega^2 L \left(\frac{C_1 C_2}{C_1 + C_2} \right) = 1$$

then

$$\frac{I_\ell}{I_i} = \frac{C_1}{C_1 + C_2}$$

The main current and inner coil current are in phase and their amplitude ratio can be fixed by choosing the appropriate capacitor ratio. Note that when the circuit is tuned this way the current ratio is independent of the inductance of the inner coil.

In addition, if the input inductor, L_o, is chosen so that: $\omega^2 L_o (C_1 + C_2) = 1$, then it can be shown that the input impedance, Z_i (where $Z_i = V/I_i$), is the following:

$$Z_i = j\omega \left(\frac{C_1}{C_1 + C_2} \right)^2 L_\ell \equiv j\omega \left(\frac{I_\ell}{I_i} \right)^2 L_\ell$$

Thus, the circuit is equivalent to an inductance equal to the load inductance degraded by the ratio $(I_\ell/I_i)^2$. In this case the effective inductance is reduced by a factor of 25. This satisfies requirement No. 2.

A photograph of one of the five coupling circuits is shown in Figure 2-6. The coil, L_o, is seen in the foreground and the coil, L, is partially seen in the background. L_o was tuned with two adjustable shorted turns (the smaller diameter turns seen in L_o of Figure 2-6). The introduction of this circuit into the inductive leg of the main circuits interrupted the dc path to ground. A large inductance was shunted across C_1 to provide this path.

2.1.2 The Mercury Feed System

The purpose of the mercury feed system is to supply neutral vapor at a steady controllable rate and with a uniform annular distribution to the space between the outer wall and inner wall of the plasma channel.

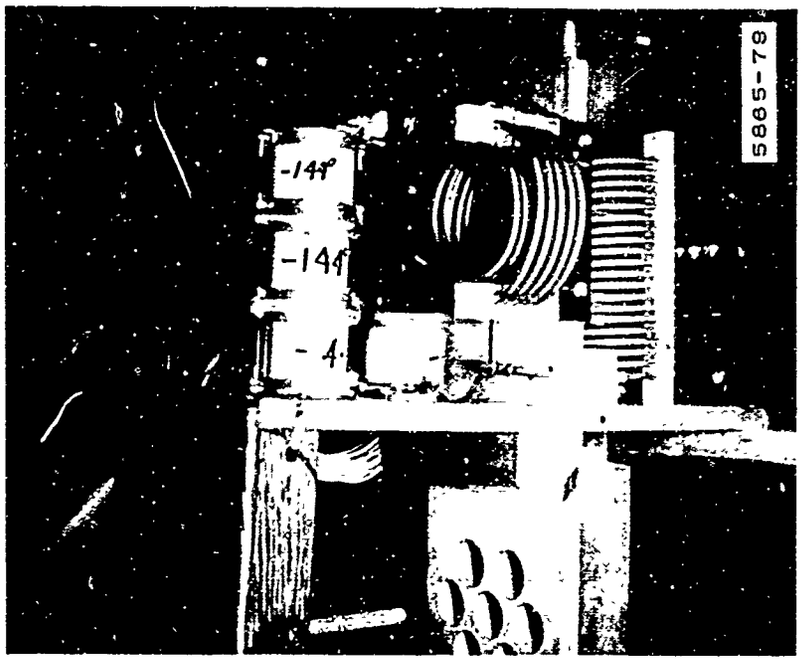

Figure 2-6. Inner Coil Coupling Circuit

It was not deemed desirable to fill a boiler with liquid mercury, and raise it to some appropriate temperature This would entail keeping a large amount of fluid at a high temperature and consequently it would be difficult to change the flow rate of vapor due to the thermal inertia of the large mass. The following method was adopted as the most promising.

The liquid mercury, driven from a reservoir at a constant volumetric rate, entered a small tube where a thermal gradient had already been established with a low temperature at the entrance end, and a high temperature at the exit end. If the upper temperature is high enough, a stationary surface of liquid is established somewhere along the tube.

The rate at which vapor leaves this surface is equal to the arrival rate of the liquid; therefore the vapor flow rate can be measured by measuring the liquid flow rate, and this rate is determined solely by the liquid pump. The evaporation tube is a small-bore tube so only small amounts of liquid are kept at a high temperature. It is only necessary to keep the following parts of the system (containing the vapor) at a temperature high enough to insure that the vapor does not condense. Figure 2-7 is a schematic drawing of the feed system (not including the pump) mounted to the Mark II (the drawing is not to scale). It consists of three sections:

1. The nozzles (eight equally spaced in the annular region)
2. The vapor containing portions (upper stem and nozzle manifold)
3. The principal heating section (lower stem).

Figure 2-8 is a photograph of the stems and manifold. The nozzles shown are not the nozzles finally adopted.

There are four separate heating circuits for the lower stem, upper stem, manifold and nozzles.

Figure 2-7 is the final configuration of the feed system, with the nozzles ending at the beginning of the field coil. Originally it was planned to inject the vapor farther downstream (well within the coil system) to prevent ions being back-reflected from the fringe field. This was changed after the Mark II was run with the long nozzles and the discharge was observed to exist too far downstream.

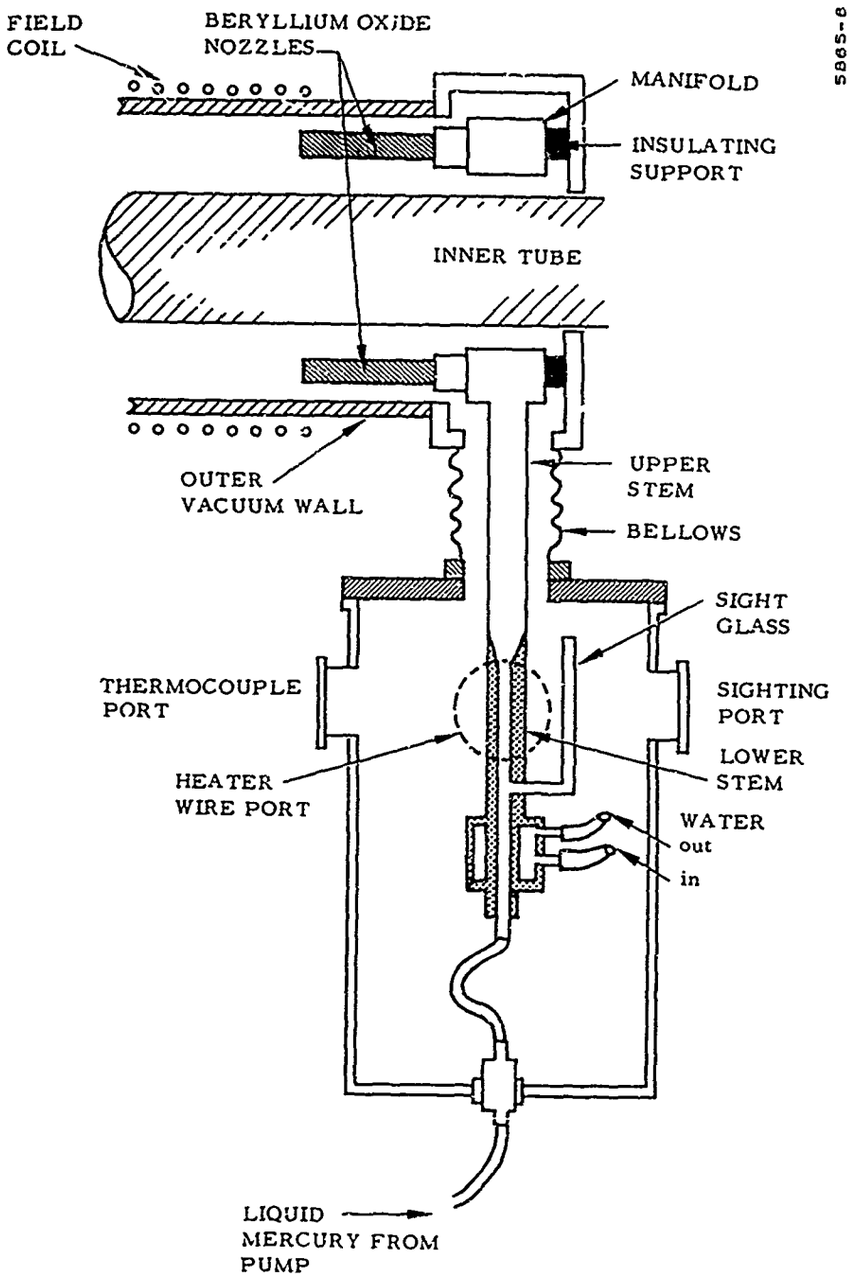

Figure 2-7. Mercury Feed System

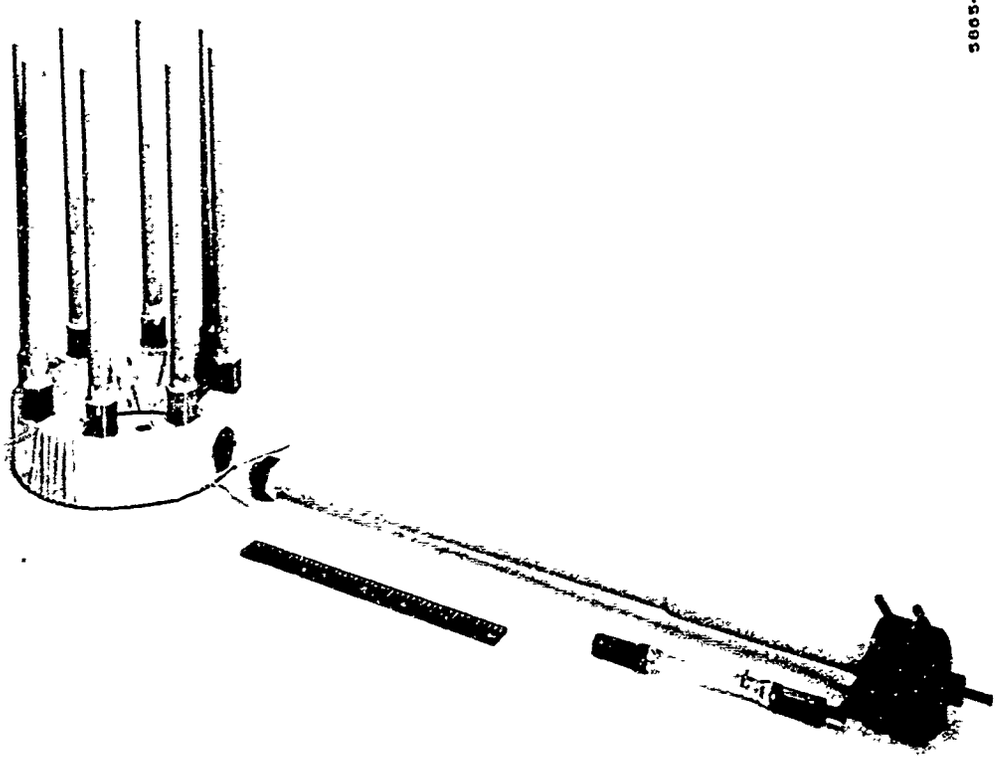

Figure 2-8. Mercury System

1. The Nozzles

Since the nozzles were originally to be in the traveling wave field and since they had to be heated, the first set was made of thin-walled steel. The heating was to be provided by eddy-current heating but this proved to be excessive and the nozzles became hot enough to be in danger of sagging. The next set was made of Grade A Lava ceramic to be heated by the nozzle manifold. The heating was inadequate and condensation occurred within the nozzles and the resulting liquid became eddy-heated by the field and vaporized at an uncontrolled rate, producing excessive surges from the power supplies. Finally, a set of beryllium oxide nozzles was made and heater wires were wound around the base (near the manifold). Since beryllium oxide has a high thermal conductivity, these nozzles proved to be quite satisfactory.

2. Upper Stem and Manifold

The upper stem and manifold are made of stainless steel. A number of coating processes were tried on these in order to obtain a reliable insulation between the heater wires and base metal. A large variety of Sauereisen cements, quartz tapes and combinations of the two were tried without much success. The coatings would not adhere well to the metal. Some of the Sauereisen cements became electrically conducting at 400 C and every failure meant an extensive tear-down process. The manifold was eventually plasma-sprayed with alumina. This system has worked well throughout a long series of repeated heatings. Not shown in Figure 2-7 are attachments (integrate with the base metal) for Conax Shielded thermocouples (one on the manifold and one on the upper stem). During operation of the system the manifold is maintained at 350 C and the upper stem at 320 C. The heater wires are Nichrome V or Tophet A throughout and the leads to the heaters are stranded nickel. No copper is used anywhere since the system is in an atmosphere of hot mercury vapor.

The upper stem is screwed into a block on the manifold and vapor leakage is prevented by finely machined mating flats, one on the manifold and one on the upper stem.

The system is attached to the accelerator enclosure by three insulating supports made of fired Grade A Lava.

3. The Principal Heating System

The section where the liquid is vaporized is a steel tube with a 1/8-inch diameter bore. It has its own heating circuit and thermocouples. A Pyrex sight glass alongside the section allows the mercury level to be observed through the side port against a scale mounted on the Pyrex. When the level has stopped changing, the system has reached steady state.

At the bottom of the lower stem is a water-cooled section which has two purposes: it fixes the temperature at the point where the liquid enters; and it keeps the flexible (Tygon) tube cool. The Tygon is needed for assembly purposes. The lower stem is welded to the upper stem and a smooth transition section joins them.

Liquid Mercury Pump

The liquid pump is shown in Figure 2-9, mounted in its normal position. It consists of a constant speed motor, variable speed reducer, gear reducer train and piston drive plus suitable valves and a mercury reservoir. The piston is sealed by two O-rings and moves in a reamed bore in a rectangular bar of Plexiglas. The piston is driven from a 40 thread/inch screw. The speed of the advance is measured on a tachometer attached to the final drive train.

Figure 2-10 shows some details of the bottom case of Figure 2-7.

Calibration of System

Figure 2-11 is a plot of the delivery rate of the pump versus tachometer reading. The calibration plot was made by attaching a calibrated precision bore glass tube to the pump output and timing the rise of the liquid. The connection between the pump and the boiler in the accelerator consists of two short sections of Tygon tubing. When a calibration of the pump was made using Tygon between the pump and precision tube the results were somewhat scattered due to the presence of compressible voids which appeared in the mercury where it passed through the Tygon. A second calibration was made using a hard connection to the tube rather than a flexible one and the plot of Figure 2-11 is the result. Vapor delivering rates are taken from this calibration even though some small error is probable.

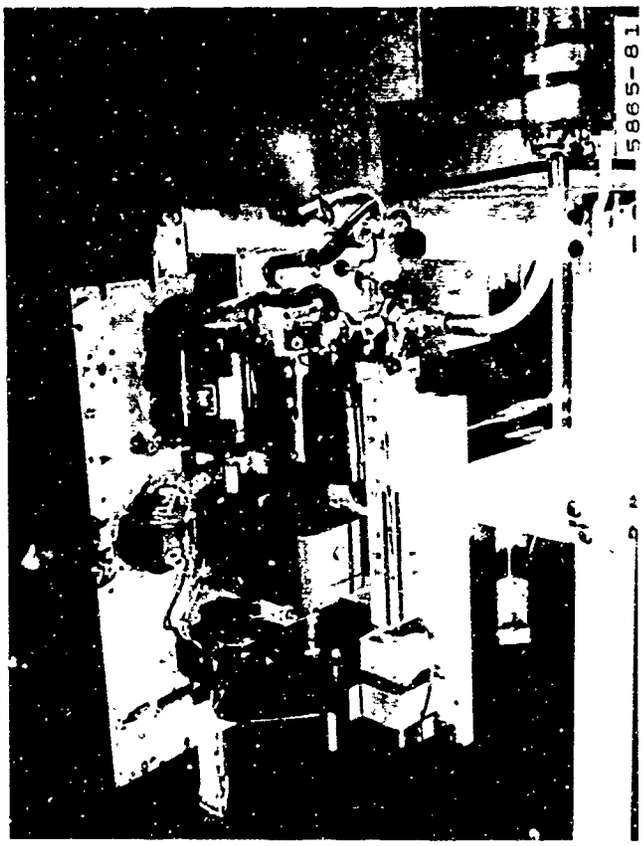

Figure 2-9. Liquid Pump

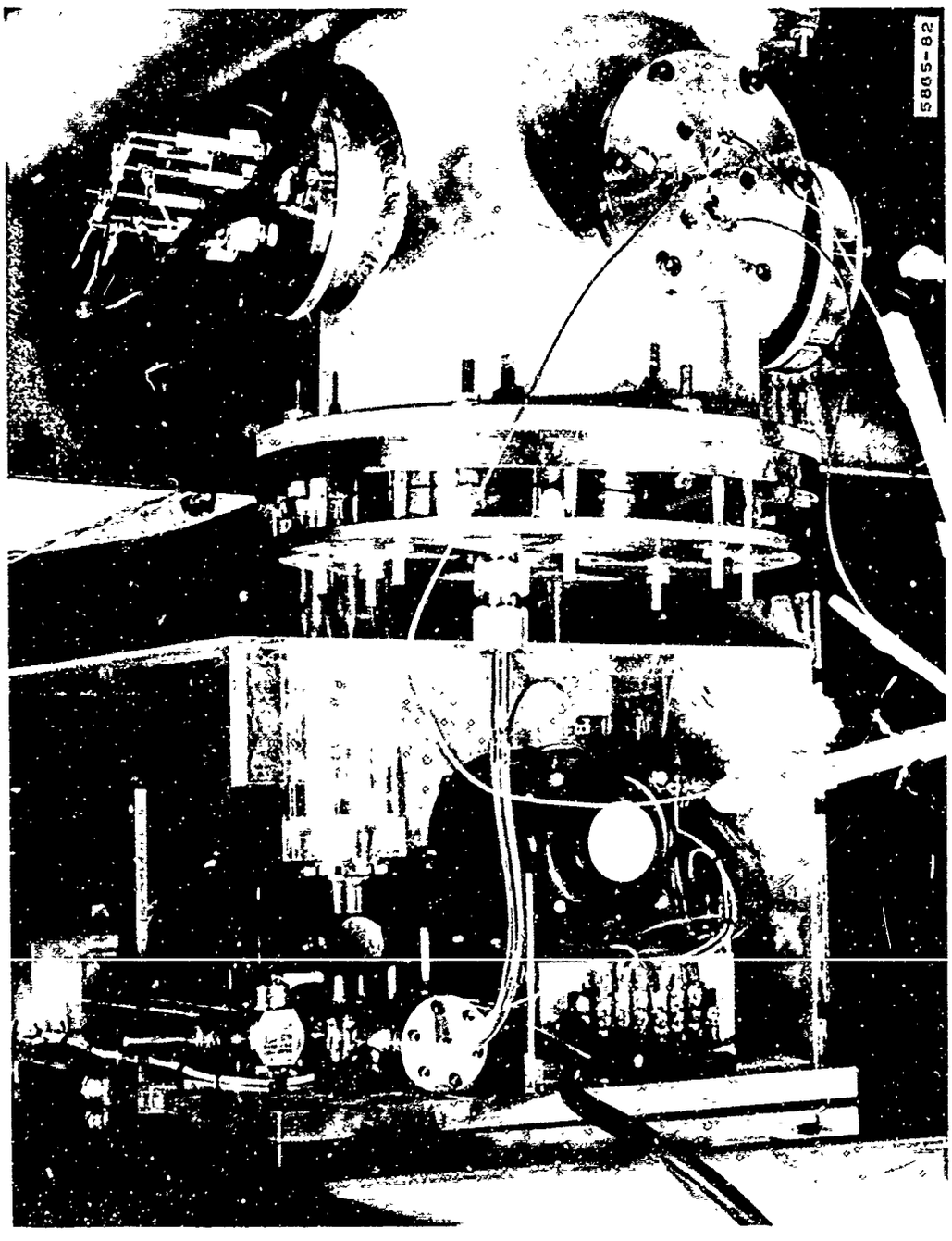

Figure 2-10. Detail of Mercury Feed System

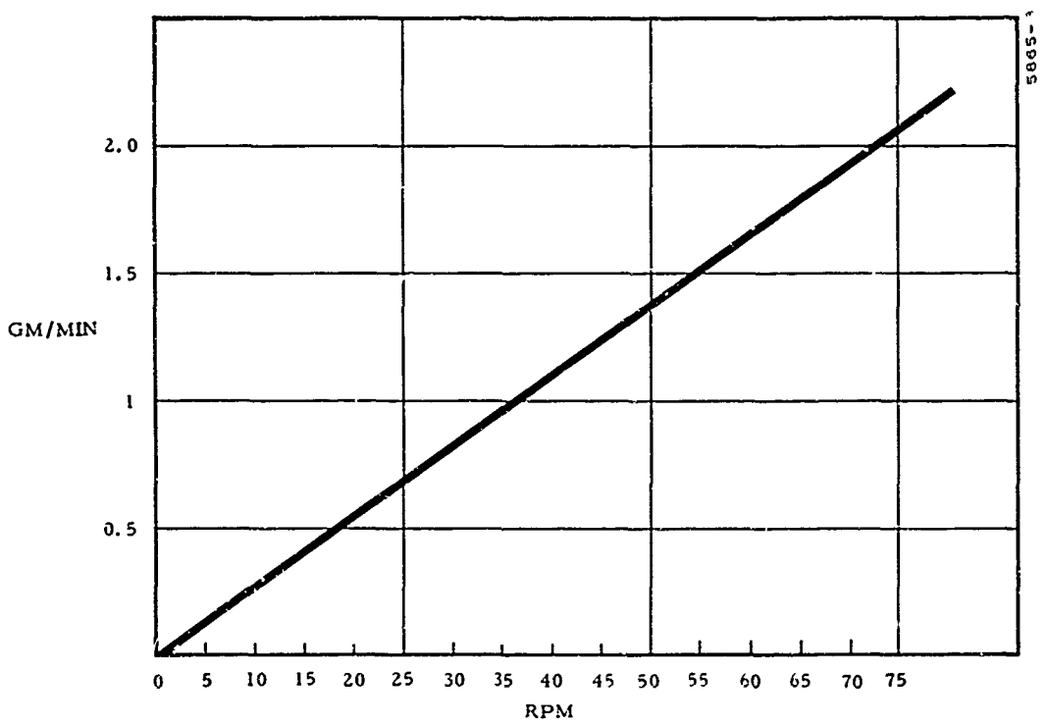

Figure 2-11. Liquid Pump Calibration

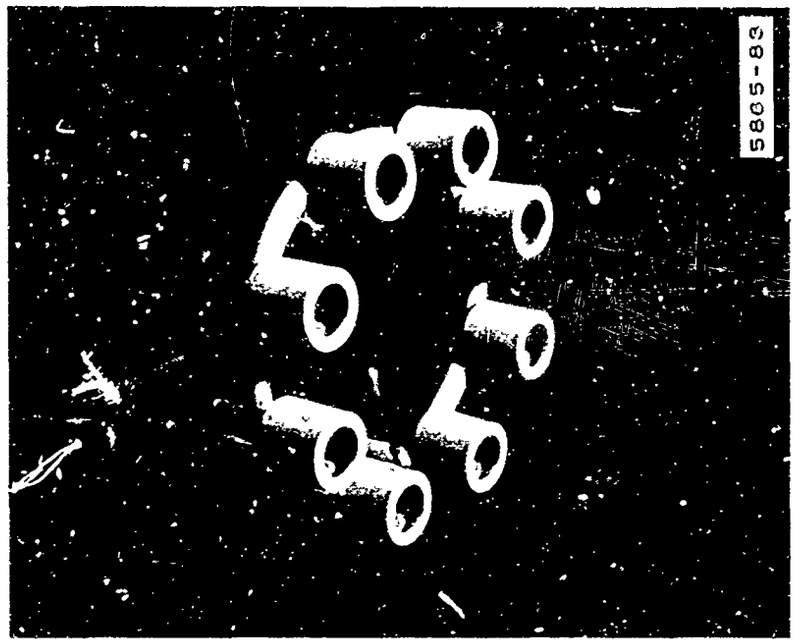

Figure 2-12. Apparatus for Symmetry Test

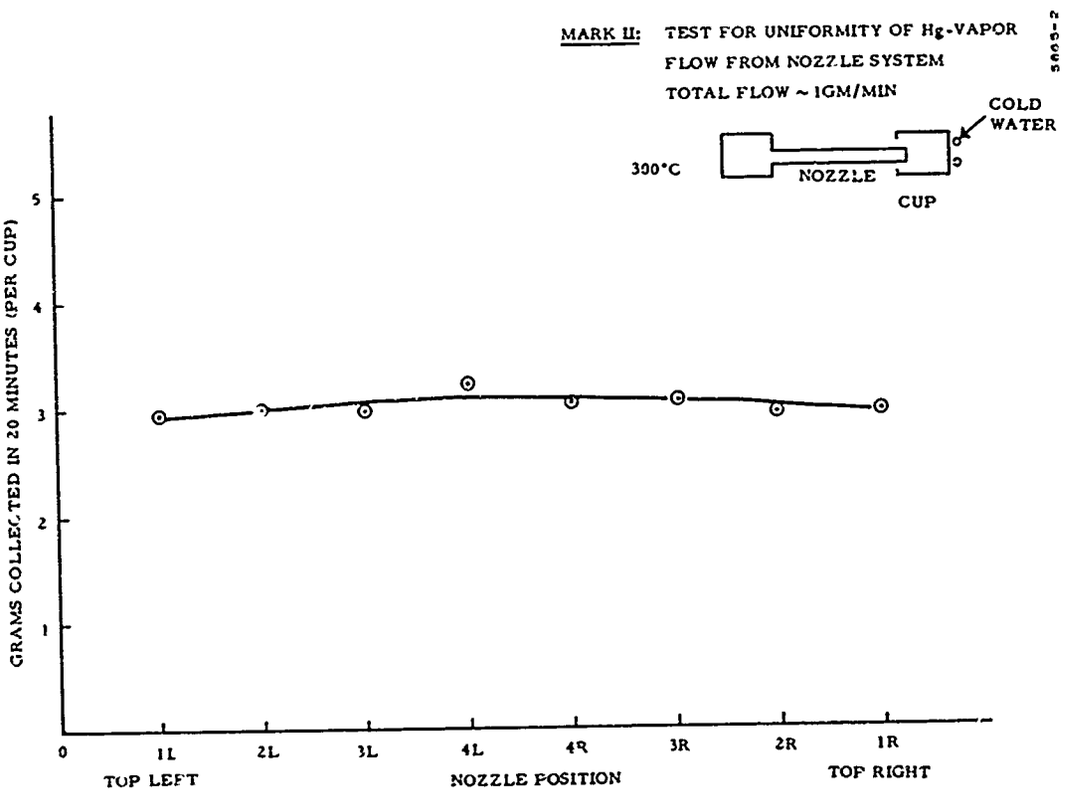

Figure 2-13. Test of Azimuthal Symmetry

Figure 2-14. Photograph of Discharge and Nozzles

An experimental observation was noted during the operation of the accelerator which appeared to confirm the need for such shielding and this is related to the theory of the neutralizing transformers. It was found that the ability to neutralize induced voltages was markedly decreased in the presence of a plasma. The phase of the residual voltages was such as to suggest a large capacitive coupling among the phases and so a shielding coat was applied to the outside of the channel wall to maintain the effect constant and independent of the plasma.

The coating was made by diluting an Aquadag suspension and applying it to a tube slowly rotating in a lathe. The shielding effect is rather insensitive to the exact value of skin resistance so the process is not critical. The coating is quite hard after air cure and showed no tendency to be affected by immersion in transformer oil (its natural environment in the accelerator).

The first tube was mounted and grounded. When the coils were excited, an arc occurred through the oil layer between the coil and coating. Inspection showed that the arc had jumped from several of the coils, each in different phases, and the current had exited from the coating at the grounding strap. The current densities were high enough to heat the coating to the point where the ceramic channel wall cracked. The cause of the arc is unknown, but it is suspected that a small amount of the aquadag came off the coating and provided a conducting path to the coil. The next Aquadag-coated tube was over-coated with PT-209*, a ceramic material. This prevented further coil-to-coating arcs. However, the coating had no significant effect on the non-neutralized induced voltages; its main effect was to make initiation of the discharge more difficult, in that a higher gas pressure was required at the same field coil voltages. The over-coated channel cracked during a subsequent experiment, and the remainder of the experiments were done with uncoated tubes.

2.1.3.2 Electrical Isolation

During a preliminary experiment concerned with the tuning of the Mark II under plasma-loaded conditions, the discharge suddenly extinguished, and oil was observed in the vacuum tank. An observer reported

*Product Techniques Inc., Downey, California

seeing a bright flash just prior to this. Upon disassembling the accelerator it was discovered that an arc strike had punctured a stainless steel bellows connecting the vacuum tank to the box containing the field coils. (Figure 2-15 is a photograph of the largest hole; there were several smaller punctures). One side of the bellows faces the plasma discharge, and the other is oil-cooled. The origin of the arc clearly lay somewhere within the plasma channel. The arc suggested the presence of an electric field directed axially down the accelerator and since the accelerator depends on a charge separation voltage to accelerate heavy ions down the machine, the arc source voltage was identified with this accelerating voltage. This effect has been previously observed*.

A rough estimate of the energy involved in the arc was obtained by calculating how much energy would be necessary to vaporize the steel. It was too high to be accounted for by some discharge of the energy stored in a capacitive field existing between the accelerator coils and the bellows.

If the arc source was the Hall voltage of the accelerator, then it was clear that one end of the accelerator should be electrically floating rather than that both ends be grounded. The end which could be isolated was the end containing the mercury feed system. This meant the isolation of the heater leads and thermocouples, and since the mercury vapor forms a conducting path the liquid mercury pump also had to be isolated.

The mechanical isolation is shown in the photograph of Figure 2-16. The bellows is separated from the floor of the box by means of a Lexan flange and the spring-loaded tie rods (ground potential) were separated from the steel shell containing the nozzle manifold by another Lexan ring. This left the shell, bellows and under-structure (not shown) isolated electrically from ground. The heaters were isolated by means of high-voltage transformers (Figure 2-17 shows two of five). When this modification was completed, the system was isolated up to about 15 kv.

In order to measure any dc voltages developed at the isolated end, a 100:1 probe was designed and the output was read on a dc microammeter. The probe is shown in Figure 2-18, and a schematic of the probe circuitry is shown in Figure 2-19.

*Smotrich, H, Janes, G. S. and Bratenahl, A., 4th Symposium on Engineering Aspects of Magnetohydrodynamics, April 1963, Berkeley, California

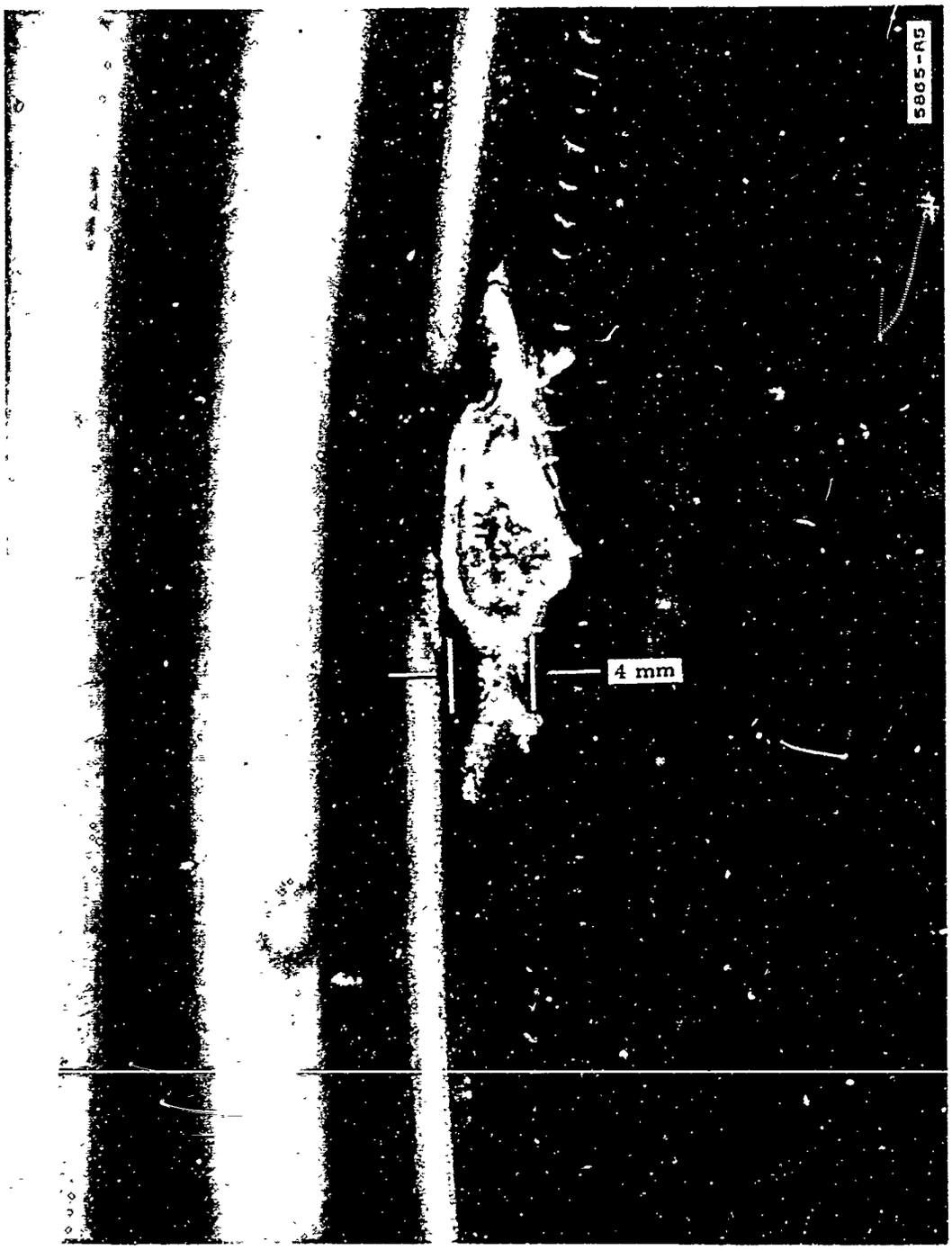

Figure 2-15. Arc Strike Puncture

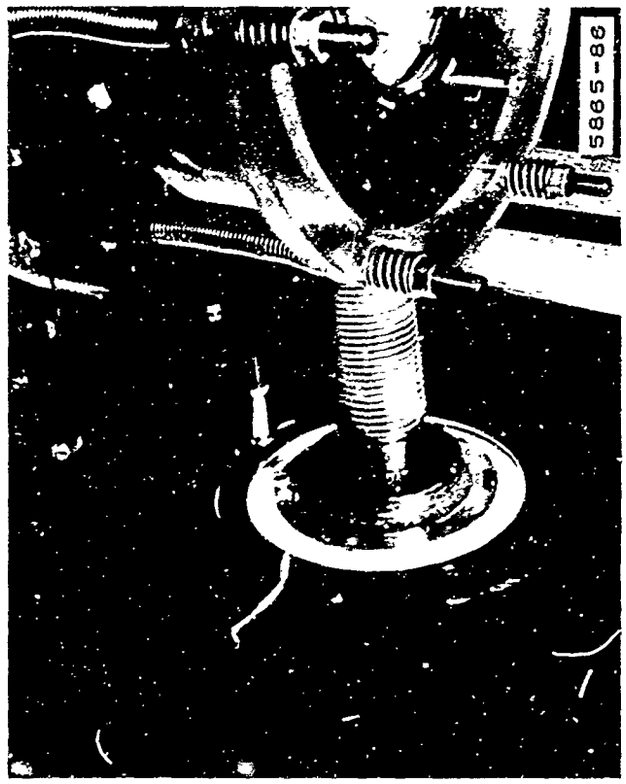

Figure 2-16. Voltage Isolation

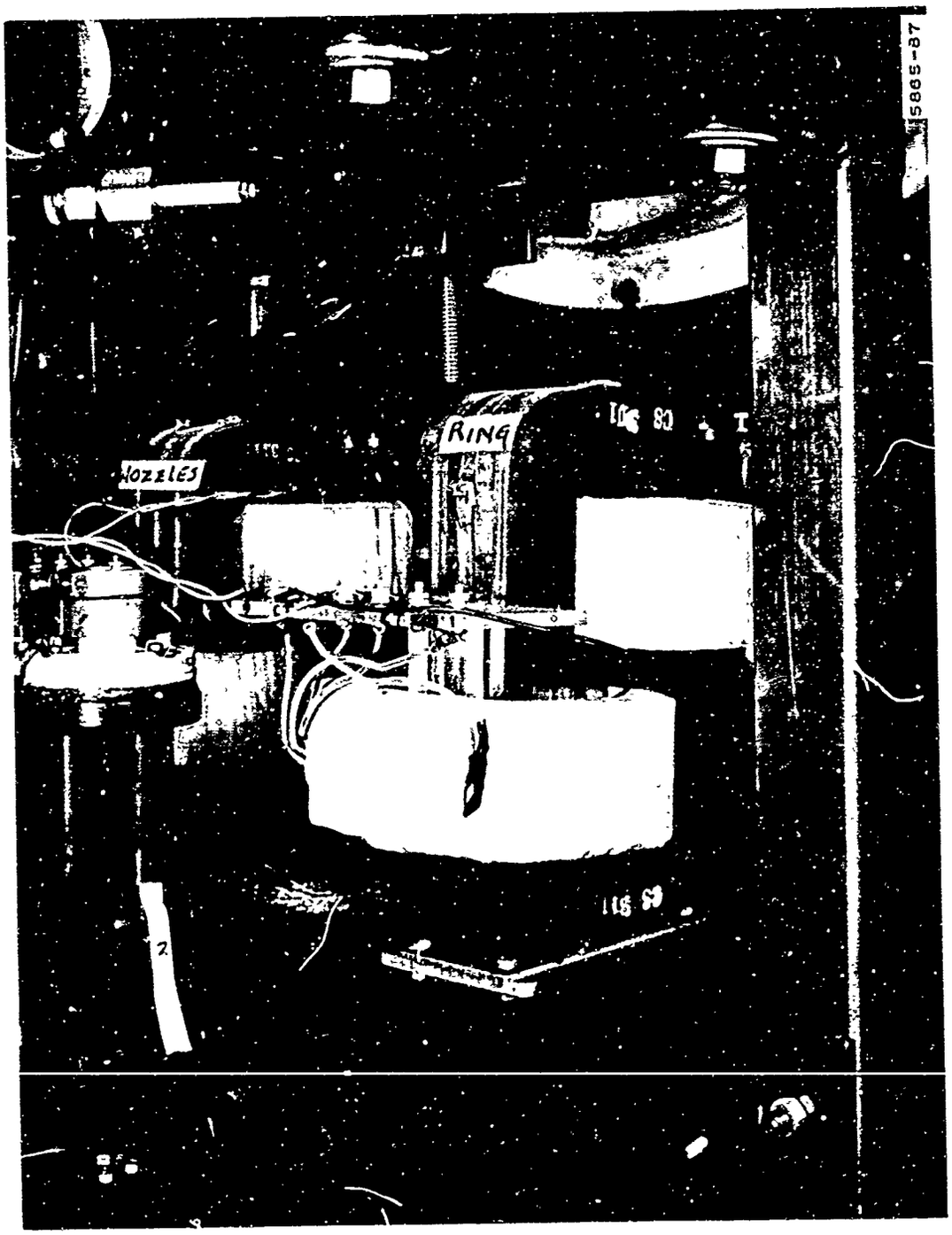

Figure 2-1?. Isolating Transformers

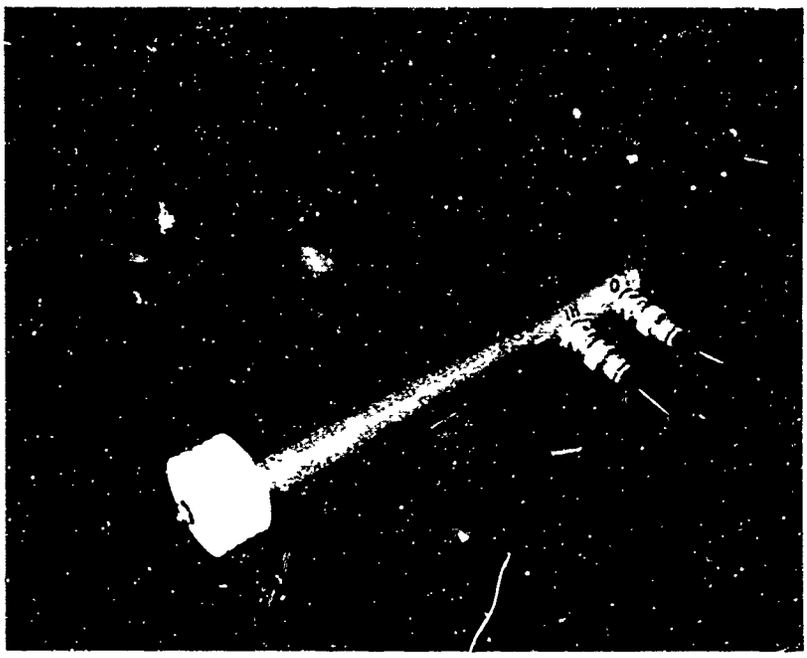

5865-88

Figure 2-18. DC Probe

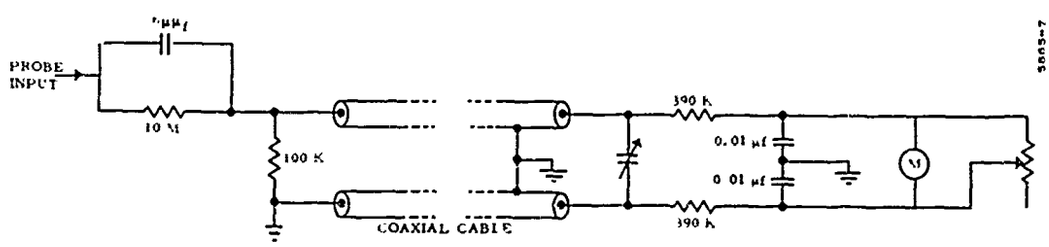

Figure 2-19. DC Probe Schematic

2.1.3.3 Field Coil Problem

The various electrical phases of the field coil are separated spatially from one another by about 0.080 inch. If the phase relation is correct between physically adjacent phases, only a nominal voltage appears between them but if the phases are wrong a large voltage difference can occur. The insulating transformer oil used in the Mark II is rated at 30 kv dc for a 0.1 inch gap but the dielectric strength at radio frequencies is lower and certain impurities can lower its strength drastically. A number of interphase coil arcs occurred during the course of the research. The site of the arc was always covered with a loose carbon deposit which had to be removed before the coil could be excited again. This usually resulted in a partial disassembly of the accelerator. Additional filters were added to the oil circulating system and they all eviated the problem somewhat. The original coil held together for a surprising time until, for a reason which is not clear, two phases blew out simultaneously (see Figure 2-20). There is a possibility that several of the power supplies went into an uncontrolled high-frequency oscillation but this is just a surmise.

A new coil was made, and insulated with Isonel 31*, a high dielectric strength varnish. This coil has proved quite reliable. A third coil was built in case the second coil was lost; this third coil had double the space between phases, but it has not been needed.

2.1.4 Diagnostic Apparatus

The Mark II accelerator is not, in the usual sense, a steady-state device. The production and acceleration of plasma toroids is essentially a transient process which occurs within a single cycle of the radio-frequency field. It is only steady in the sense that the traveling field is on for a time long compared with its period. The measurement of gross parameters, such as power input, gives only an indication that the accelerator is working in a manner consistent with the underlying theory. In the final analysis it is necessary to detect the critical transient phenomena, that is, the plasma toroids.

*Schenectady Varnish Co. Inc., Schenectady, N. Y.

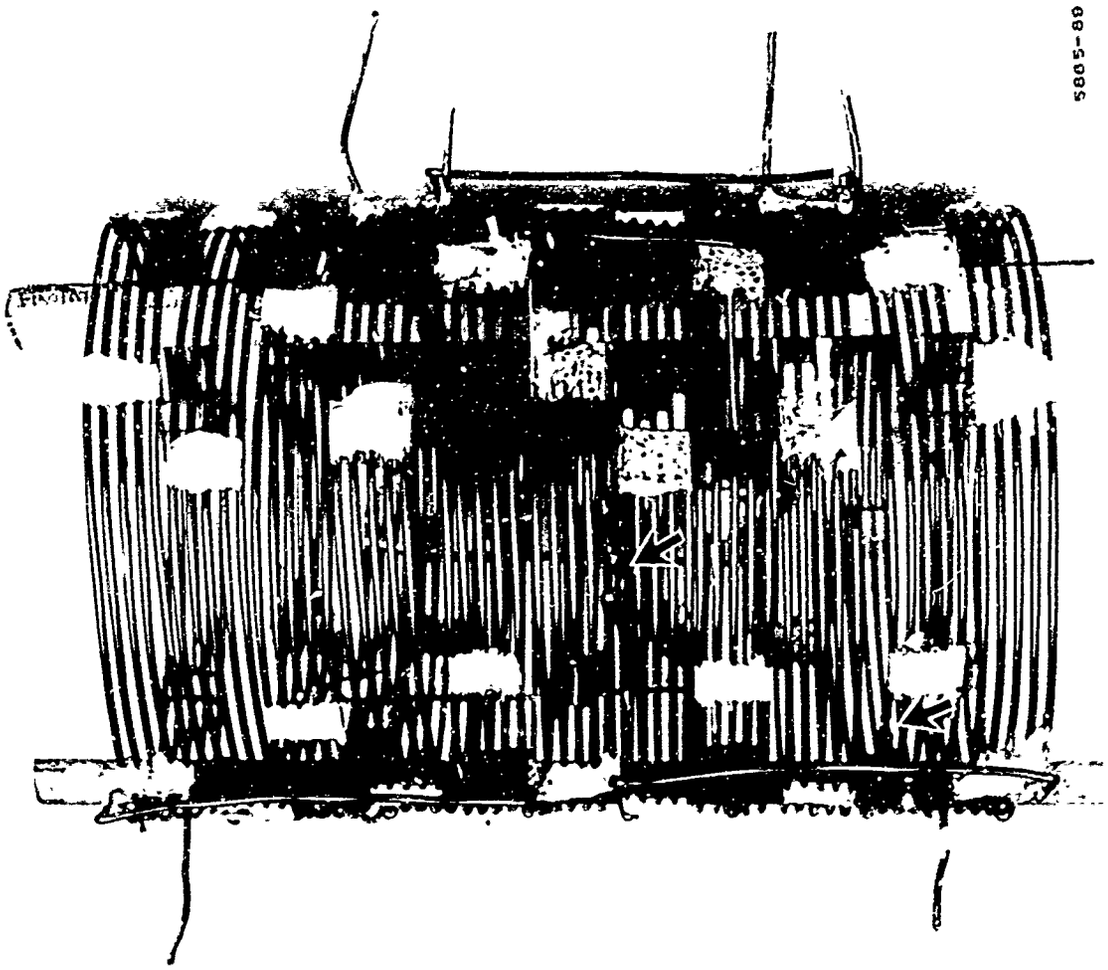

Figure 2-20. Blown Field Coil

The apparatus with which attempts were made to detect the toroids can be divided into two main categories:

1. Field Detectors
   a. Magnetic flux probes
   b. Electrostatic probes
   c. Dc voltage probe
2. Optical Detectors
   a. Optical spectroscopy
   b. Image converter
   c. Light pulsation detection

1. a. Magnetic Flux Probe

Of the various techniques the one relied on most heavily was the magnetic flux probe. The reason for this follows:

The toroids should exit the accelerator pinched by their self-currents and the current should exist for times of the order of a mean collision time. Since they should be traveling at speeds in excess of 5×10^4 meters/sec, they will occupy a finite spatial region and the magnetic field associated with the self-current should extend farther. The magnetic flux probes are used to detect the self-fields of the toroids. The probes are multiturn coils which are meant to intercept the toroids and give a voltage output which is proportional to the rate-of-change of that part of the self magnetic field of the toroids which threads the coil. Figure 2-21 is a schematic drawing of the coil position relative to the exit of the accelerator, and of the electrical connections of the coil to the oscilloscope.

Each probe consisted of two coaxial coils of the same diameter and number of turns electrically connected so that a uniform time varying flux gave no net output voltage. This was done to remove as much accelerator fringing field background as possible. The two output lines of the coils went into a shield which was attached to the common connection between the coil halves. The lines were brought out of the vacuum system via

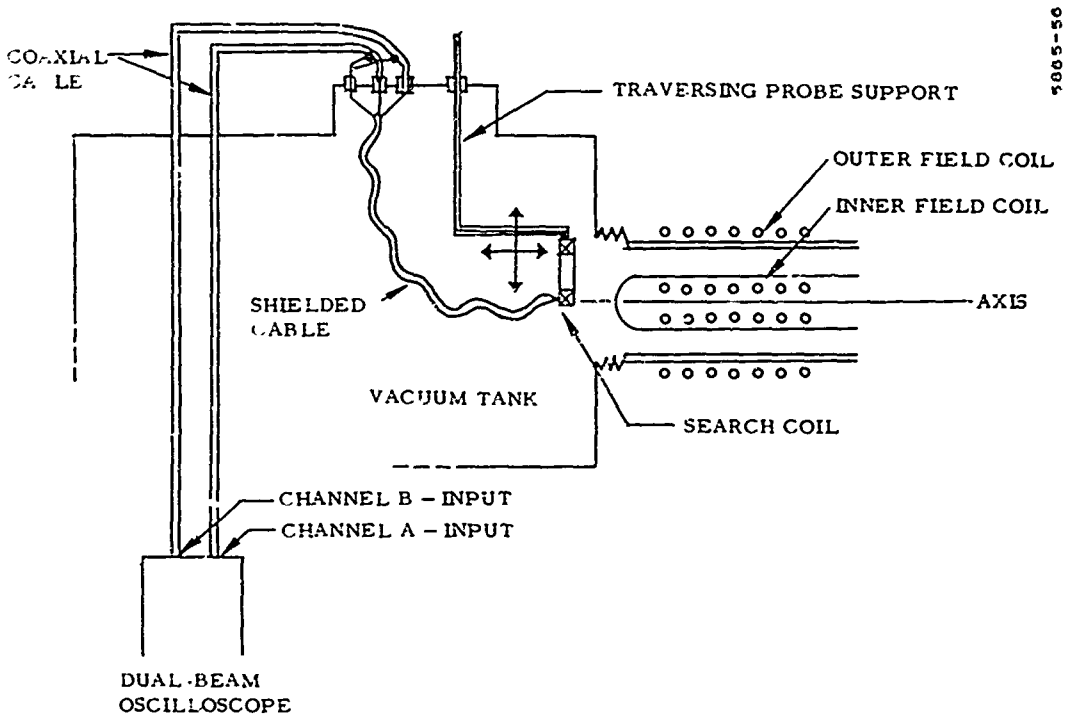

Figure 2-21. Flux Probe in Accelerator

feedthroughs and continued to the dual beam oscilloscope (Tektronix 555) in coaxial cable. The lines were connected to the A and B amplifiers and the oscilloscope trace was taken A minus B, to give the voltage across the coil. The lines were terminated at the scope with the characteristic impedance of the coax cable. Both A and B amplifiers were balanced by feeding into them a common signal and adjusting the gains to give a zero signal on the A minus B mode. Figure 2-22(a) is a schematic of the search coil.

Another device was used in conjunction with the search coil. Since the coils are in the fringe field of the field coil a question will always arise as to the legitimacy of any output signals. An insulating probe was built whose purpose was to interrupt any toroidal currents. This probe could be moved axially into the annular channel to form a solid radial spoke. If toroids were being emitted from the accelerator, this block in the channel should disrupt the azimuthal self-current resulting in a radical change in the search coil signal. Figure 2-22(b) is a photograph of a search coil and the blocker probe (constructed of ceramic and boron nitride). The blocker occupies about 1/300 of the circumference of the annular channel and therefore its effect on any axial flow phenomena is negligible. The blocker was used towards the end of the program.

1. b. Electrostatic Probe

The electrostatic probes consisted of four bare 0.005-inch diameter tungsten wires in the plasma stream. the probes were used in pairs, each pair being fed into the A and B channels of the scope amplifier in a manner similar to the magnetic flux probe. By choosing pairs among the four probes a spatial variation in the detected fields can be established.

1. c. DC Voltage Probe

This is the probe discussed in section 2.1.3.1.

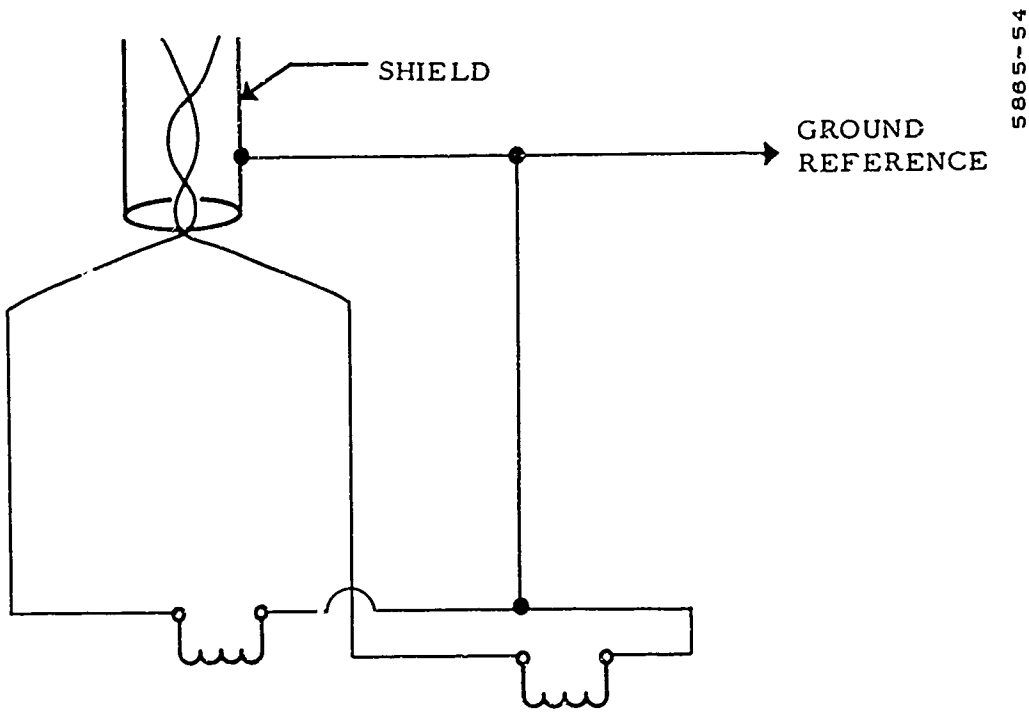

BOTH COILS FORWARD WOUND

Figure 2-22a. Schematic of Search Coil

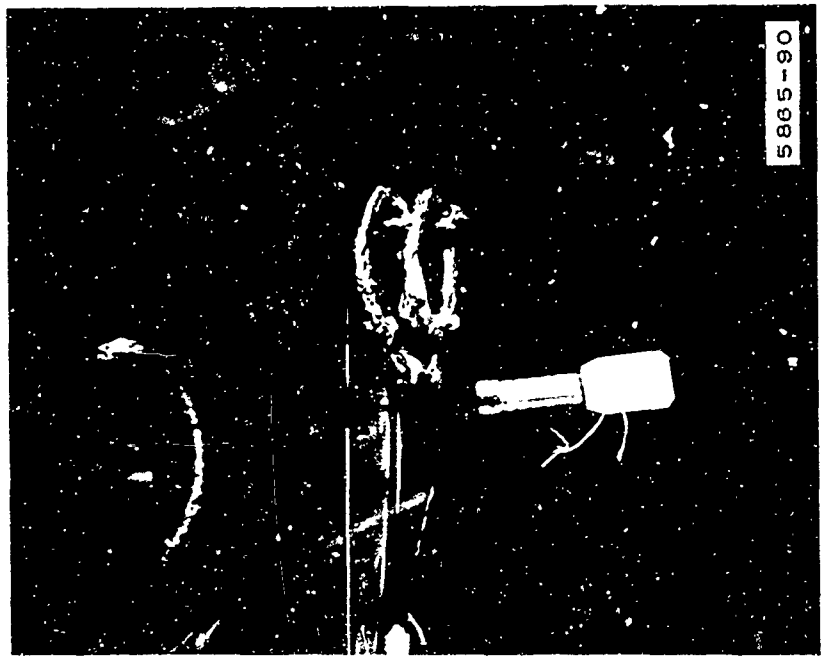

Figure 2-22 b. Search Coil and Blocking Probe

2. a. Optical Spectroscopy

The spectrograph is a Hilger and watts, type E-528 with 60 cm glass optics. The dispersion ranges from 15 Å/mm at 4000 Å to 100 Å/mm at 9000 Å. The film used was Eastman Kodak type 1F. The position of the spectrometer is shown in Figure 2-23.

2. b. Image Convertor

An STL Image Converter camera, in the framing mode, was used in an attempt to photograph the toroids. The light level of the discharge at the exit was too low and no images were obtained.

2. c. Light Pulsation Detection

A bundle of incoherent fiber optics were stationed at the exit of the accelerator as shown in Figure 2-23. The light output of the optics was directed into a photomultiplier whose output was displayed on an oscilloscope.

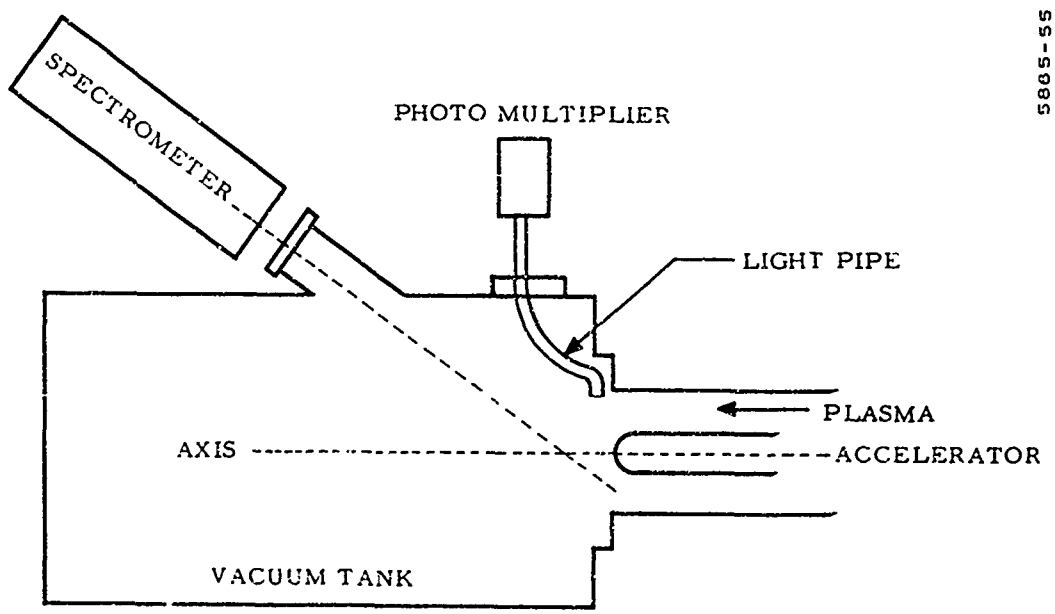

Figure 2-23. Position of Optical Apparatus

2.2 EXPERIMENTS WITH THE PLASMA DISCHARGE

Introduction

Now we describe that part of the experimental phase of the program which involved the plasma discharge. Early in this research program, before the first model of the mercury feed system was completed, it was decided to operate the Mark II with a low pressure argon discharge. A light ballistic pendulum was mounted at the output of the accelerator as an indication of performance. Two conclusions were reached as a result of this experiment:

1. The pendulum deflection was zero when one of the five phases was far out of electrical alignment.
2. It would be necessary to replace the Pyrex glass of the vacuum channel with a material more resistant to thermal effects.

The experiments conducted after the preliminary study are reported below. Except for a few higher mass flow-attempts, the mass flow rate of mercury was between 0.3 and 0.4 grams/minute.

2.2.1 Operation of the Accelerator

Certain steps are taken to prepare the accelerator for a series of experimental runs.

The vacuum system is always left evacuated (and valved off from the pumps) overnight; the insulating oil is pumped out of the box holding the field coils and into a storage tank. Initially the system is pumped down to $<10^{-4}$ Torr and the oil is pumped back into the coil box. The oil is circulated past a pair of resistors dissipating 10 kw in order to heat it. It is necessary to pre-heat the outer and inner vacuum channel walls with the hot oil (to about 40C) to prevent condensation of mercury in the vacuum channel. In parallel with this procedure the mercury boiler and feed system is brought up to its operating temperatures. During this interval the power supplies are turned on and checked. The phases of the currents are observed to insure that the phase servos are operating properly.

Although initial adjustments are made to roughly equalize the amplitudes of the currents in the five primary phases, the final adjustment must be made with a plasma. When these preliminary conditions are established, mercury is admitted into the boiler, the mercury pump turned on, and the flow-rate set. The flow and temperature reach their steady-state values in about 15 minutes.

2.2.2 Operation of the Accelerator with Plasma

The final tuning of the accelerator is accomplished by exciting the phases one at a time with gas in the vacuum channel. When the mercury flow rate has reached steady-state, argon is injected to a pressure of few microns to initiate the discharge. The argon pressures used are not known with accuracy since the gauges used to measure pressure deteriorated fairly rapidly in the mercury environment. Argon is added as a seed because usually mercury alone would not break down, though on occasion, and under apparently identical conditions, it discharged easily.

The phases are run separately and the induced currents in the unexcited phases are reduced by adjusting the neutralizing transformers. This is not as straightforward as it sounds since it is observed that two modes of single-phase discharge occur, one rather low intensity mode which does not couple the circuits tightly, and a second mode which is brighter and produces a much larger coupling. While one mode is being neutralized the discharge can flip into the other mode upsetting the neutralization. Several rounds usually have to be made in order to minimize the induced currents. The neutralization is very effective if the gas is argon but not as effective with mercury. In addition to this, the primary currents are brought to equal amplitude by changing the biases on the power amplifiers. When these adjustments are satisfactory, the accelerator is ready to be run polyphase.

When the system is run polyphase a further series of adjustments must be made to bring the coil currents to equal value.

Because of the short running times (see Section 2.2.2.1) the tuning of the accelerator is a trial and error adjustment rather than a systematic adjustment. There are the following possible tuning (in the broad sense) variables:

1. Ten neutralizing transformers
2. Five power supply biases
3. Five tuning capacitors
4. Five phase-servo range changers

It was found that the phase-servo ranges (i.e., the range of phase correction over which they work), rarely had to be altered. One attempt was made to change the power supply bias during polyphase operation and the result was a broken channel wall. In practice the only workable system of equalizing the coil currents is the following: the accelerator is turned on polyphase and the currents noted; it is turned off and the biases adjusted and the accelerator turned on again and the currents noted, and so on until the currents are more or less equal. Sometimes it was found impossible to accomplish equalization for the biases no longer controlled the voltage output of the supply and the voltages were determined more by the mutual coupling. Data was taken whenever reasonable equalization was obtained.

2.2.2.1 Thermal Overload Problems

All the adjustments which have been discussed previously should be made during **continuous** polyphase operation since the plasma conditions (and hence the couplings) are considerably different than with single-phase operation. It is at this point where the most serious problems with the accelerator arose. This can most graphically be illustrated by the photograph of Figure 2-24. The cylinders shown in the figure are the outer vacuum wall of the accelerator. Numbers 1, 2, and 3 are made of Mullite (an Alumina-Silica ceramic) and number 4 is a 94 percent Alumina ceramic. All of these cylinders cracked during polyphase operation with mercury. None of these runs lasted more than five seconds. The break in cylinder No. 1 was accompanied by a break, at the same axial position, in the inner quartz vacuum wall. In order to protect the quartz tube, an alumina cylinder 2 inches in length was slipped over the quartz and was located between the nozzle tips and the quartz tube. At this time the mercury feed nozzles were long and admitted the mercury vapor about one-third of the way into the field coil. The remaining cylinders broke with shortened nozzles. The breaks in cylinders 2, 3 and 4 are at the end of the accelerator where the plasma exits and the breaks are just downstream of the last turn of the field coil. It is noted that the breaks occur at the same axial position within 1/4 inch.

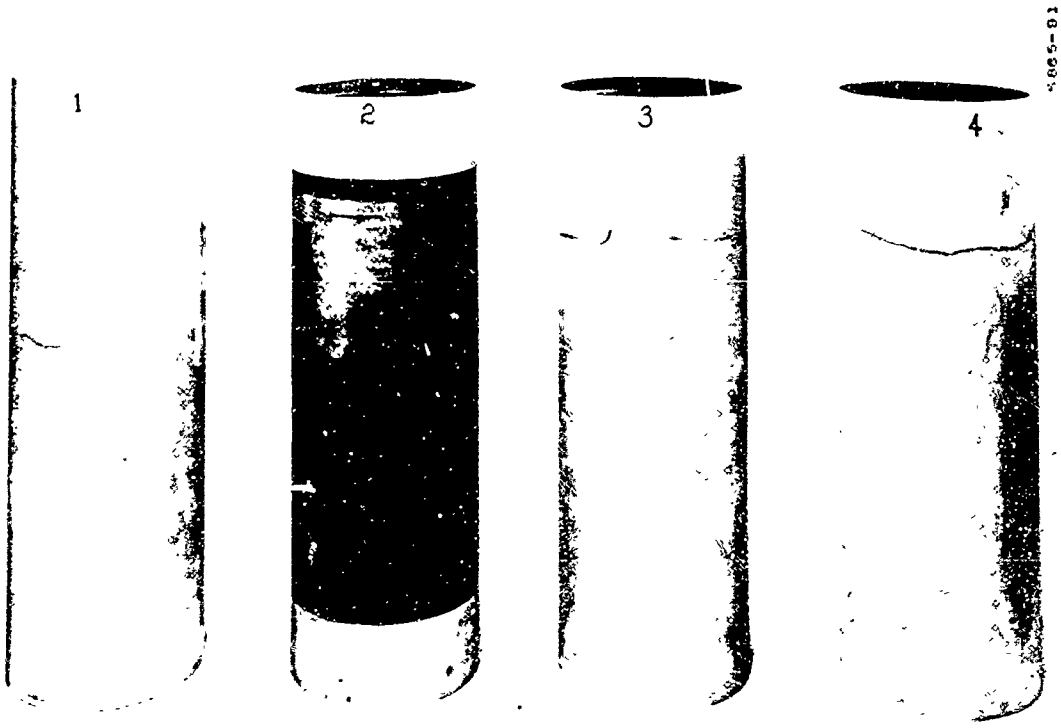

Figure 2-24. Broken Ceramic Vacuum Channels

Cylinder No. 4 was procured in the hope that the higher thermal conductivity of the Alumina (6 to 7 times higher) would alleviate the thermal problem but it broke after a 2.3 second run.

A consistent electrical characteristic of the accelerator was that the power supplies which excite the final two phases (those closest to the breaks) invariably together delivered about twice as much power as the sum of the other three sources. This is probably the immediate source of the high local thermal overload.

2.2.3 Experimental Results and Interpretations

This section presents the experimental results obtained during the contract period. The working gases were mercury, argon, and argon-seeded mercury. As mentioned previously, the double-coil flux probes constituted the principal plasma diagnostic tool.

The model of the plasma toroid is that of a simple ring current with associated self-flux. Figure 2-25 is a drawing of that model impacting upon the double-coil probe and it shows the expected output as a function of time. As noted in Section 1 the plasma toroids should occur every half-cycle of the rf (or at 480,000 cps). The alternate toroids should, in principle, be alike except that their currents should be reversed. Therefore, alternate coil signals, separated by a half-wave length, should be inverted. A speed measurement depends on the toroid interacting with both halves of the coil. Figure 2-26 is a series of sketches of the expected coil signal if the signals from the two sides of the coil are of equal amplitude. Each sketch represents a different toroid speed (therefore the different time delays of the signals). The solid lines of Figure 2-26 are the net outputs of the coil. The detailed shape and size of the actual flux probe signals is highly dependent on the relative orientation of the toroid and coil and also depends on the electrical characteristics of the probe circuit. However the general shape must be similar to that shown.

In order to derive a speed measurement from the search coil output (the resultant signal of Figure 2-26) it would be necessary to have an analytical model of a single coil signal that could be used with some degree of confidence. It can be seen from Figure 2-26 that the position on the resultant at which the transit time would be measured is highly dependent on the exact shape of the unsummed signals. Only a lower limit to the speed can be derived using the zero-crossing width of the output signal. These lower limits were found to be of the order of half the field speed.

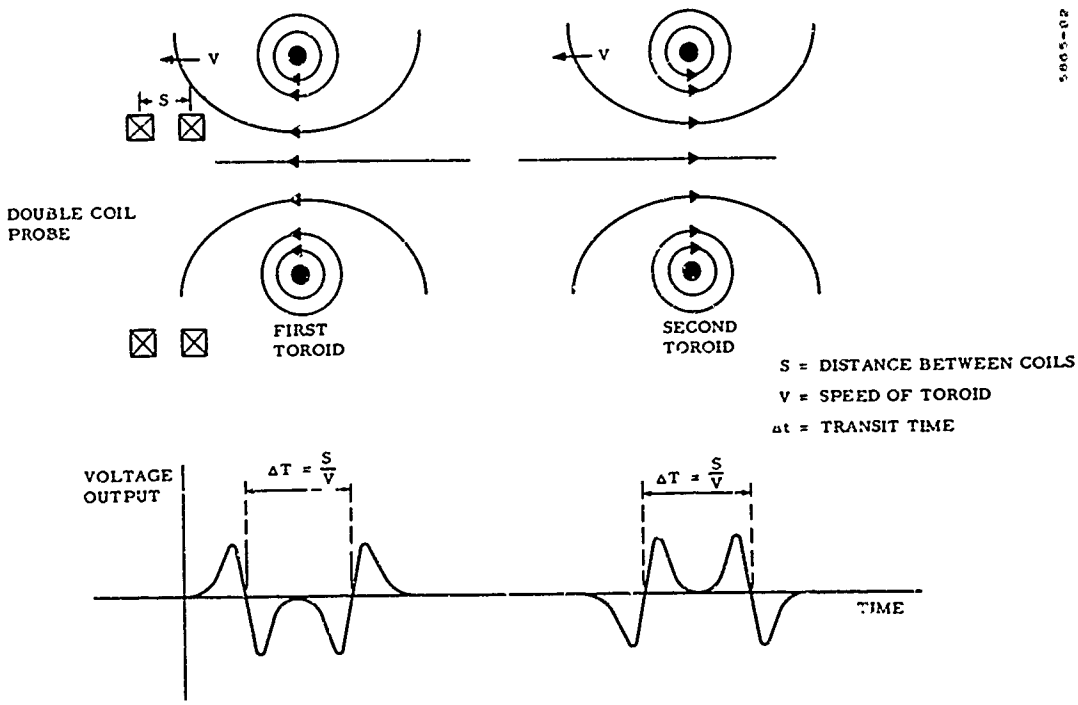

Figure 2-25. Ring Current Model

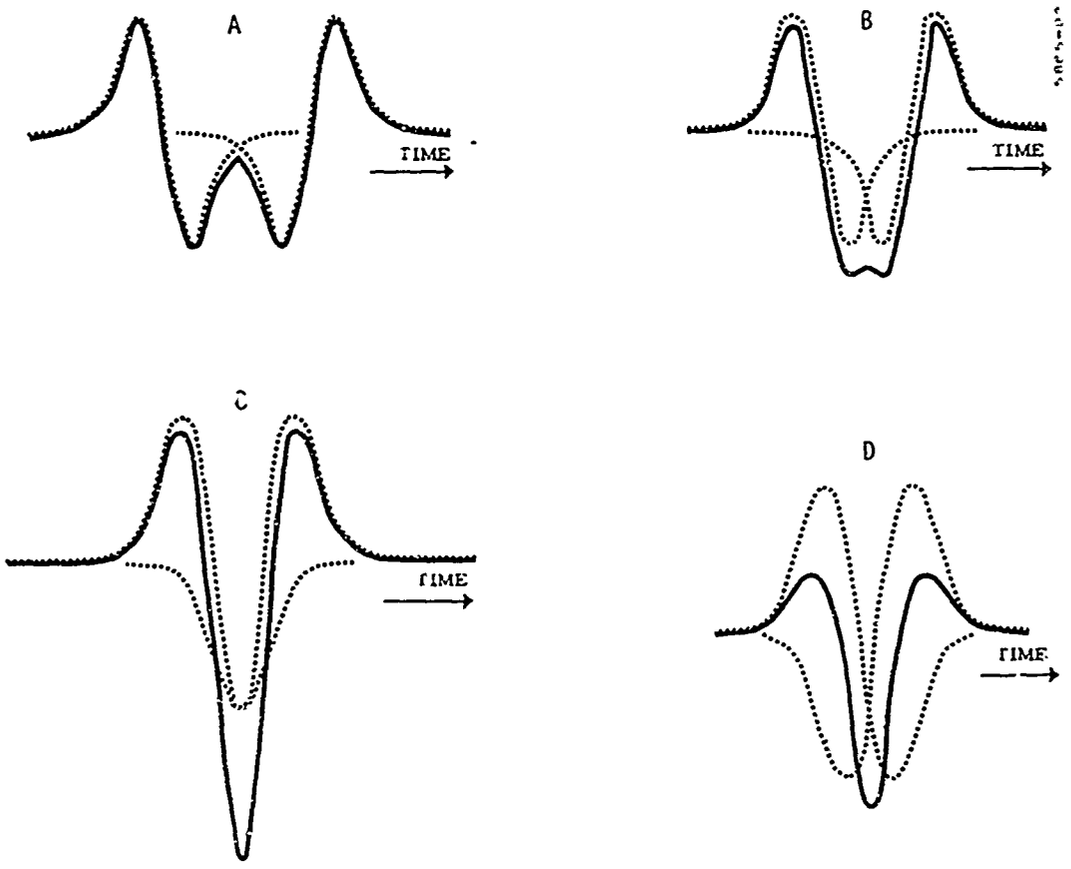

Figure 2-26. Resultant Search Coil Signals

2.2.3.1 Magnetic Flux Probe Oscillograms

The set of figures from Figure 2-27(a) to Figure 2-38 are oscillogram traces of the magnetic flux probe together with photographs of the remote control console. The console meters show the accelerator conditions during the run when the particular oscillogram was taken. The round-face meters on the console are the rf field coil currents. Immediately below them are the output tube plate current meters for the corresponding power supply, and below them are the grid current meters. Figure 2-27(a) is a photograph of the search coil signal with the field coils excited at 40 rms amperes but no plasma discharge. It is a typical signal under these conditions (approximately equal current amplitudes and correct phase relations). Figure 2-27(b) shows the standard source signals and the signals fed back from the pick up loop which monitors the phase of the field coil currents. The signal pip display is that described in Appendix J of 64-1340.

The flux probe traces shown in this document are a small sample of the many taken. The number showing significant features (relative to the ring-current model) are a small fraction of the total. Many of the traces showed no discernable features (a few are reproduced). Most of the oscillograms were obtained with a repetitive sweep and therefore show an average condition over many cycles of the rf. When single traces were taken on immediately succeeding runs (under closely similar conditions) it was clear that the previous picture was indeed an average. The single sweep generally showed that the interesting features did not repeat cycle-to-cycle with great regularity.

The sine wave accompanying the flux probe signal is a trace of the master oscillator and is always at 240 kc and it served as a time marker and as the scope trigger.

2.2.3.2 DC Voltage

The end-to-end dc voltage along the accelerator was measured with the probe of Figure 2-19.

No dc voltage ever appeared when the accelerator was run without plasma.

UPPER TRACE
MASTER OSCILLATOR

2-27(a)

LOWER TRACE
SEARCH COIL SIGNAL
AT 40 AMPS FIELD COIL
CURRENT - NO PLASMA
DISCHARGE

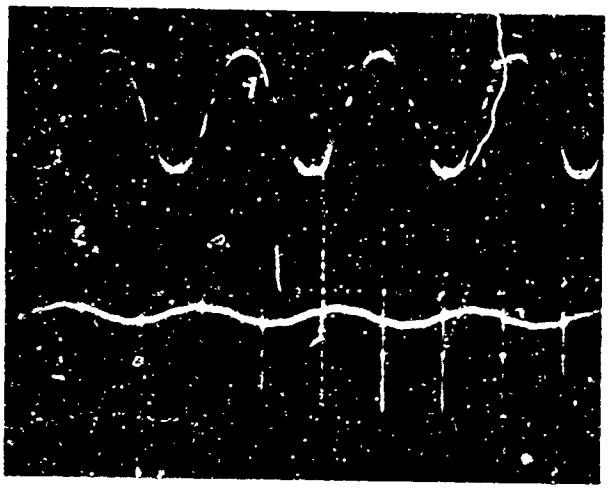

5885-94

UPPER TRACE
PHASES OF FIELD
COIL CURRENTS

2-27(b)

LOWER TRACE
STANDARD PHASES

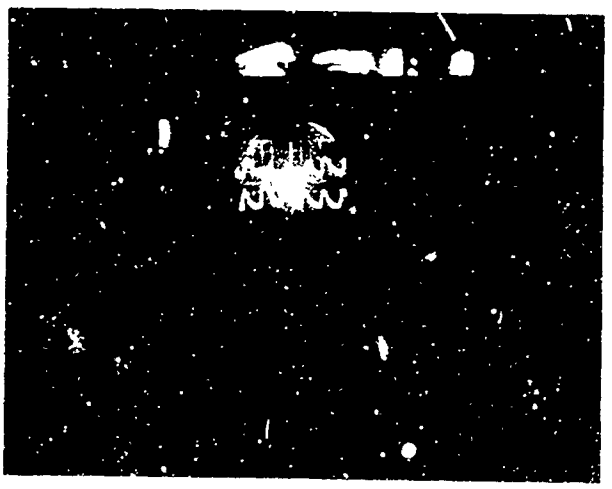

Figure 2-27. Oscilloscope Display

SINGLE SWEEP

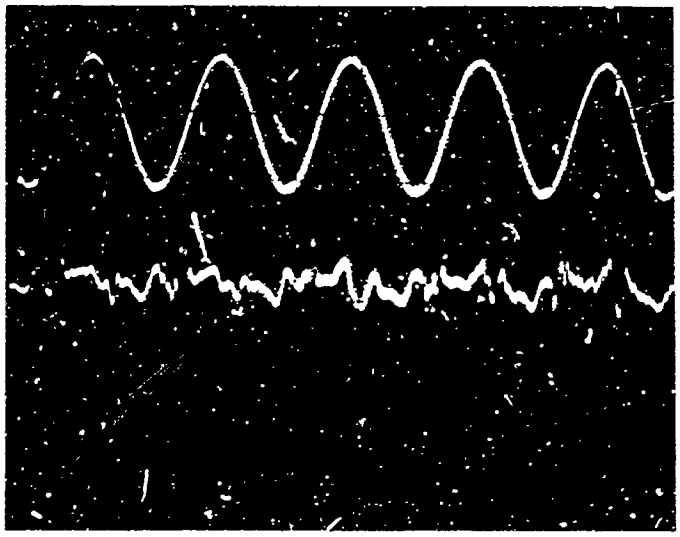

5885-95

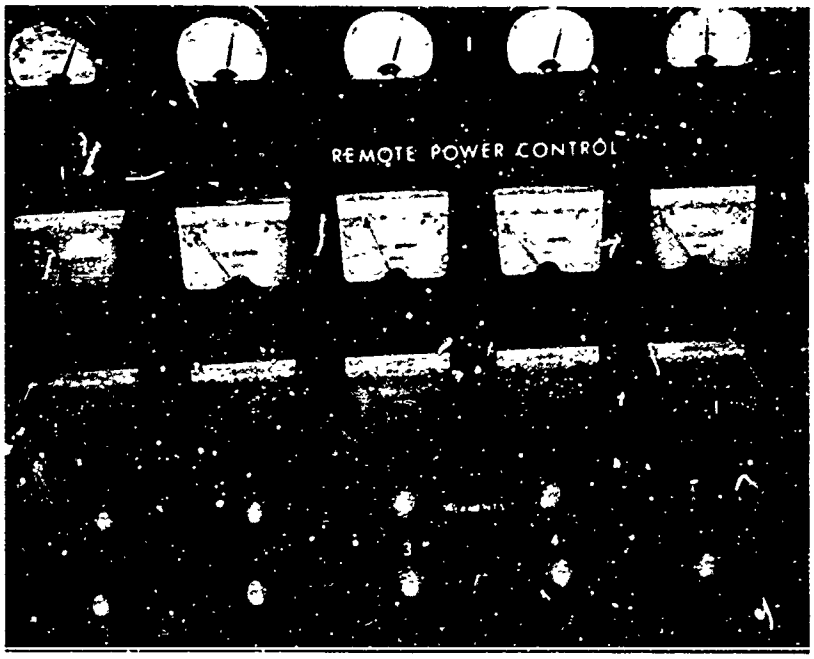

Figure 2-28. Probe Trace, Mercury

SINGLE SWEEP

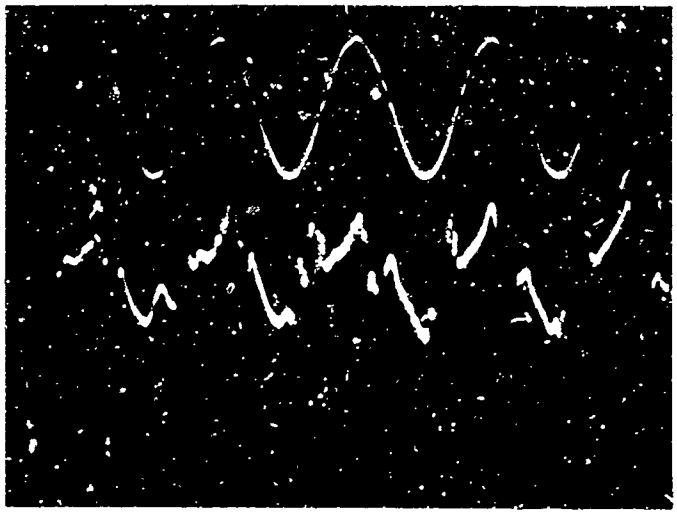

5885-98

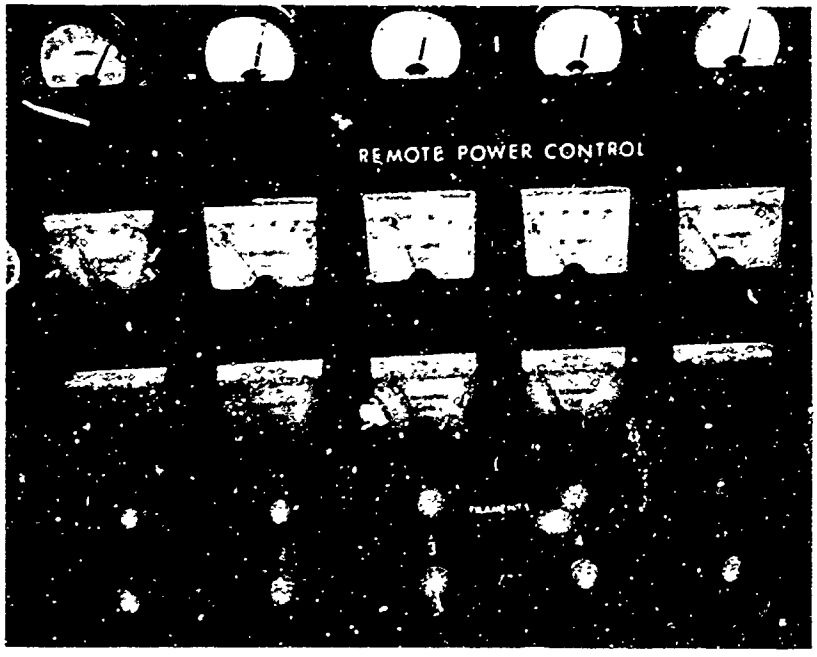

Figure 2-29. Probe Trace, Mercury

SMALL COIL

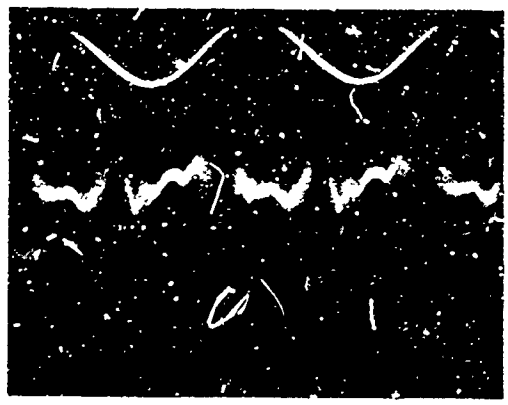

LARGE COIL

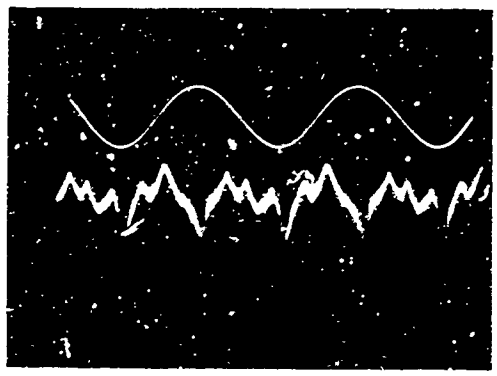

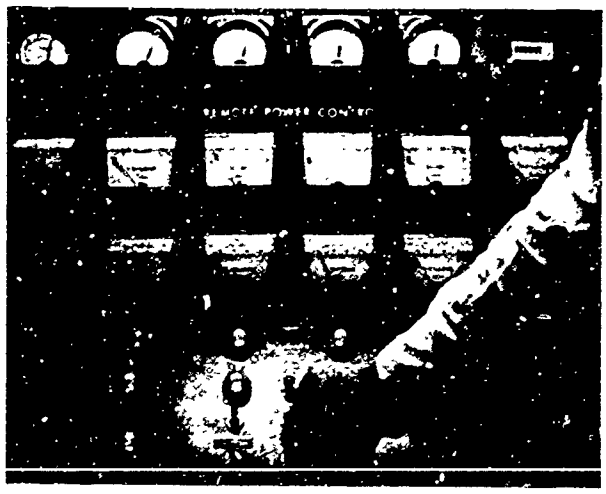

SIMULTANEOUS FLUX MEASURENT WITH TWO SEARCH COILS

Figure 2-30. Probe Trace, Mercury

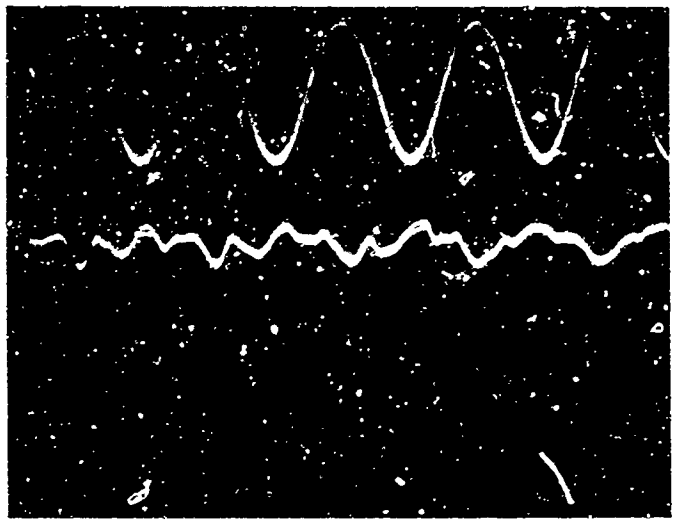

5865-98

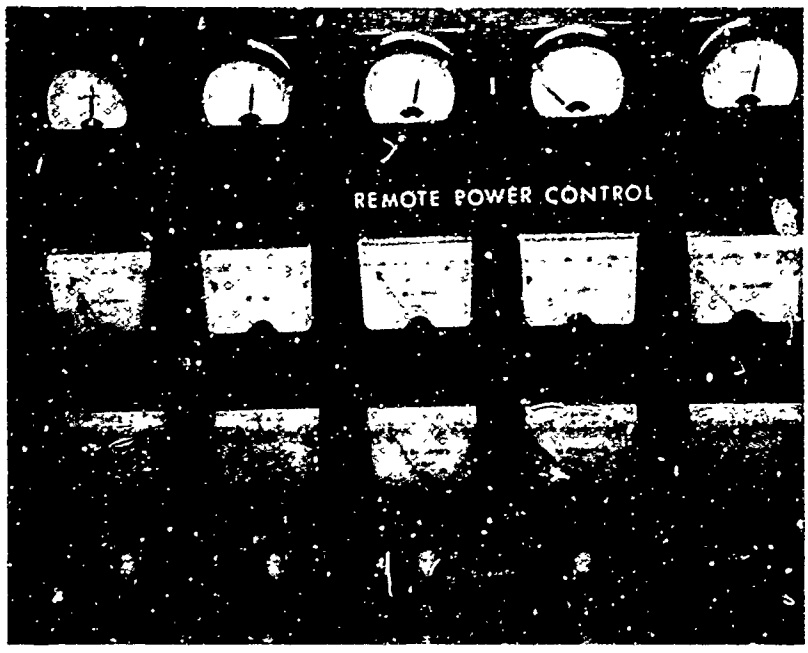

NOTE: ONE POWER SUPPLY AND CORRESPONDING PHASE OUT. COMPARE WITH FIG. 2-32 FOLLOWING.

Figure 2-31. Probe Trace, Argon

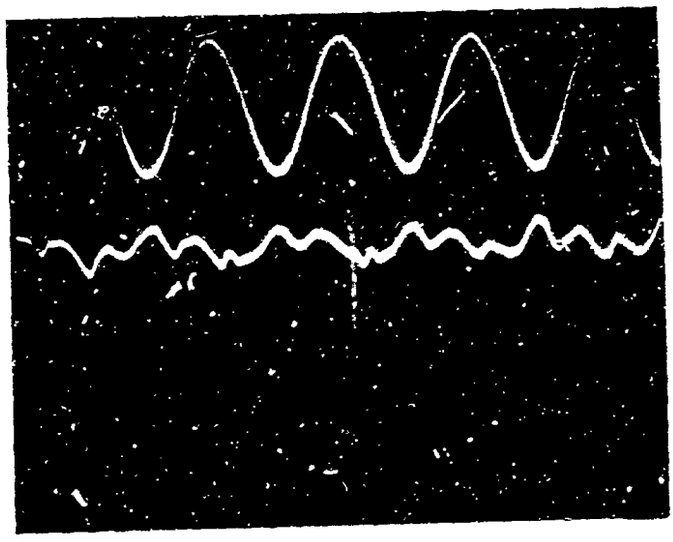

5885-77

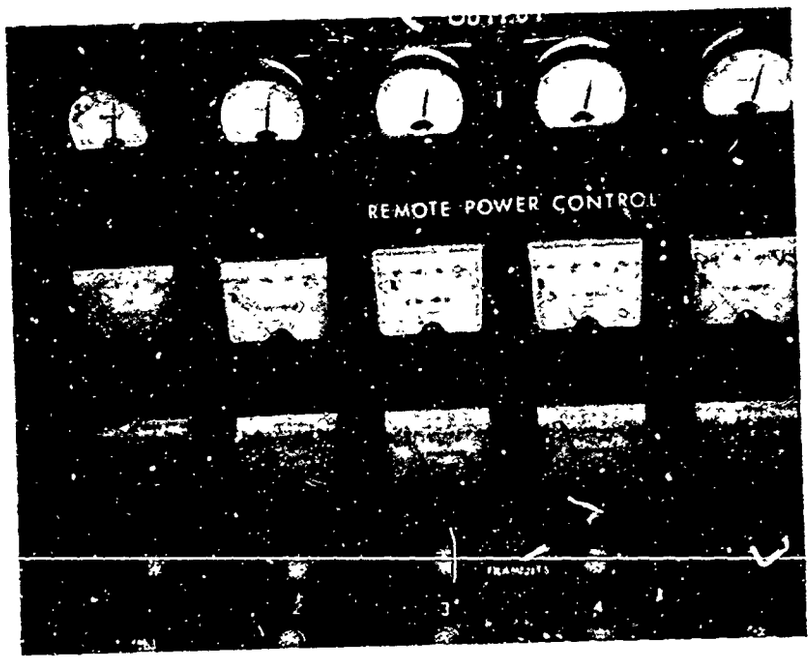

Figure 2-32. Probe Trace, Argon

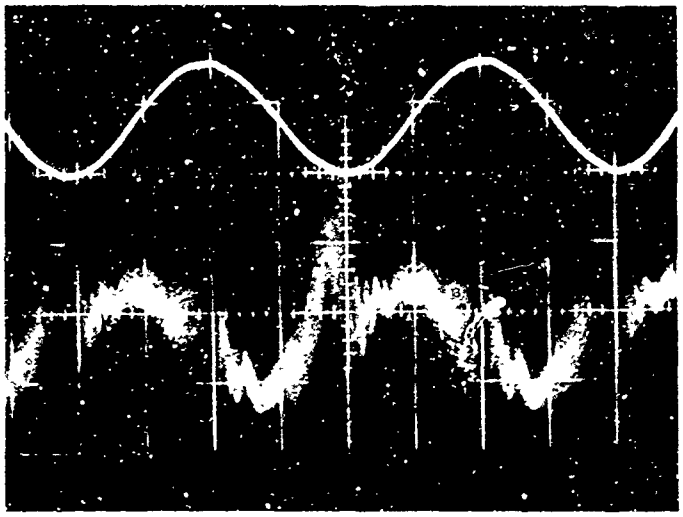

5885-99

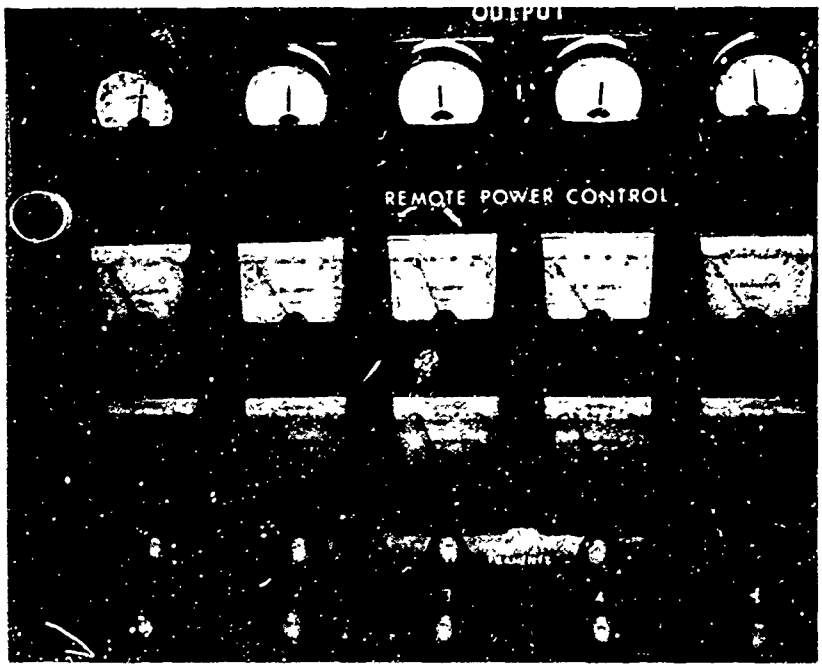

Figure 2-33. Probe Trace, Mercury-Argon

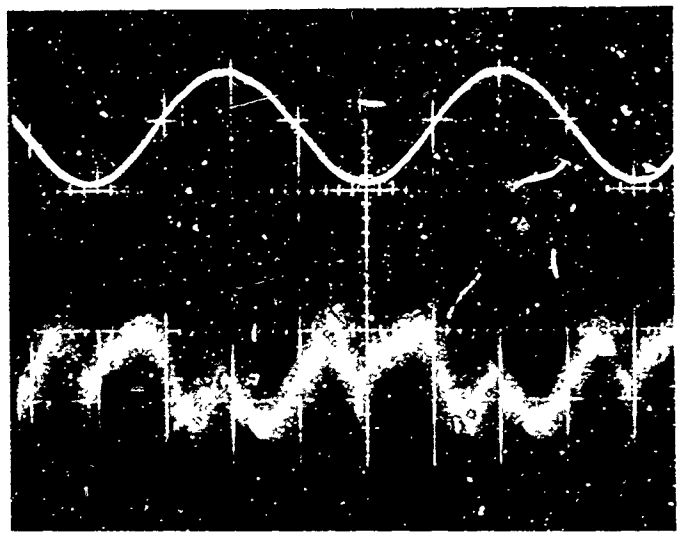

5865-100

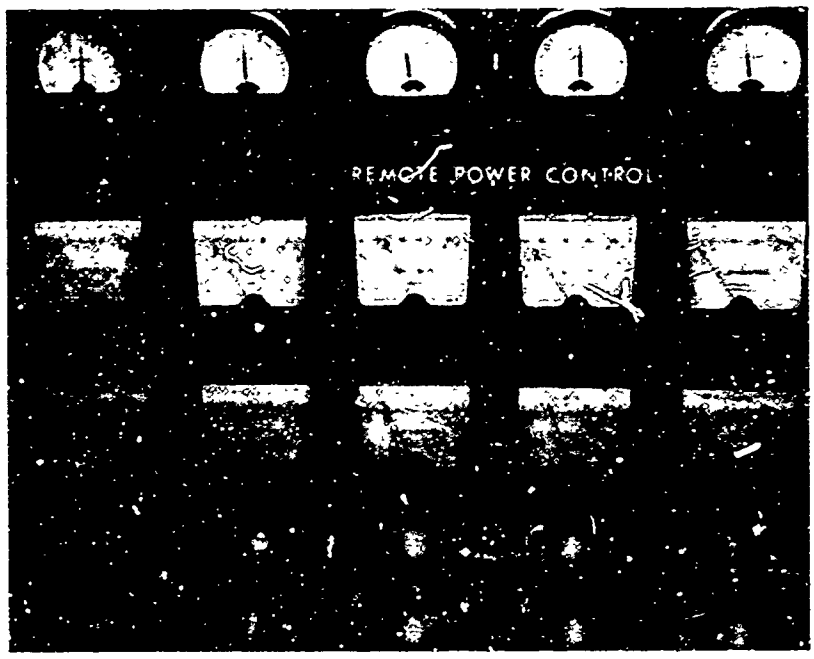

Figure 2-34. Probe Trace, Mercury-Argon

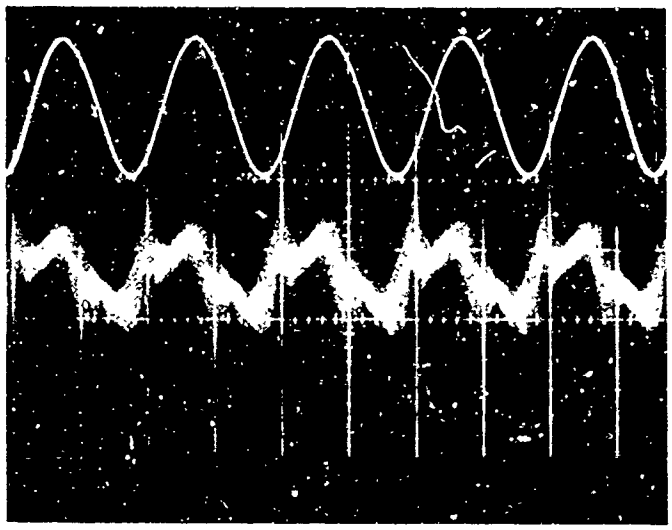

5865-101

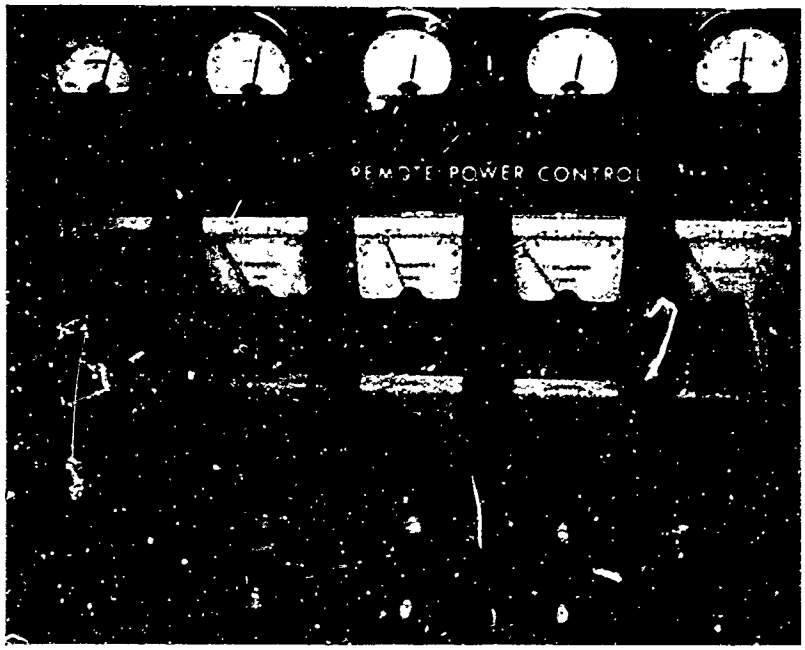

Figure 2-35. Probe Trace, Mercury-Argon

OSCILLOGRAM
REPETITIVE SWEEP

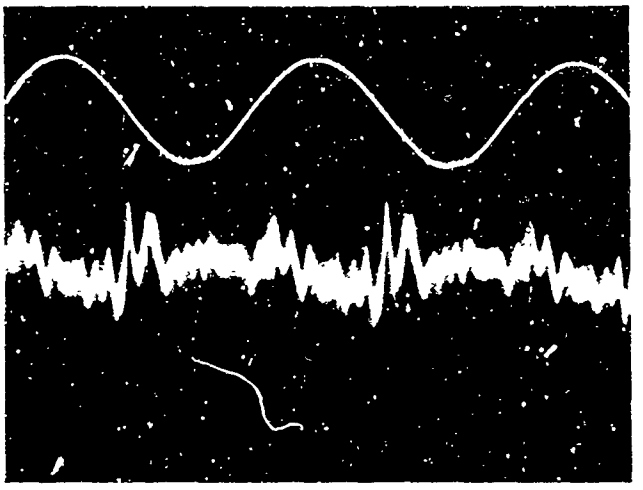

5865-102

(COIL CURRENTS = 32 AMPS)

OSCILLOGRAM
SINGLE SWEEP ON
FOLLOWING RUN

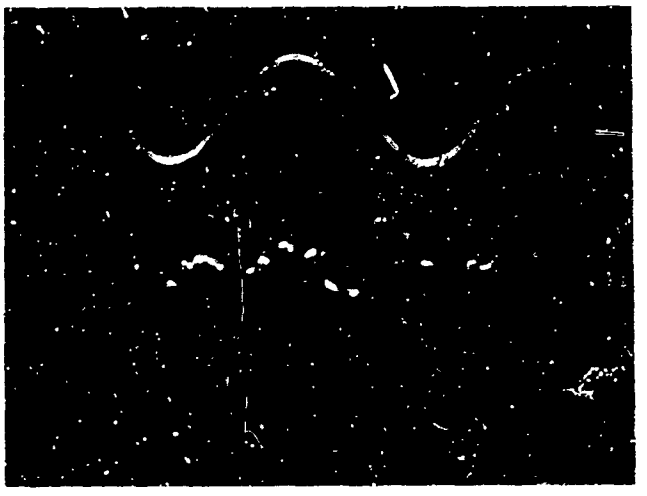

Figure 2-36. Probe Trace, Mercury-Argon

SINGLE SWEEP

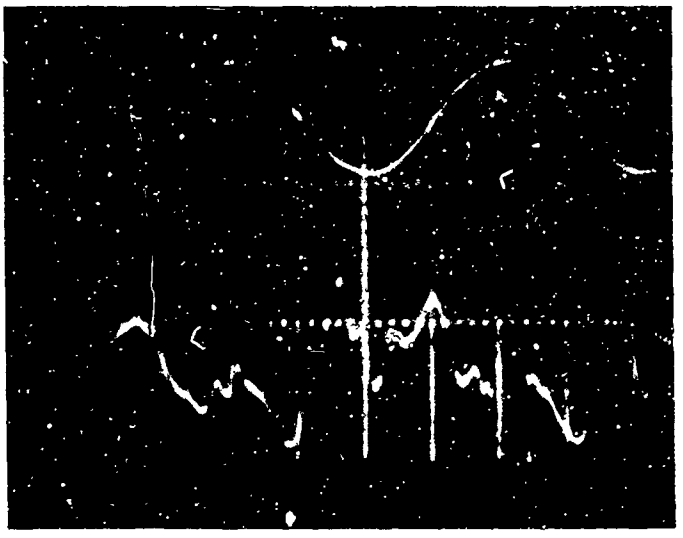

5865-103

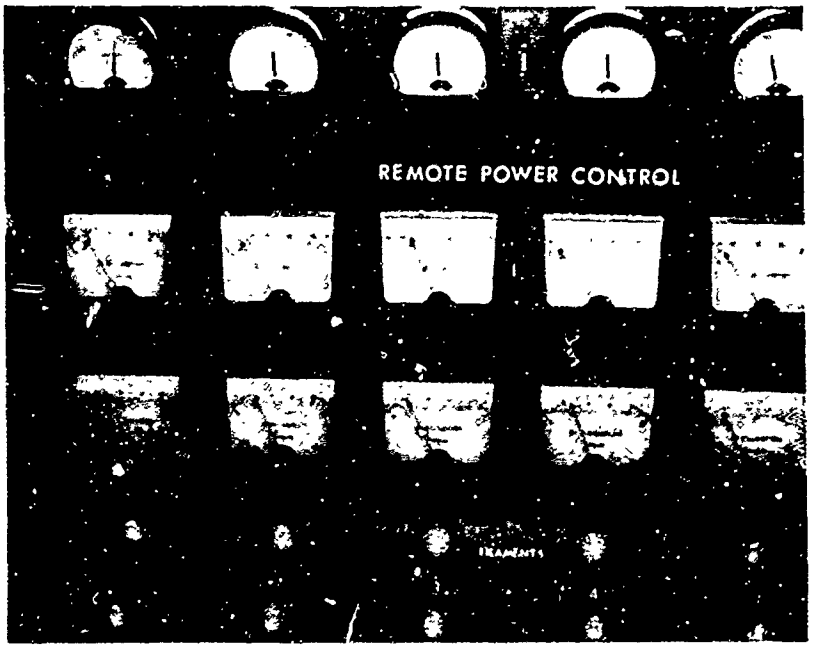

Figure 2-37. Probe Trace, Mercury-Argon

BLOCKER OUT

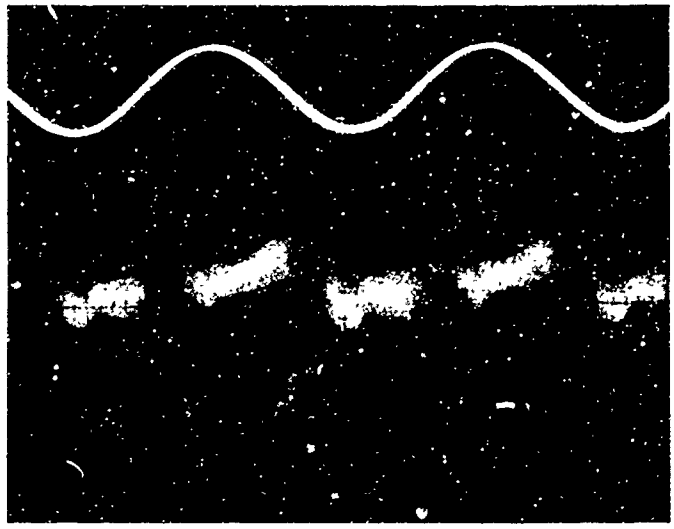

5865-104

BLOCKER IN

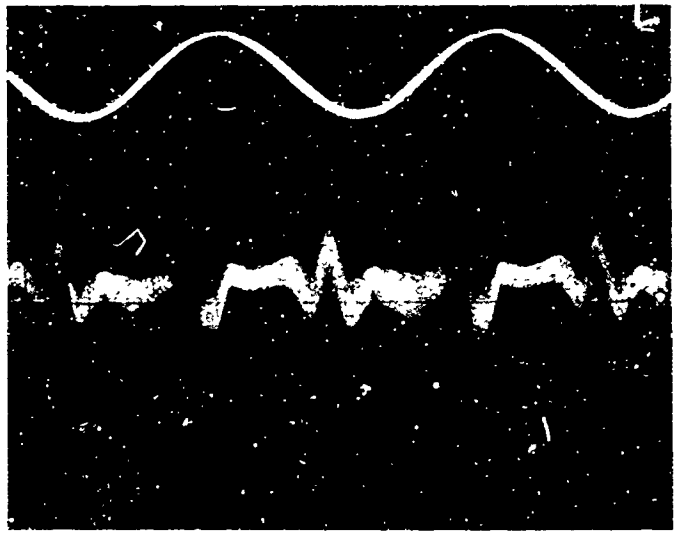

NOTE: FLUX PROBE SHIELDED ELECTROSTATICALLY

Figure 2-38. Effect of Blocker on Probe Signal

The graph of Figure 2-40 shows a correlation between field coil current and dc voltage when argon-seeded mercury was the working gas. (There is not enough data with mercury alone to look for such a correlation.) The graph was obtained by averaging all observed results at chosen values of coil current (the current is the average over the five phases). Some points were excluded because the coil currents differed greatly. The voltage was always positive with respect to ground (the exit end of the accelerator). Therefore this voltage is of the correct polarity to accelerate ions towards the exit of the accelerator.

Some rather puzzling results occurred when argon alone was used. The argon was usually fed into the vacuum tank which is at the exit end of the accelerator and the voltage developed was always negative with respect to ground. Negative voltages as high as -2000v were observed under this condition, though usually the voltage was under -300v. When the voltages were first measured only small negative voltages appeared but at the end of the research period large negative voltages were quite frequent. It is not known why this happened. The argon feed was changed to allow some argon to enter the nozzles at the end of the accelerator where the mercury vapor was usually admitted. When argon was admitted through the nozzles the dc voltage rose to +200 volts but the power supplies continually blew circuit breakers so very little data is available. It was later demonstrated that by feeding argon both into the vacuum tank and into the nozzle space (but not through the nozzles), the voltage was much less negative (~ -300v) than feeding it into the vacuum tank alone (~ -1500v).

The probe measures the net dc voltage down the accelerator and does not measure the axial voltage distribution. The peak voltages inside the accelerator may be much higher.

The relation shown in Figure 2-40 can be used to speculate about the operation of the accelerator. The Mark II was built to produce a slingshot effect (i.e., toroids exiting at up to twice the field speed). The depth of the inductive potential (V^L) well (see Section 4.1.2 of 64-1340) must be at least equal to the ion energy at the exiting velocity and the depth depends on the coil current, I, through the relation

$$V^L \propto \Phi^2 \propto I^2$$

where Φ is the magnetic flux.

The relation between the dc voltage (V_{DC}) and coil current has a shape which suggests an equation

$$V_{DC} = 0.5\, I^2$$

where a rough fit to a parabolic form was made. If we assume that the ions exit at energies given by V_{DC} we can calculate the coil currents needed to produce a slingshot effect in mercury. This amounts to about 150 rms amps which is about three times more current than the present design would allow, or 75 rms amps if the ions were to just come up to the field speed.

2.2.3.3 Optical Spectroscopy

A number of plates of the mercury plasma discharge at the exit end of the Mark II were taken. One of the plates is reproduced in Figure 2-41. In no plate is there evidence of Hg II. The exposure times were <3 seconds. The identified lines are Hg I, H_α and H_β. The slit length was 8 mm and the width was 0.1 mm.

2.2.3.4 Light Pulsation Detector

None of these traces are presented in this report. It was proved that the time-dependant signal output was completely due to stray effects.

2.2.3.5 Electrostatic Probes

Figure 2-39 shows typical electrostatic probe signals. They exhibit no significant patterns.

2.2.3.6 An Interesting Incident

During one of the final runs made with the Mark II an interesting incident occurred which may shed some light on the accelerator performance.

The accelerator was running at an input power level of about 90 KW (20 KW of this are circuit losses), with an argon-seeded mercury plasma. The discharged changed suddenly. The pips in the search coil signal disappeared and the dc voltage fell from +800 to +200 volts. Afterwards

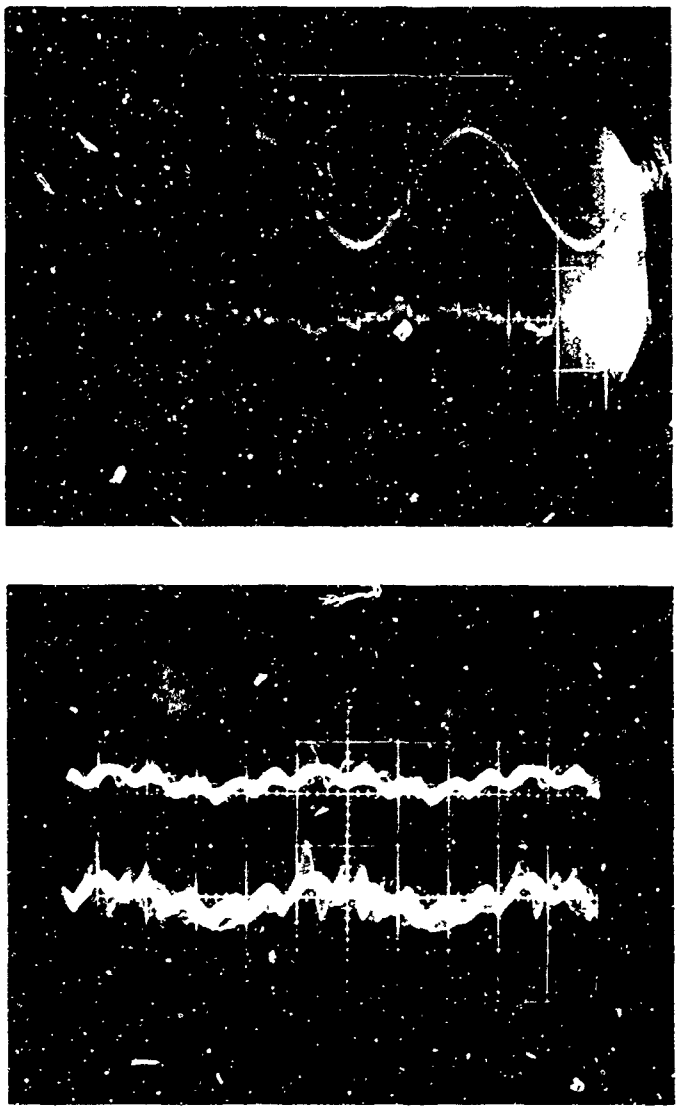

5865-105

Figure 2-39. Electrostatic Probe Traces

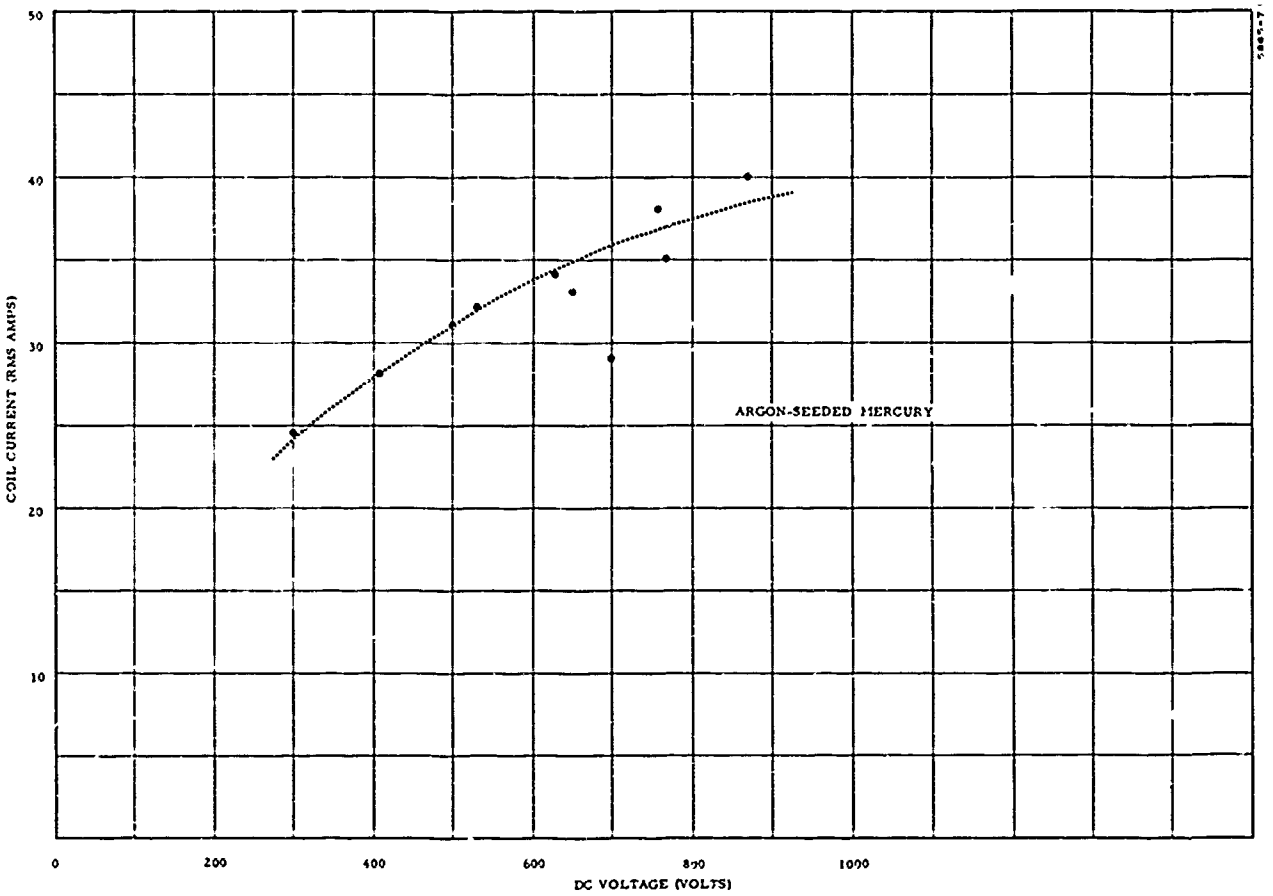

Figure 2-40. Relation of DC Voltage to Coil Current

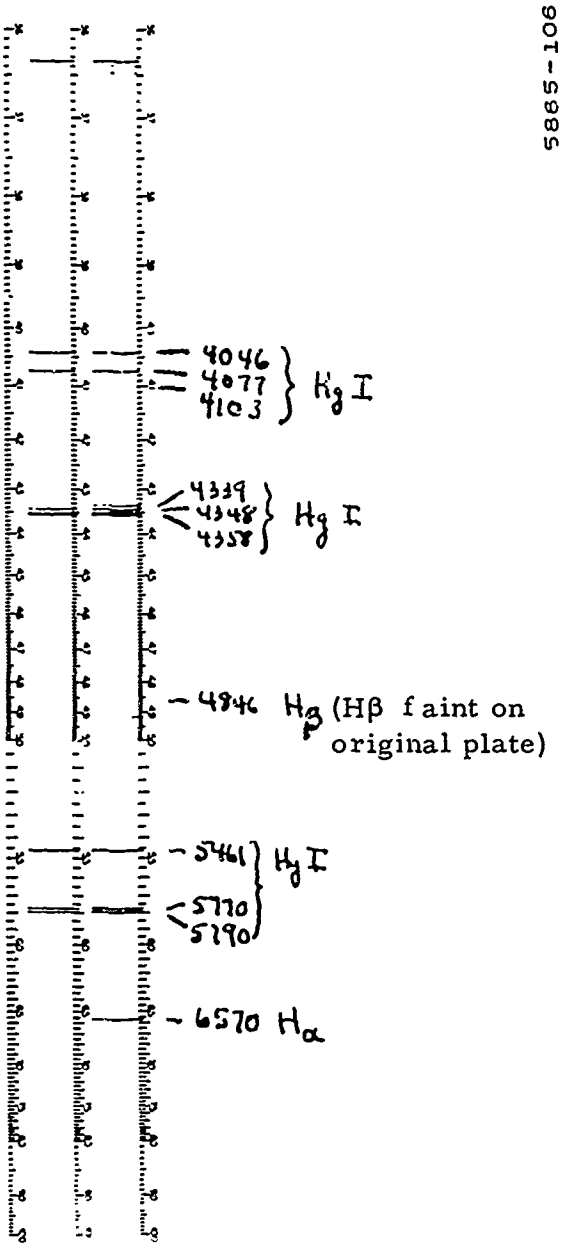

Figure 2-41. Spectrogram of Mark II Discharge

it was discovered that the alumina shield (see Section 2.2.2.1) on the inner quartz wall had broken and fallen into the annular channel but not in a position such as to distort the mercury vapor flow from the nozzles.

It is in this section of the accelerator that the electron avalanche must occur which initiates the formation of pinched currents. The broken ceramic would act like the blocking probe in that it would interrupt azimuthal currents. The effect of the blocking probe at the exit of the accelerator was pronounced but not definitive (Figure 2-38). The effect of the accidental "blocker" at the nozzle end was unmistakeable.

3. SUMMARY AND CONCLUSIONS

The early research conducted with the Mark I accelerator, and the subsequent development of the inductive potential concept applied to the motion of charged particles in a traveling wave magnetic field, made it possible to consider a device which would continuously form and accelerate plasma toroids into a region of free space where their behavior and properties could be studied.

The development of this device, the Mark II accelerator, has taken place over a period of several years but it cannot be said to have reached its design goal. The theory behind the accelerator and many of the techniques developed for the accelerator have proven fruitful when applied to various other programs.*

The major obstacle to the successful operation of the Mark II has been the wall thermal problem which limited the experimental runs to a few seconds. The tuning and neutralizing adjustments which were developed to correct for the results of the reaction of the discharge on the circuits producing the traveling field could not be properly applied because the operating time necessary to make them was not available. This made it impossible to pursue a systematic study either of the operation of the accelerator or the discharge phenomena; the two are tightly coupled. If the Mark II were performing according to its basic concept, that is as a device in which transient processes were dominant. the excessive Joule heating and thermal shock would not exist. This is clearly not the case in the experiments.

*An example of this is a slip-type traveling wave accelerator, investigated as a re-entry simulator for AFFDL, (RTD), AFSC. This device utilizes the neutralizing transformers and high-voltage polyphase electrical design methods employed in the Mark II.

The production of outgoing toroids depends on a three-step process. First the electron avalanche must occur in a fraction of an rf cycle, second the electron current must increase at a rate fast enough for the pinch forces to develop before the current is destroyed by Joule heating, and third the pinched current must be accelerated out of the machine. Even an accelerator without the thermal shock problem and with the best traveling wave capable of being produced might not operate successfully because of the non-occurence of the fast initial step in the formation process.

It can be inferred from the search coil study that outcoming plasma currents have been found in the Mark II. Their occurrence is random and apparently uncorrelated with the field coil strength. At best the process was marginal. The relation derived from the experimentally observed correlation between accelerator coil current and Hall voltage suggests that about three times the present operating coil current is required to produce the effects predicted for the Mark II. That is to say, a polyphase rf system capable of handling up to 200 rms amperes would be needed. This would require a completely different circuit design than presently exists in the Mark II accelerator.

This report brings to a close the work on the Mark II accelerator. It is now clear that the initial objective of the work - the attainment of a steady stream of high-speed pinched plasma toroids - is not attainable with the existing apparatus. This results in spite of a long and arduous effort. Evidence has been obtained which indicates that the performance of the accelerator falls short of the mark by several factors of two in the strength of the magnetic field. In addition, severe limitations were found to occur from the materials available for construction of the channel walls.

It is important to recognize that the conclusions of this work in no way bear on the prospects for other types of electromagnetic accelerators which do not require the generation of highly localized plasma structures with attendant operation which departs greatly from steady state. Indeed, this laboratory has recently experienced a significant advance in the operation and control of a traveling wave accelerator of the slip-type; and, in addition, the prospects for a plasma propulsor of the fringe-field variety appear bright.

NOTE: Work on the Mark II accelerator was continued past the end of the contract period under Litton sponsorship. Since the results of this work were available at the time of final printing of this report they have been included (Appendix B) for the sake of completeness.

APPENDIX A

FRINGE FIELD INVESTIGATION

1. INTRODUCTION

The purpose of this appendix is twofold:

1. To investigate the effects due to amplitude and phase disturbances resulting from the fringe fields associated with a finite length $J \times B$ accelerator; and
2. To investigate a method for modifying (tailoring) the magnetic field so as to reduce the undesirable fringing field behavior to an acceptable level.

The electromagnetic field region at the entrance and exit of the acceleration channel is a region in which variations in both field velocity and magnetic flux amplitude are encountered. These variations result in detrimental deceleration and joule heating of the test gas as it enters and leaves the acceleration channel.

The end field or fringe field region may be considered as consisting of the coherent superposition of two fields, a fringe field having a field velocity that is considerably greater than the field velocity in the accelerator channel, and a standing wave field having a field velocity that is zero. The standing wave will produce a deceleration of the gas because the gas velocity exceeds the wave velocity. The fringe field will produce an excessive joule heating of the gas since the gas velocity is less than $\gamma-1/\gamma$ times the field velocity.[6] Both fields will produce joule heating because of the axial variations in magnetic flux intensity.

For purposes of analysis, the vacuum electromagnetic field at one end of an accelerator of semi-infinite length is considered.

2. THEORETICAL FORMULATION

Consider the field produced by an axially symmetric current, composed of current filaments, traveling in the +Z direction. The vector potential A_ϕ for a current filament can be written as[1]

$$A_\phi = \frac{\mu R}{4\pi} \int J(Z_o)\, dZ_o \int_0^{2\pi} \frac{\cos\phi\, d\phi}{\left[r^2 + R^2 - 2Rr\cos\phi + (Z - Z_o)^2\right]^{1/2}} \quad (1)$$

where R is the radius of the cylinder of the current sheet (refer to Figure A-1).*

$$J_\phi \equiv J(Z_o)\, \delta(r_o - R) \quad (2)$$

Now defining

$$\alpha = r/R$$

$$\beta = Z/R$$

$$\beta_o = Z_o/R$$

Eq. (1) becomes

$$A_\phi = \frac{\mu R}{4\pi} \int J(\beta_o)\, d\beta_o \int_0^{2\pi} \frac{\cos\phi\, d\phi}{\left[1 + \alpha^2 - 2\alpha\cos\phi + (\beta - \beta_o)^2\right]^{1/2}}$$

If we change variables, letting $\theta = \phi/2$ and utilize the trigonometric identity $\cos\phi = 2\cos^2\phi/2 - 1$

$$A_\phi = \frac{\mu R}{2\pi} \int \frac{J(\beta_o)\, d\beta_o\, \zeta}{2\sqrt{\alpha}} \int_0^{\pi} \frac{(2\cos^2\theta - 1)\, d\theta}{\left(1 - \zeta^2\cos^2\theta\right)^{1/2}} \quad (3)$$

*MKS units are employed throughout this appendix.

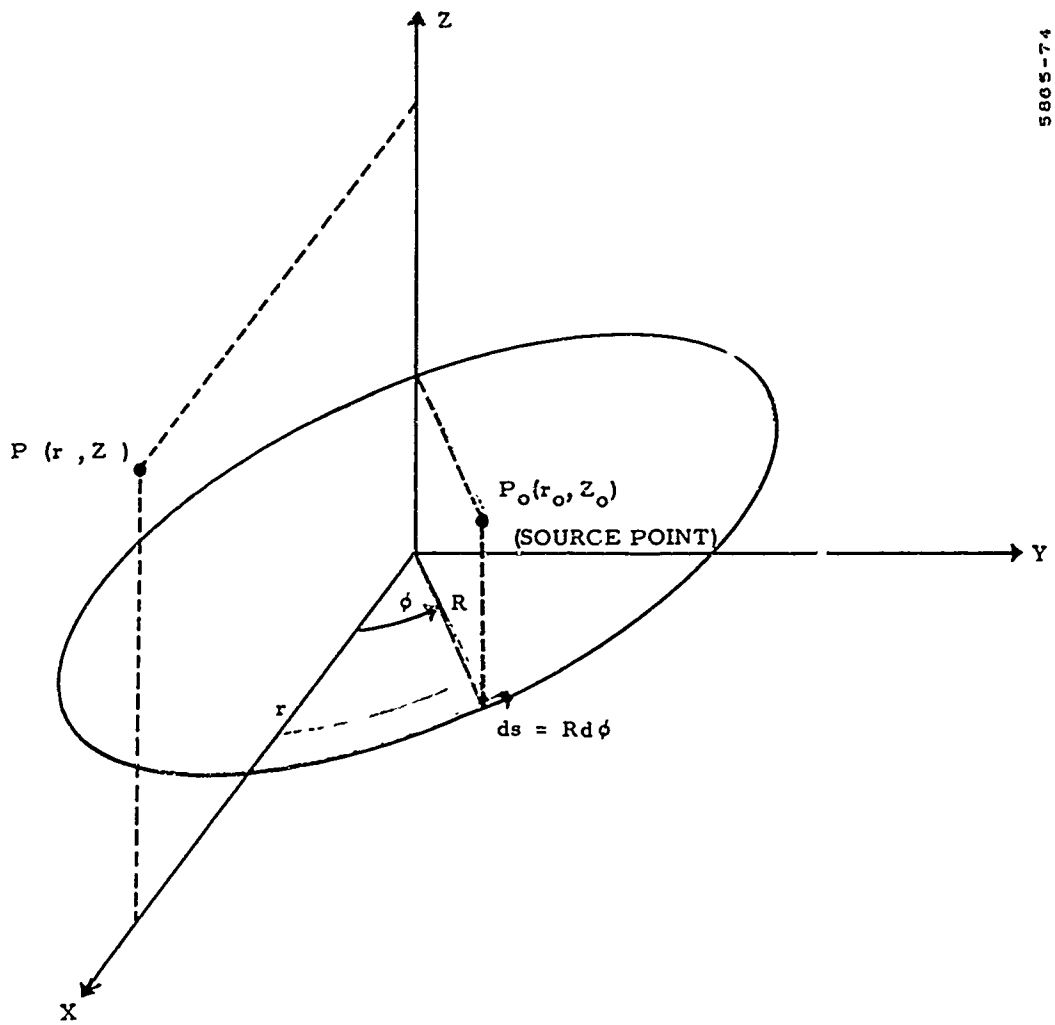

Figure A-1. Coordinate System

where

$$\zeta^2 \equiv \frac{4a}{(1 + a)^2 + (\beta - \beta_o)^2}$$

Let $\theta = \pi/2 - \phi$ and Eq. (3) may be written as

$$A_\phi = \frac{\mu R}{\pi} \int \frac{\zeta J(\beta_o)}{2\sqrt{a}} d\beta_o \int_0^{\pi/2} \frac{-1 + 2\sin^2\phi}{\sqrt{1 - \zeta^2 \sin^2\phi}} d\phi \tag{4}$$

The second integral in Eq. (4) is an elliptic integral and may be evaluated by using the following relation from Jahnke and Emde[2]

$$-K + 2D = \zeta^2 C(\zeta) \tag{5}$$

where $K(\zeta)$ and $D(\zeta)$ are the complete elliptic integrals of the first and second kinds, respectively. The superposition of contributions from all current loops is expressed as

$$A_\phi = \frac{\mu R}{2\pi} \int_{-\infty}^{\infty} J(\beta_o)\, S(a, \beta - \beta_o)\, d\beta_o \tag{6}$$

where

$$S(a, \beta - \beta_o) \equiv \frac{\zeta^3}{\sqrt{a}} C(\zeta) \tag{6a}$$

The parameters ζ and S are plotted as a function of $\beta - \beta_o$, for two a's in Figures A-2 and A-3, respectively. The significance and applicability of these curves will discussed later.

The mutual inductance between the current filament and a similar one of radius r located at z is

$$M = \mu r\, S(a, \beta - \beta_o) \tag{7}$$

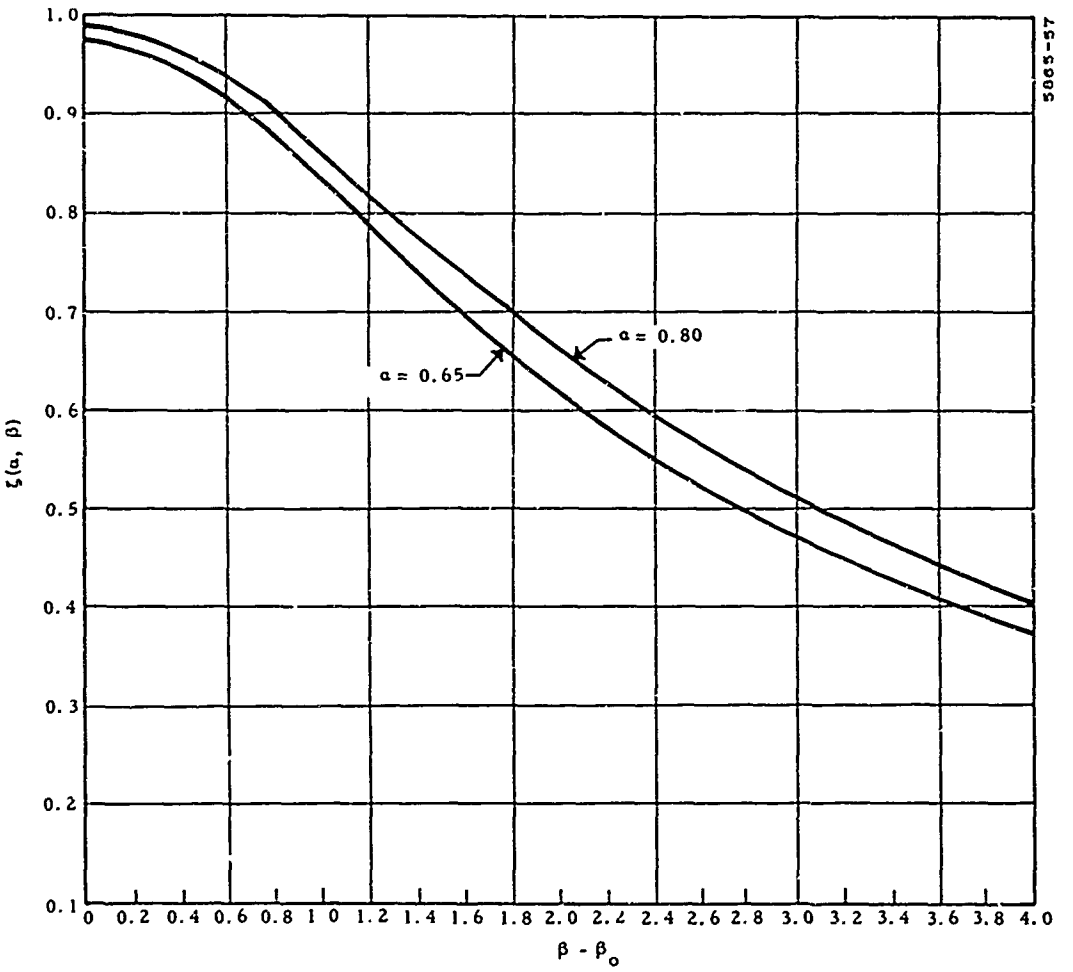

Figure A-2. ζ versus $\beta - \beta_o$

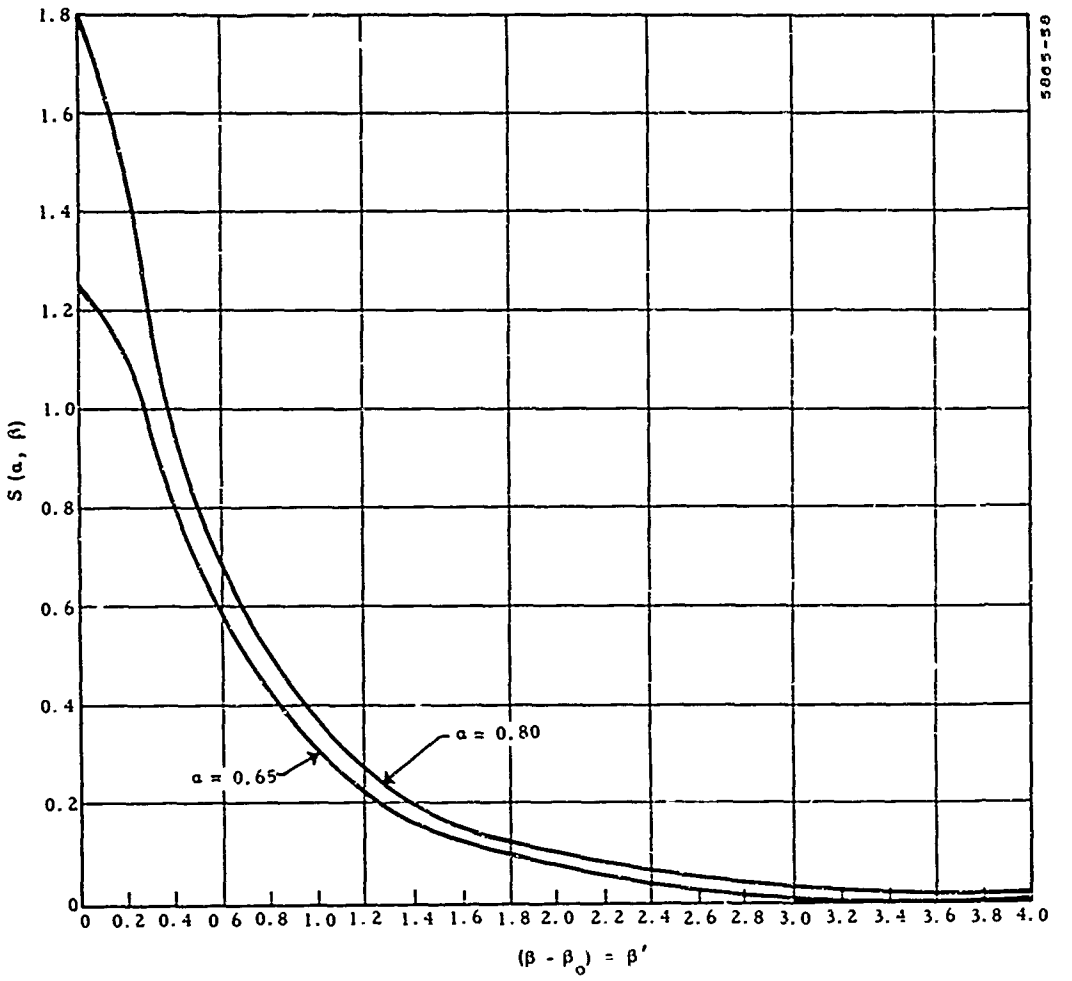

Figure A-3. S versus $\beta - \beta_o$

which can be derived recalling that the magnetic flux Φ is given by

$$\Phi = MI$$

or

$$\Phi = 2\pi\ rA$$

Values for M are tabulated in Grover.[3]

In general the magnetic field components are

$$B_r = -\frac{\partial A}{\partial z} \tag{8}$$

$$B_z = \frac{1}{r}\frac{\partial rA}{\partial r} \tag{9}$$

and the magnetic flux, Φ is

$$\Phi \equiv 2\pi \int_0^r rB_z\, dr = 2\pi rA \tag{10}$$

Now let

$$J(\beta_o) = J_o \cos(\omega t - \delta z_o/R)$$

where $kR = \delta$ and $-L \le z_o \le 0$ which defines the current sheet length.

Eq. (6) may be expressed as

$$A_\phi = \frac{\mu R J_o}{2\pi} \int_{-L/R}^{0} \cos(\omega t - \delta\beta_o)\, S\left[a,\ (\beta - \beta_o)\right] d\beta_o \tag{11}$$

If $\beta - \beta_o$ is now replaced with β' throughout the above equation, the result is

$$A_\phi = \frac{\mu R J_o}{2\pi}\left[\cos(\omega t - \delta\beta)\int_{\beta'=\beta+z/R}^{\beta'=\beta+L/R} S(\alpha, \beta')\cos\delta\beta' d\beta' - \sin(\omega t - \delta\beta)\int_{\beta'=\beta}^{\beta'=\beta+L/R} S(\alpha, \beta')\sin\delta\beta' d\beta'\right] \tag{12}$$

For $-4 \le \beta' \le 4$ and $L/R > 8$ we can set the upper limit $(\to\infty)$. The validity of using the above values as limits can be seen from Figure A-3 where the function S has fallen to a few percent of its original value at $\beta = \pm 4$. The asymptotic values were determined by expanding $S(\alpha, \beta)$, Eq. (6a), in a series (see Jahnke and Emde[2]) as a function of ζ^2 where $\zeta^2 \ll 1$. It was found that the ζ^6 term contributed less than 1 percent.

Let

$$C_S \equiv \int_\beta^\infty S(\alpha, \beta')\cos\delta\beta' d\beta'$$

$$S_S \equiv \int_\beta^\infty S(\alpha, \beta')\sin\delta\beta' d\beta' \tag{13}$$

then Eq. (12) becomes

$$A_\phi = \frac{\mu J_o R}{2\pi}\left\{\left[C_S(\alpha, \beta, \delta) - C_S(\alpha, \beta+\frac{L}{R}, \delta)\right]\cos(\omega t - \delta\beta) - \left[S_S(\alpha, \beta, \delta) - S_S(\alpha, \beta+\frac{L}{R}, \delta)\right]\sin(\omega t - \delta\beta)\right\} \tag{14}$$

This expression contains a contribution from each end of the current sheet. In general if $L/R > 5$ the two contributions will not overlap and interact with each other. Assuming this and defining

$$\bar{A}_o(\alpha, \beta, \delta) \equiv \left[C_S(\alpha, \beta, \delta)^2 + S_S(\alpha, \beta, \delta)^2\right]^{1/2}$$

$$\theta(\alpha, \beta, \delta) \equiv \tan^{-1} \frac{S_S(\alpha, \beta, \delta)}{C_S(\alpha, \beta, \delta)} \tag{15}$$

the expression for the potential becomes

$$A_\phi = \frac{\mu J_o R}{2\pi} \bar{A}_o(\alpha, \beta, \delta) \cos(\omega t - \delta\beta + \theta) \tag{16}$$

The behavior of the field can be determined from this expression.

In general for a pure traveling wave $\theta \equiv 0$, thus θ is a measure of the departure from this condition.

Now for $\beta \rightarrow -\infty$ (recalling that the current sheet stretches from the origin to negative infinity), S_S, the sine based on the kernel of S, approaches zero while C_S, the cosine based on the kernel of S, approaches a constant (see Figures A-4 and A-5 which plot C_S and S_S, respectively, versus β for two α's and three δ's). The amplitude function, $\bar{A}_o$, is plotted versus β in Figure A-6.

The solution for the internal magnetic flux produced by an infinite cylindrically symmetric current sheet is in the form of modified Bessel functions of order one.[4] In the limit the fringe field solution should approach this solution which is

$$\phi = 2\pi \mu J_o R r\, I_1(\delta\alpha)\, K_1(\delta) \tag{17}$$

Utilizing Eq. (10) and evaluating Eq. (16) in the limit of $\beta \rightarrow -\infty$, the azimuthal components of the vector potential can then be written as

$$A_\phi = \mu R J_o I_1(\alpha\delta) K_1(\delta) A_o(\alpha, \delta, \beta) \cos(\omega t + - \delta\beta + \theta) \tag{18}$$

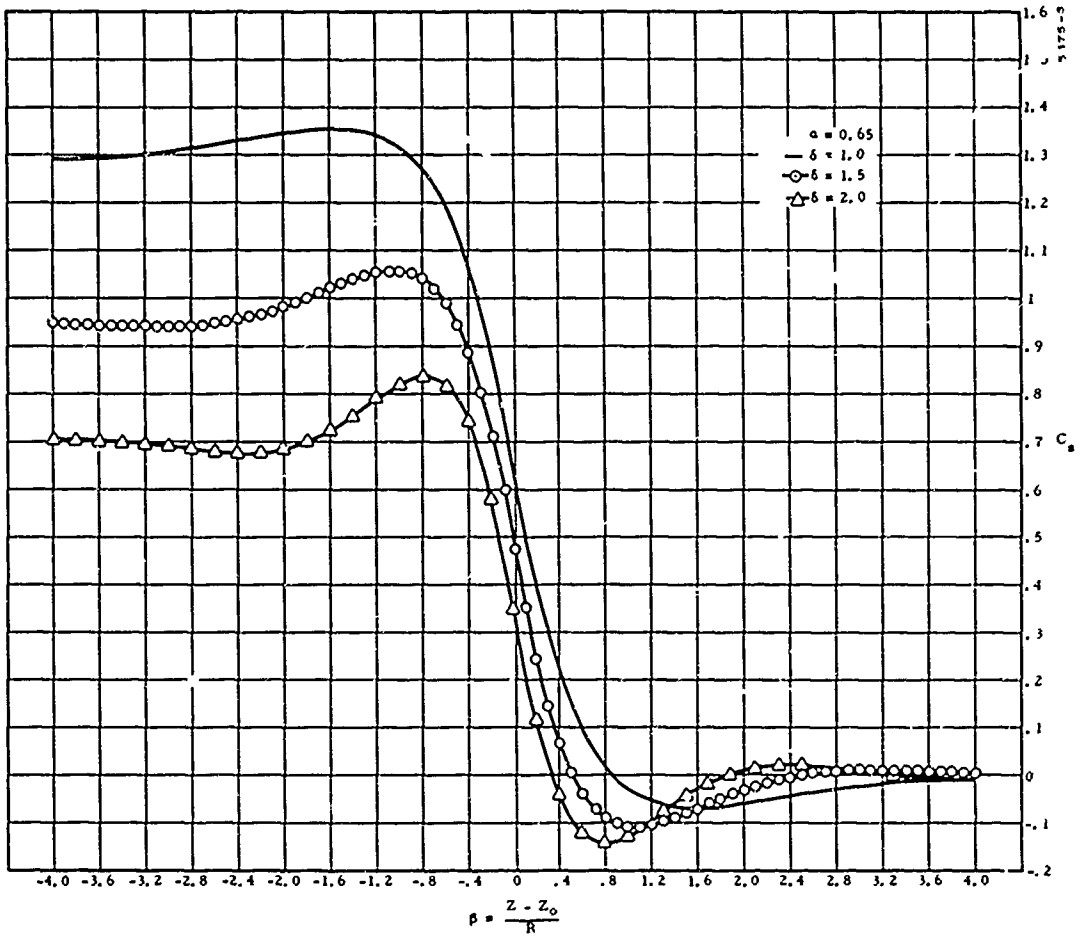

Figure A-4. C_S Dependence

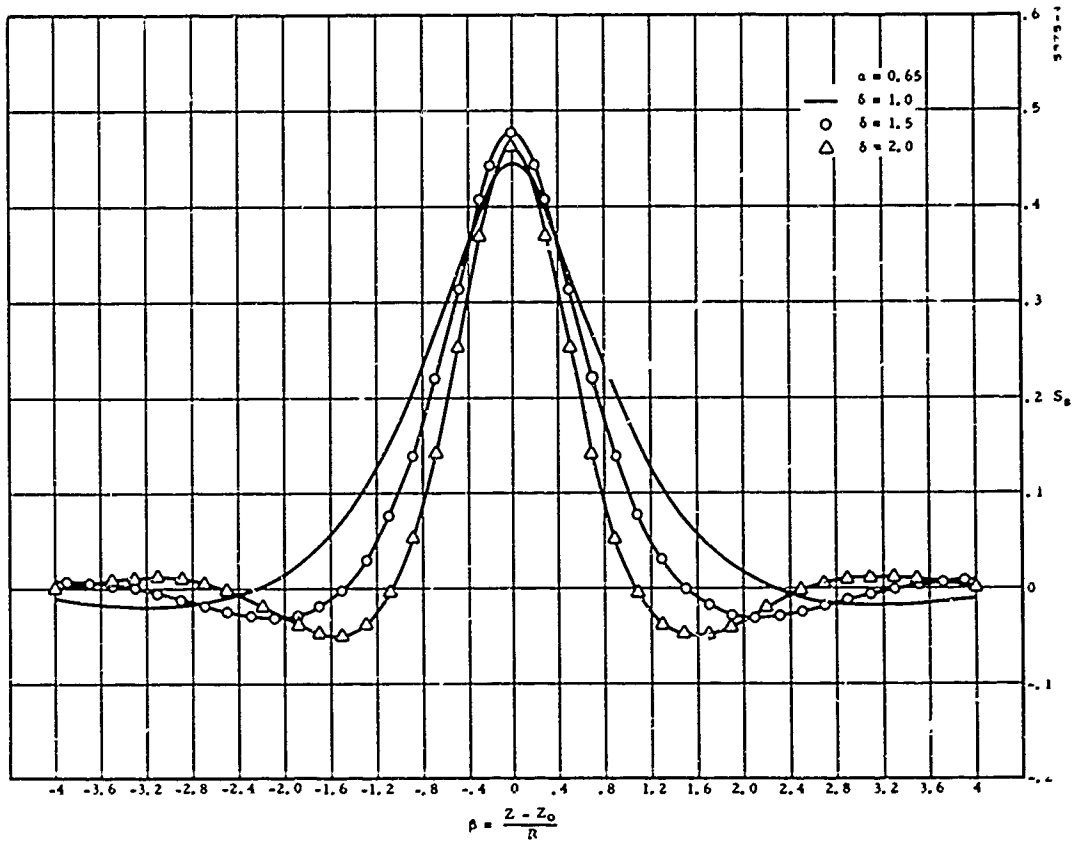

Figure A-5. S_S Dependence

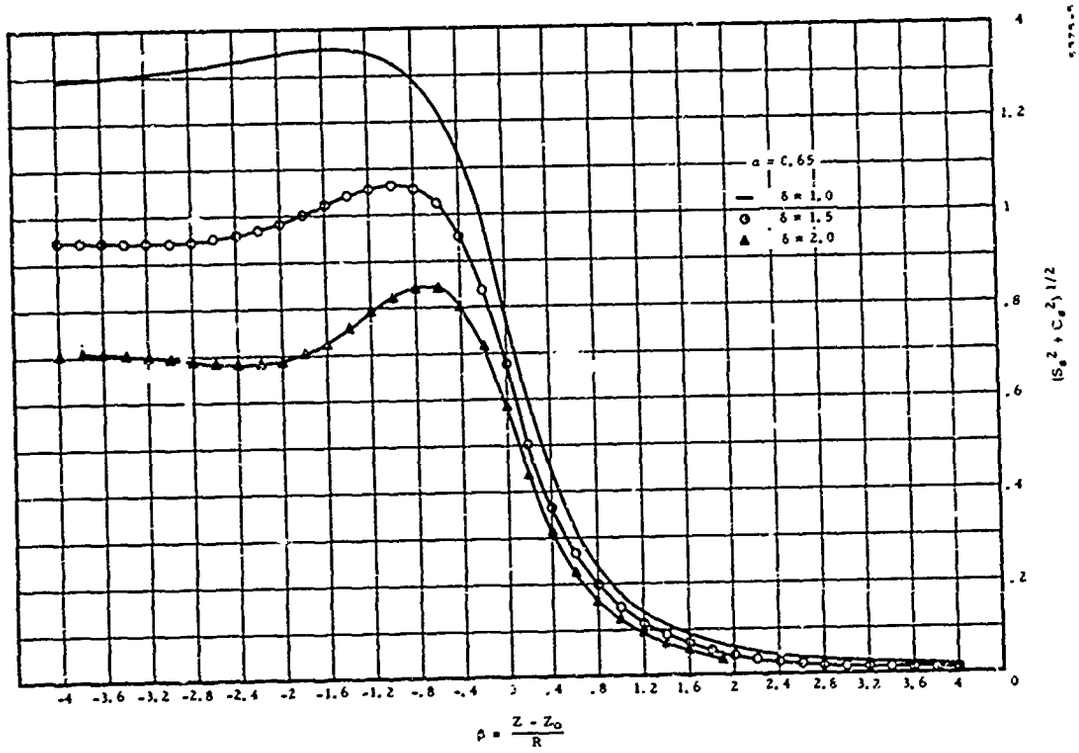

Figure A-6. Amplitude Function, $\overline{A}_o$

where

$$A_o \equiv \frac{\left(C_S^{\,2} + S_S^{\,2}\right)^{1/2}}{2\pi\, I_1\,(\delta a)\, K_1\,(\delta)}$$

which is normalized to allow study of departure from the ideal situation. A_o approaches unity as one physically moves back into the current sheet (coil system).

The magnetic flux, Φ, is then given by

$$\Phi = (\mu J_o R^2)\, a\, A_o\,(a,\ \beta,\ \delta)\cos(\omega t - \delta\beta + \theta) \tag{19}$$

From Eq. (19) the azimuthal electric field, E_θ, and the radial magnetic field component can be evaluated.

$$E_\theta = -\frac{1}{2\pi r}\frac{\partial\Phi}{\partial t}$$

$$E_\theta = \frac{\mu J_o}{2\pi} R\omega\, A_o \sin(\omega t - \delta\beta + \theta) \tag{20}$$

$$B_r = -\frac{1}{2\pi r}\frac{\partial\Phi}{\partial z}$$

$$B_r = -\frac{\mu J_o}{2\pi}\left[-\frac{\partial A_o}{\partial\beta}\cos(\omega t - \delta\beta + \theta) + A_o\frac{\partial(\theta - \delta\beta)}{\partial\beta}\sin(\omega t - \delta\beta + \theta)\right] \tag{21}$$

When the partial derivatives are evaluated, Eq. (21) can be written

$$B_r = \frac{\mu J_o}{2\pi}\underbrace{S\,(a,\ \beta)\cos\omega t}_{A} - \underbrace{\delta A_o \sin(\omega t - \delta\beta + \theta)}_{B} \tag{22}$$

Thus B_r consists of two parts:

1. A standing wave part (A), and
2. A traveling wave part of varying speed and amplitude (B).

The traveling wave velocity is defined by

$$V_f = \frac{\omega}{k} = \frac{R\omega}{\delta} \tag{23}$$

Rewriting B_r in terms of V_f

$$B_r = \frac{\mu J_o}{2\pi}\left[S(\alpha, \beta) \cos \omega t\right] - \frac{E_\theta}{V_f} \tag{24}$$

The electric field experienced by the gas moving in the field is

$$E'_\theta = -\frac{1}{2\pi r}\frac{d\Phi}{dt}$$

$$E'_\theta = E_\theta + UB_r \tag{25}$$

where U is the gas velocity in the axial direction.

Let us now look at the partition of the electromagnetic energy addition to the gas stream, namely

$P = \vec{J} \cdot \vec{E}$, total power transferred to the gas stream per unit volume

$P_{work} = (\vec{J} \times \vec{B}) \cdot \vec{U}$, work done on the gas stream per unit time per unit volume

$P_{joule} = \vec{J}^2/\sigma$, rate of joule heating per unit volume

Denoting time averages by an overline

$$\overline{P} \propto \overline{E'_\theta E_\theta} = \overline{E_\theta^2} + \overline{UB_r E_\theta} \tag{26}$$

$$\overline{P}_{work} \propto -\overline{UE'_\theta B_r} = -\overline{UB_r E_\theta} - \overline{U^2 B_r^2} \tag{27}$$

$$\overline{P}_{joule} \propto \overline{E'^2_\theta} = \overline{E_\theta^2} + \overline{2UE_\theta B_r} + \overline{U^2 B_r^2} \tag{28}$$

If temporal variations of U are neglected in evaluating the averages, one finds, recalling Eq. (19) and (20) and with $\theta - \delta\beta \equiv \phi$:

$$\overline{P} \propto (R\omega A_o)^2 \left(1 + \frac{U}{R\omega} \frac{\partial\phi}{\partial\beta}\right) \tag{29}$$

$$\overline{P}_{work} \propto (R\omega A_o)^2 \left[\left(\frac{U}{R\omega} \frac{\partial\phi}{\partial\beta}\right)\left(-1 + \frac{U}{R\omega} \frac{\partial\phi}{\partial\beta}\right) - \left(\frac{U}{R\omega A_o} \frac{\partial A_o}{\partial\beta}\right)^2\right] \tag{30}$$

$$\overline{P}_{joule} \propto (R\omega A_o)^2 \left[\left(1 + \frac{U}{R\omega} \frac{\partial\phi}{\partial\beta}\right)^2 + \left(\frac{U}{R\omega A_o} \frac{\partial A_o}{\partial\beta}\right)^2\right] \tag{31}$$

From the above results it is evident that the term $\partial A_o/\partial\beta$ is always detrimental in that it decreases the electromagnetic energy partitioned to the body forces while increasing the joule heating.

When the partial derivatives are evaluated, Eqs. (29) through (31) become:

$$\overline{P} \propto (\delta V_f)^2 \left[A_o^2 \left(1 - \frac{U}{V_f}\right) + \frac{A_o S}{\delta} \left(\frac{U}{V_f}\right) \sin(-\delta\beta + \theta)\right] \tag{32}$$

$$\overline{P}_{work} \propto (\delta V_f)^2 \left[A_o^2 \left(1 - \frac{U}{V_f}\right)\frac{U}{V_f} - \frac{A_o S}{\delta}\left(\frac{U}{V_f}\right)\left(1 - \frac{2U}{V_f}\right)\sin(-\delta\beta + \theta) + \left(\frac{S}{\delta}\right)^2 \left(\frac{U}{V_f}\right)^2\right] \tag{33}$$

$$\overline{P}_{joule} \propto (\delta V_f)^2 \left[A_o^2 \left(1 - \frac{U}{V_f}\right)^2 + \frac{2A_o S}{\delta}\left(\frac{U}{V_f}\right)\left(1 - \frac{U}{V_f}\right)\sin(-\delta\beta + \theta) + \left(\frac{S}{\delta}\right)^2 \left(\frac{U}{V_f}\right)^2\right] \tag{34}$$

Let us now consider that the traveling wave accelerator is to be used to augment a hyperthermal arc in a re-entry simulator facility. The one-dimensional equations of motion for steady-state acceleration of a perfact gas in a channel show (see the Resler-Sears phase plane[5]) that the accelerator must operate at a ratio of $U/V_f > \gamma\text{-}1/\gamma$ (which for the free electrons is $U/V_f > 0.4$) for supersonic acceleration to be achieved. Choosing $U/V_f = 1/2$, Eq. (32) through (34) reduce to

$$\overline{P} \propto A_o^2 + \frac{A_o S}{\delta} \sin(-\delta\beta + \theta) \tag{35}$$

$$\overline{P}_{work} \propto 1/2 \left[A_o^2 - \left(\frac{S}{\delta}\right)^2\right] \tag{36}$$

$$\overline{P}_{joule} \propto 1/2 \left[A_o^2 + \frac{2A_o S}{\delta} \sin(-\delta\beta + \theta) + \left(\frac{S}{\delta}\right)^2\right] \tag{37}$$

A plot of these power densities versus β for $\alpha = 0.65$ and $\delta = 2.0$ is shown in Figure A-7. Recalling that the traveling wave magnetic field coil system runs from $-\infty$ to 0, it is important to note that the joule heating peak occurs almost at the end of the machine whereas the $J \times B$ forces reach their minimum value at this point. The joule heating also extends downstream of the last coil which is part of the linear array that forms the current sheet. These conditions are undesirable for a traveling wave accelerator being considered for supersonic acceleration. The joule heating phenomena at the exit of the field system is detrimental in all traveling wave devices as the excess heating can produce Mach effects (thermal) leading to performance degradation.

Let us now investigate a method for fringe field corrections. To facilitate this study, consider one coil at $z_o = D$ and another at $z_o = -L$ (the ends of the current sheet) whose amplitude variance from J_o is described by a delta function $\delta(Z)$, and whose phase departs by X from the phase of the traveling wave. This can be expressed as

$$J(z_o) = J_o \Big[\cos(\omega t - kz_o + \theta) + a\delta(z_o)\cos(\omega t + X) - a\delta(z_o + L)\cos(\omega t + X)\Big] \tag{38}$$

for $-L \le z_o \le 0$.

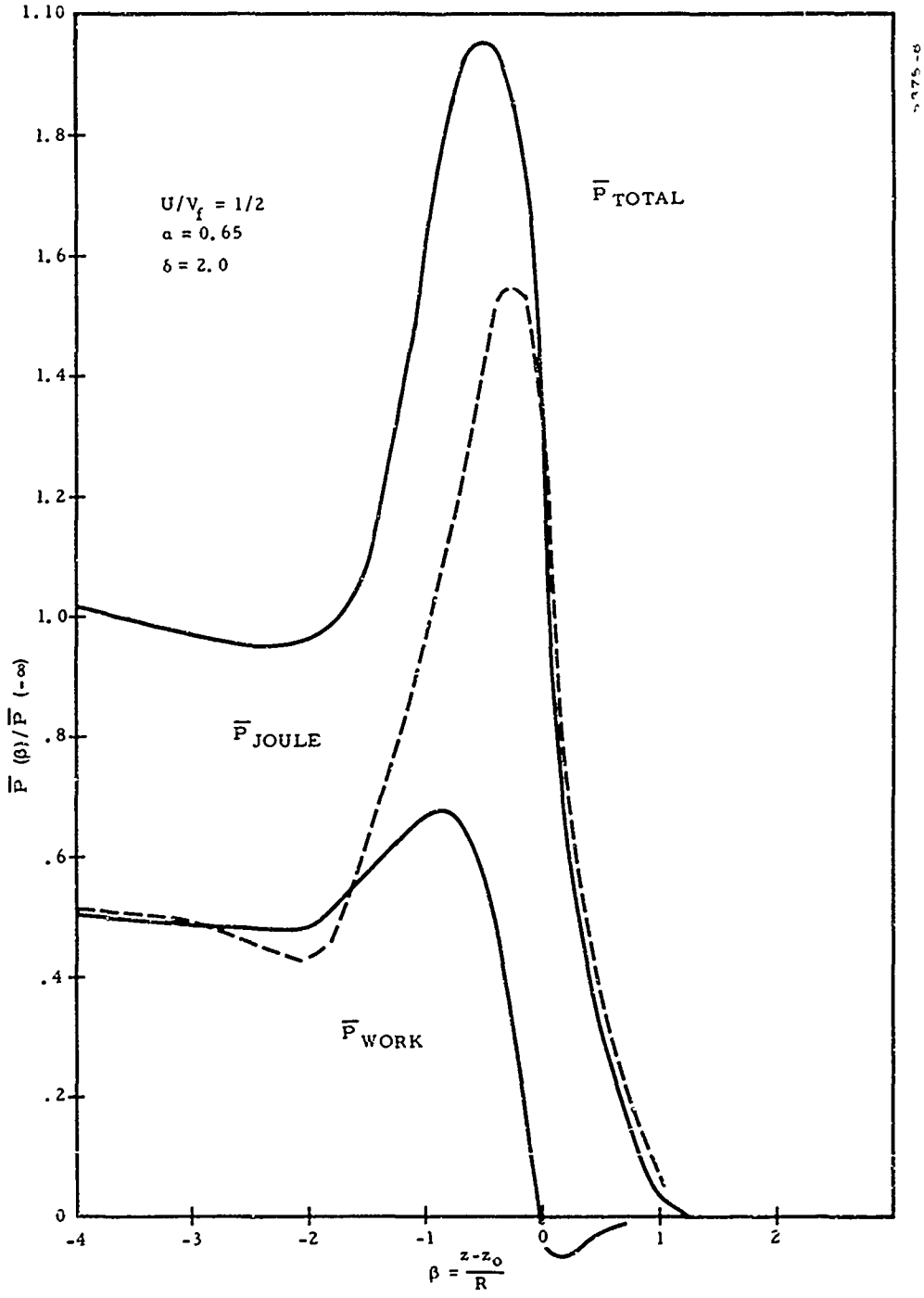

Figure A-7. End Field Effects

Then starting with Eq. (12) and using Eq. (38) the vector azimuthal component of A_ϕ in terms of S_S and C_S is

$$A_\phi = \frac{\mu J_o R}{2\pi} \left\{ \left[C_S(\alpha, \beta) - C_S\left(\alpha, \beta + \frac{L}{R}\right) \right] \cos(\omega t - \delta\beta) - \left[S_S(\alpha, \beta) - S_S\left(\alpha, \beta + \frac{L}{R}\right) \right] \sin(\omega t - \delta\beta) + \frac{a}{R} S(\alpha, \beta) \cos(\omega t + X) - \frac{a}{R} S\left(\alpha, \beta + \frac{L}{R}\right) \cos(\omega t + X) \right\} \tag{39}$$

For $L/R \geq 8$ and $-4 < \beta$, $C_S(\alpha, \beta + L/R)$ and $S(\alpha, \beta + L/R)$ are essentially zero (refer to Figures A-3 and A-4). This allows the effects of the correction coil at one end to be evaluated independently of the other end. Using these assumptions, Eq. (17) through (19), and some algebra, Eq. (39) can be written as

$$A_\phi = \mu J_o R\, I_1(\alpha, \delta)\, K_1(\delta)\, A_o(\alpha, \beta)\, B_o(\alpha, \beta) \cos(\omega t + \Phi) \tag{40}$$

where $B_o(\alpha, \beta) \cos(\omega t + \Phi) = \cos(\omega t + \Phi) + \frac{a}{R}\left[\frac{S(\alpha, \beta)}{A_o}\right] \cos(\omega t + X)$.

A graphical method was used to determine B_o, Φ and a/R for a given X. By iteration of the graphic solution a X of +63.5 degrees was found to be optimum under these conditions; however 60 degrees is the value of X chosen since this theory will first be applied to a three-phase accelerator. 60 degree phase shifts are, in practice, easy to obtain electrically in this case.

Eq. (29) through (31) are put in a form amenable to calculation using the data obtained from the graphic technique.

$$\overline{P} \propto (A_o)^2 \left(1 + \frac{U}{\delta V_f} \frac{\partial\phi}{\partial\beta}\right) \tag{41}$$

$$\overline{P}_{work} \propto (A_o)^2 \left[\left(\frac{U}{\delta V_f} \frac{\partial\phi}{\partial\beta}\right) \left(-1 + \frac{U}{\delta V_f} \frac{\partial\phi}{\partial\beta}\right) - \left(\frac{U}{\delta V_f A_o} \frac{\partial A_o}{\partial\beta}\right)^2 \right] \tag{42}$$

$$\overline{P}_{joule} \propto (A_o)^2 \left[\left(1 + \frac{U}{\delta V_f} \frac{\partial \phi}{\partial \beta}\right)^2 + \left(\frac{U}{\delta V_f A_o} \frac{\partial A_o}{\partial \beta}\right)^2 \right] \tag{43}$$

Because A_o in the above equations is for the ideal current sheet without the correction coil addition, A_o is replaced by $A_o B_o$ to account for the amplitude effect of the correction coil in these equations. For $U/V_f = 1/2$ and $\delta = 2.0$ these equations yield

$$\overline{P} \propto (A_o B_o)^2 \left(1 + 1/4 \frac{\partial \phi}{\partial \beta}\right) \tag{44}$$

$$\overline{P}_{work} \propto (A_o B_o)^2 \left[\left(\frac{1}{4} \frac{\partial \phi}{\partial \beta}\right) \left(-1 + \frac{1}{4} \frac{\partial \phi}{\partial \beta}\right) - \left(\frac{1}{4A_o} \frac{\partial A_o}{\partial \beta}\right)^2 \right] \tag{45}$$

$$\overline{P}_{joule} \propto (A_o B_o)^2 \left[\left(1 + \frac{1}{4} \frac{\partial \phi}{\partial \beta}\right)^2 + \left(\frac{1}{4A_o} \frac{\partial A_o}{\partial \beta}\right)^2 \right] \tag{46}$$

These expressions can now be evaluated using Figure 6 and the graphic solution. The results are plotted in Figure A-8. The beneficial effect of the correction coil is seen when magnitudes of $\overline{P}$, $\overline{P}_{work}$ and $\overline{P}_{joule}$ in Figure A-8 are compared to those in Figure A-7. The peak reduction in joule heating, $\overline{P}_{joule}$, is approximately a factor of two.

While some experimental optimization will be necessary, these results clearly point out the way to proceed when designing a traveling wave field for application to a continuous slip-type accelerator. The applicability of this theory to the Mark II accelerator was not clear since the Mark II operation apparently lay midway between pure resistive and pure inductive behavior. However the appropriate modification of the Mark II field coil would have required a major engineering effort and time did not permit.

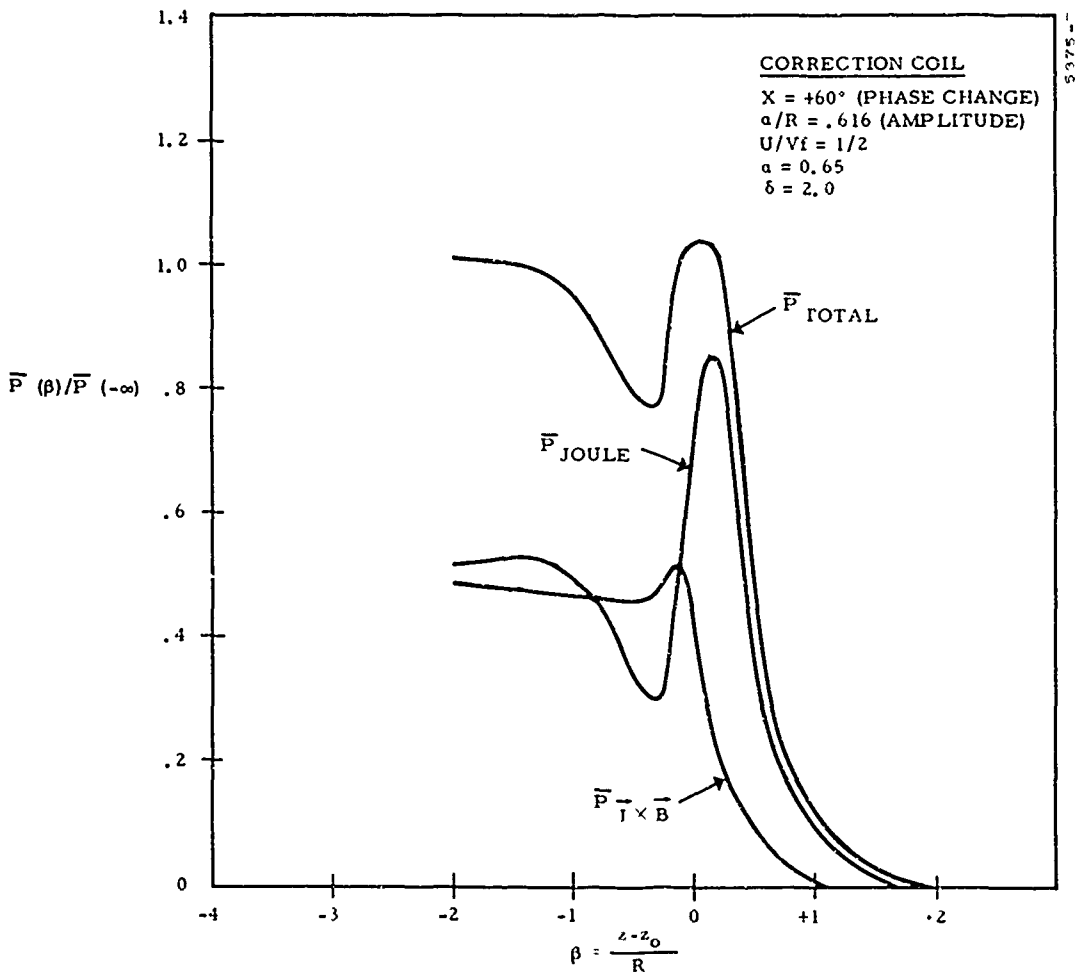

Figure A-8. Reduction of End Field Effects

REFERENCES

1. E. Weber, Electromagnetic Fields, Volume 1, John Wiley & Sons, Inc., 1950, p 140.

2. E. Jahnke and F. Emde, Tables of Functions, Dover S133, 4th Edition, 1945, p 73.

3. F. W. Grover, Inductance Calculations - Working Formulas and Tables, Dover S974, 1962, p 80

4. A. S. Penfold and R. M. Rosen, "Research on Electromagnetic Plasma Acceleration," AFOSR Sci. Doc. 64-1340, June 1964.

5. E. L. Resler, Jr. and W. R. Sears, Journal of Aerospace Sciences, Volume 25, No. 4, 235 (1958).

6. J. A. Thornton, G. R. Seemann, and A. S. Penfold, "Development of a Continuous Flow Electromagnetic Alternating Curr[illegible] Traveling Wave Accelerator for High-Density, Hypervelocity Wind [illegible]nnel Applications," Final Report AF 33(615)-2548 - Litton Publication 5212.

APPENDIX B

ADDITIONAL INVESTIGATIONS

At the conclusion of Contract AF 49(638)-1251 the investigation of the Mark II accelerator was extended for another 30 days under Litton sponsorship. The data which resulted from this additional work is reported here in Appendix B. The work was conducted by Dr. G. R. Seemann and it involved the operation of the Mark II with the entire inner body and inner coil structure removed.

A summary of the findings is as follows:

1. For a specified mass flow rate and power supply setting the power which could be transferred to the gas was smaller than when the inner body was present. Thus the wall thermal problem was reduced and longer run times were obtained. Some runs were as long as 13.5 seconds. The longer run times allowed more time for making the necessary tuning and decoupling adjustments so that a better "tune" was obtained.
2. The "tune" which could be obtained with no inner body was generally better and closer to ideal than with the inner body.
3. The various experimental observables (such as probe signals) were more reproducible, day-to-day, than when the inner body was present.
4. The blocker had a co sistent pronounced affect on the magnetic flux probe signals in contrast to the situation with the inner body present where the effect was erratic.
5. While the available diagnostic techniques were insufficient to establish an absolute identity for the source of the observables, it seems clear that current filaments traveling at or near the field velocity were created and ejected from the accelerator.

Experimental Investigation

The modification to the Mark II changed the channel geometry from annular to cylindrical. The electrical system as described in Section 2.1.1 was otherwise basically unchanged.

A 1-1/2 inch diameter magnetic flux probe, which could be traversed along a diameter, with electrostatic shielding was positioned at the outer periphery of the plasma channel. A 3-1/2 inch diameter probe with shield was fixed downstream from the smaller coil. The small coil had the same electrical geometry as in the previous research.

Two new blockers were made. They were both structures which were one inch wide and 1/8 inch thick. One of them was designed to be placed on a channel diameter and to extend over 7/8 of a diameter. The other was designed to be placed on a cord rather than a diameter of the channel.

Accelerator Operation

With argon only, or mercury only, it was found that by iterating the adjustments of the neutralizing coils and the main tuning capacitors, the mutual inductances could be reduced to 10% or less of the primary inductances. The Q's of the circuits with the inner coil removed were about 25% higher than previously.

Another general property of the system was that the power supplies loaded much more uniformly than previously, though generally at a lower total power level. In contrast to the previous conditions, the five primary phases were easily adjustable for equal currents in the range 35 amperes to 50 amperes (rms). At the upper current level the peak-to-peak voltages across the circuits were about 32 KV and corona and voltage breakdowns in supply cabling began to occur.

Dummy load calibration tests for low plate currents (0.5 - 2.0 amps) were used to supplement the existing calibrations and the remote meters at the Mark II console were also re-calibrated. The power to the plasma varied from 0.5 to 4 KW for argon, and from 3 to 12 KW for mercury. The mercury flow rate was varied from 0.09 to 0.54 gm/mm resulting in chamber pressures ranging from 1μ to 5μ.

Experimental Results

The results obtained from the dc voltage probe (the Hall voltage probe) described in Section 2.1.3.2 of the main text will now be described. A positive polarity indicates that the upstream end of the accelerator was positive with respect to the downstream end (lab ground).

1. Argon Gas

   a. When argon gas was injected into the system from a location downstream of the accelerator a dim, or weak, discharge mode would sometimes result from simultaneous operation of all the phases. A voltage of about -1200 volts appeared under these conditions.

   b. When argon gas was injected into the system from a location downstream of the accelerator a bright mode discharge usually appeared. The voltage was +100 volts when the phases were operated one at a time and nearly zero when all the phases were in operation.

   c. When argon gas was injected into the accelerator from an upstream location (near the nozzles) +15 volts appeared with all phases in operation. The operation was bright mode.

2. Mercury Gas

   a. With mercury flowing through the nozzles and no argon present the voltage was +100 volts with single phase excitation. When all phases were operated this voltage dropped to the range +20 to +50 volts.

The introduction of a blocker probe reduced the voltage in both argon and mercury discharges.

Sample oscillogram traces from the magnetic flux probes are shown in Figures B-1 to B-5. Figure B-1 includes a photograph of the control console which shows that the coil currents varied, phase-to-phase, by less than ±2 rms amperes and that the power supply plate currents were also very nearly equally balanced. The degree of balance indicated in this photograph was typical of that obtained for all the runs reported here.

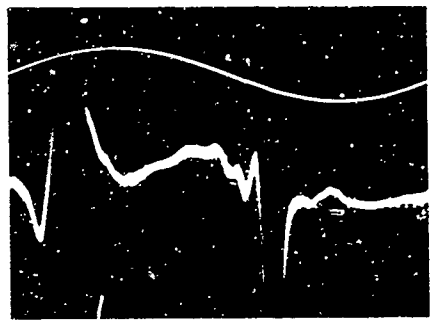

ARGON ONLY
$p \simeq 3\mu$

(a)

SMALL COIL
0.2 V/CM

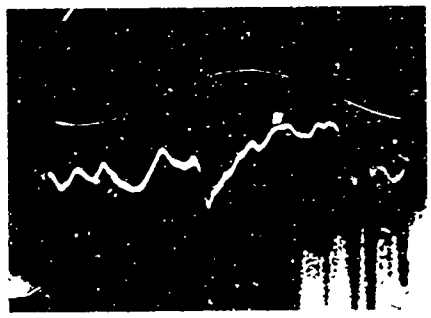

LARGE COIL
0.2 V/CM

(b)

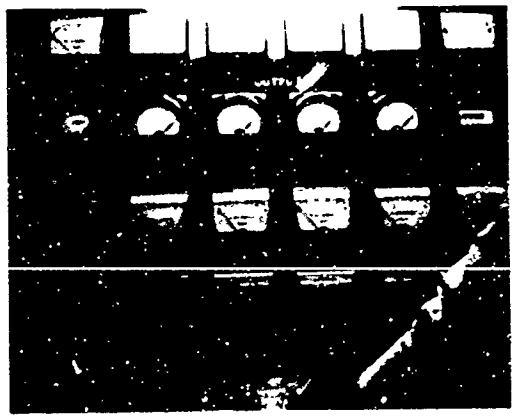

CONSOLE

(c)

I_{COIL} = 48 ± 1 AMP

NOTE: SMALL BUT
RELATIVELY
UNIFORM PLATE
CURRENTS (I_p)

Figure B-1. Probe Traces, Argon

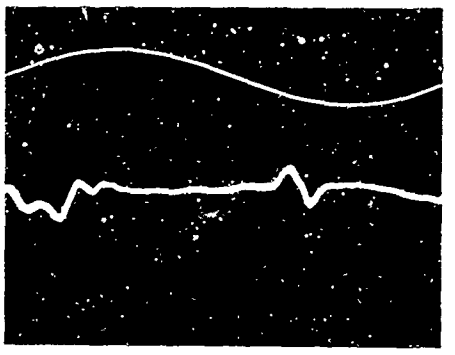

ARGON ONLY

$P \approx 3\mu$

0.2 V/CM

SMALL (ORIGINAL, UNEXTENDED) BLOCKER IN CHANNEL

I_{COIL} = 48 AMPS

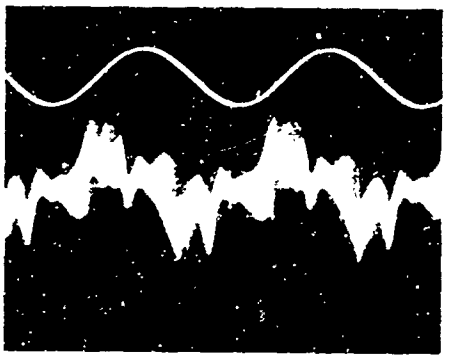

MERCURY + ARGON

$P_{TOTAL} \approx 1\mu$

0.5 V/CM

I_{COIL} = 42 AMPS

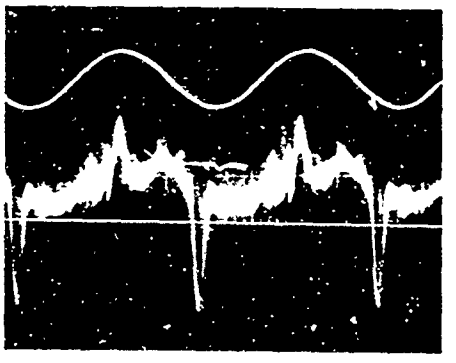

MERCURY ONLY

0.36 GM/MIN

0.5 V/CM

I_{COIL} = 42 AMPS

Figure B-2. Probe Traces, Argon and Mercury

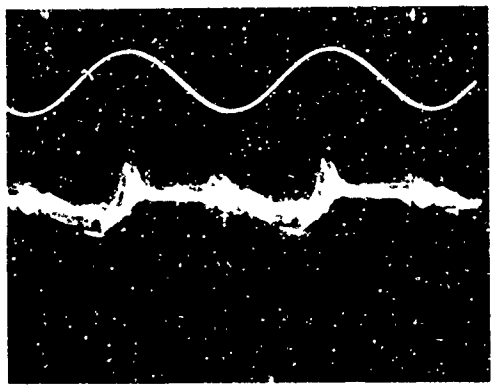

MERCURY ONLY
0.36 GM/MIN
0.5 V/CM (a)

LARGE (EXTENDED)
BLOCKER IN PLACE

I_{COIL} = 43 AMP

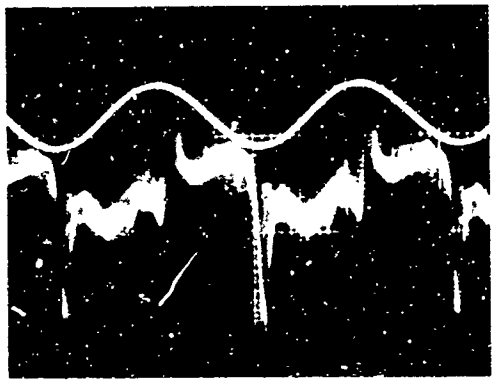

MERCURY ONLY
0.30 GM/MIN
1.0 V/CM (b)

I_{COIL} = 50 AMP.

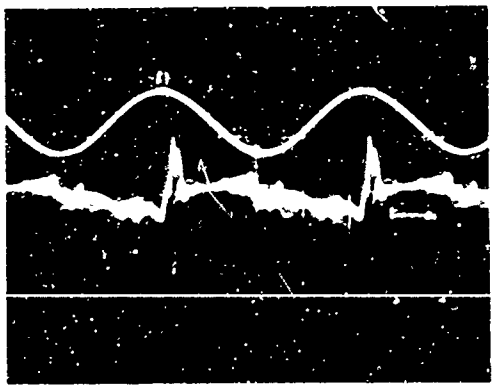

MERCURY ONLY
0.30 GM/MIN
1.0 V/CM (c)

LARGE (EXTENDED)
BLOCKER IN PLACE

I_{COIL} = 50 AMP.

Figure B-3. Probe Traces, Mercury

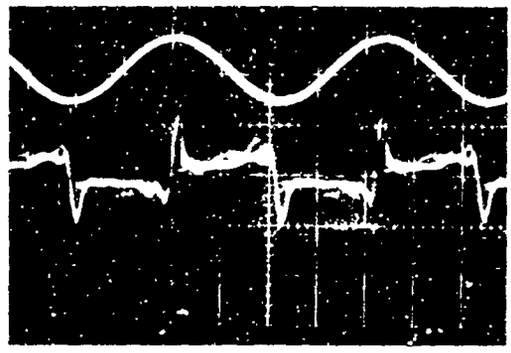

MERCURY ONLY
0. 30 GM/MIN
1. 0 V/CM

LARGE (EXTENDED)
BLOCKER IN PLACE (a)

SINGLE SWEEP

I_{COIL} = 50 AMP.

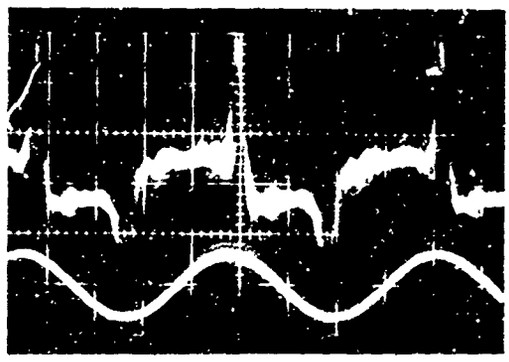

MERCURY ONLY
0. 30 GM/MIN
1. 0 V/CM (b)

I_{COIL} = 50 AMP.

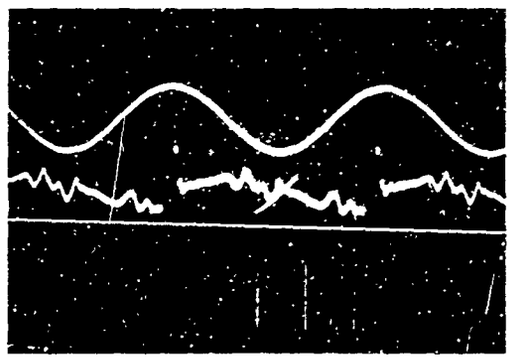

MERCURY ONLY
0. 30 GM/MIN
1. 0 V/CM (c)

BLOCKER EXTENDED
ACROSS CHORD OF
CHANNEL (RATHER THAN
DIAMETER).

I_{COIL} = 50 AMP

Figure B-4. Probe Traces, Mercury

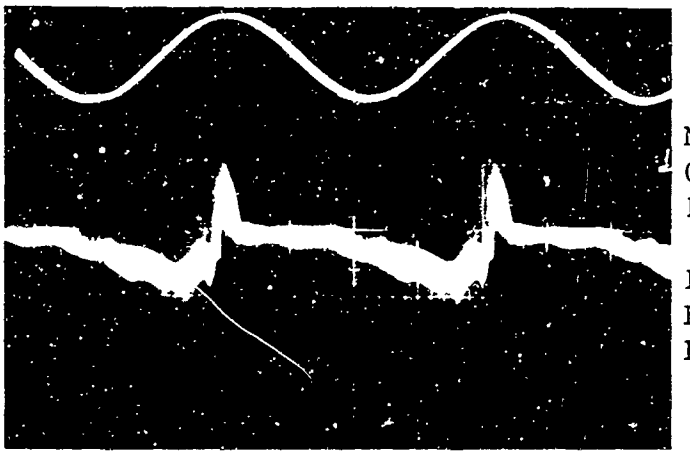

MERCURY ONLY
0. 30 GM/MIN
1. 0 V/CM (a)

LARGE (EXTENDED)
BLOCKER IN PLACE
I_{COIL} = 50 AMP

6126-5

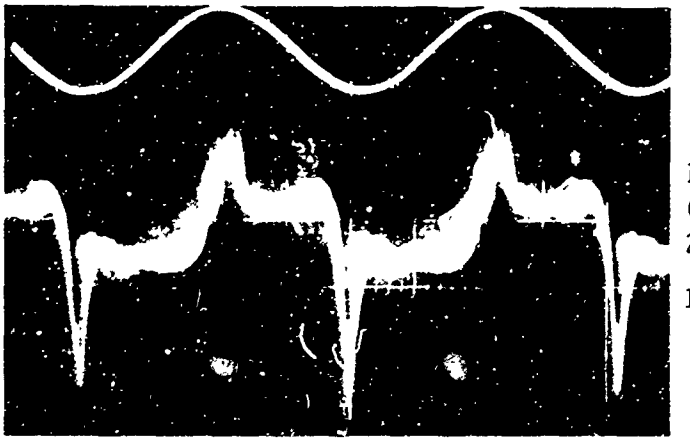

MERCURY ONLY
0. 15 GM/MIN
2. 0 V/CM (b)

I_{COIL} = 50 AMP

Figure B-5. Probe Traces, Mercury

The large-coil magnetic flux probe showed features which mirrored those revealed by the smaller probe, but they were generally less distinct. An oscillogram taken from the large coil is shown in Figure B-1. It is the only example given here.

The small coil was traversed from the periphery of the channel to the axis of the channel. In general the signal shape remained invariant to position along the traverse but the amplitude dropped by a factor of 2.5 as the channel axis was approached.

Figures B-3(b) and B-5(b) show the effect of a decrease in the mercury mass flow rate on the amplitude of the probe signals. The trend of increasing amplitude with decreasing flow rate, at constant field coil currents, was characteristic of the results. A decreasing mercury flow rate produced a lower vacuum tank pressure while the power input to the gas remained nearly constant.

Each of the Figures B-1 through B-5 shows a portion of a 240 KC sine wave from which the time scale of the figures may be determined. Other pertinent data is given to the right of the photographs.

Interpretation of Results

The interpretation of the magnetic probe traces is made on the basis of the ring-current model of Section 2.2.3. The model (shown in Figure 2-26) is really over-simplified in that it does not take into account the fact that as the toroid speed increases the peaks displayed in Figure 2-26 should become sharper. In addition it does not take account of the essential asymmetry of the double coil system (the forward coil perterbation of the plasmoid). However, a zero-crossing estimate combined with the 2 cm double coil spacing yields a speed $\sim 5 \times 10^4$ meters/sec which is the accelerator field speed. Now collisionless mercury ions accelerated up to the field speed should yield an end-to-end voltage of approximately +2500 volts. In the previous work with the inner body, it was estimated that the probe signals gave about half the field speed and dc voltages were recorded which reached +800 volts. In this work the dc voltages were very low (< + 50 volts). High toroid speeds are really not reconcilable with very low voltages except by using the argument that the end-to-end voltage does not necessarily represent the peak voltages in the accelerator.

Another peculiarity is the fact that the blocker generally attenuates alternate signals (compare Figures B-3(b) and B-3(c)). The accelerator

theory states that the only difference between successive toroids should be current polarity. With the inner body absent the entire volume of the channel is available to toroids so it is conceivable that there is also a spatial variation among toroids and the blocker only intercepts toroids of one sign. The coil signals with no inner body show an asymmetry such that positive pulses are always smaller than negative pulses. Figure B-5(b) should be compared to Figure 2-30 (small coil trace). In the latter the characteristic pulses have the same height.

The effect on coil signal amplitude with flow rate noted in the previous section bears some interpretation. Since total power does not drop proportionate to the flow rate one can say that the power input per unit mass increases. This implies that more mass may be accelerated or the same mass may be accelerated to higher speeds. Increased mass also leads to increased currents and the signal amplitude would increase with both higher currents or faster toroids. The oscillograms are not good enough to distinguish these effects. The decrease of tank pressure with decreasing flow rate tends to make the system more collisionless and this would also tend to increase probe signals since the plasma currents would not decay as fast.

UNCLASSIFIED
Security Classification

DOCUMENT CONTROL DATA - R&D
(Security classification of title, body of abstract and indexing annotation must be entered when the overall report is classified)

1. ORIGINATING ACTIVITY (Corporate author) Space Sciences Laboratories Litton Systems, Inc. 336 North Foothill Road Beverly Hills, California	2a. REPORT SECURITY CLASSIFICATION Unclassified 2b. GROUP NA

3. REPORT TITLE RESEARCH ON ELECTROMAGNETIC PLASMA ACCELERATION
VOL I: THE DEVELOPMENT OF A CW TRAVELING WAVE ACCELERATOR FOR THE PRODUCTION OF PINCHED PLASMA TOROIDS

4. DESCRIPTIVE NOTES (Type of report and inclusive dates)
Final Report November 1963 through December 1966

5. AUTHOR(S) (Last name, first name, initial)
Penfold, Alan S. and Rosen, Richard M.

6. REPORT DATE January 31, 1967	7a. TOTAL NO. OF PAGES 92	7b. NO. OF REFS Total of 7
8a. CONTRACT OR GRANT NO. AF 49(638)-1251 b. PROJECT NO. c d	9a. ORIGINATOR'S REPORT NUMBER(S) 6126 9b. OTHER REPORT NO(S) (Any other numbers that may be assigned this report) AFOSR 67-0979	

10. AVAILABILITY/LIMITATION NOTICES

11. SUPPLEMENTARY NOTES	12. SPONSORING MILITARY ACTIVITY United States Air Force Office of Scientific Research

13. ABSTRACT

The development of a CW traveling wave accelerator for the production and acceleration of high-speed pinched plasma toroids is described. The accelerator is a polyphase-driven electrical system. Mercury and argon-seeded mercury were used as test gases. A comprehensive technology was developed to compensate for the inductive back-reaction of the plasma discharge on the coils producing the traveling wave field. Severe and rapid thermal overloading of the walls of the plasma channel limited the run times to a few seconds. Several types of ceramic channels were tried but the problem remained. The short run times made proper utilization of the back-reaction compensating circuits an impossibility. However, evidence of plasma acceleration was obtained and macroscopic discrete ring-currents were observed in the plasma efflux. The axial Hall voltage was monitored and a maximum value of 1000 volts was recorded.

DD FORM 1 JAN 64 1473

UNCLASSIFIED
Security Classification

UNCLASSIFIED
Security Classification

14. KEY WORDS	LINK A ROLE	LINK A WT	LINK B ROLE	LINK B WT	LINK C ROLE	LINK C WT
Plasma Acceleration						
Plasma Accelerator						
Electromagnetic Acceleration						
Traveling Wave Accelerator						
EM-Plasma Interactions						
Inductive Discharge						
Electrodeless Discharge						

INSTRUCTIONS

1. ORIGINATING ACTIVITY: Enter the name and address of the contractor, subcontractor, grantee, Department of Defense activity or other organization *(corporate author)* issuing the report.

2a. REPORT SECURITY CLASSIFICATION: Enter the overall security classification of the report. Indicate whether "Restricted Data" is included. Marking is to be in accordance with appropriate security regulations.

2b. GROUP: Automatic downgrading is specified in DoD Directive 5200.10 and Armed Forces Industrial Manual. Enter the group number. Also, when applicable, show that optional markings have been used for Group 3 and Group 4 as authorized.

3. REPORT TITLE: Enter the complete report title in all capital letters. Titles in all cases should be unclassified. If a meaningful title cannot be selected without classification, show title classification in all capitals in parenthesis immediately following the title.

4. DESCRIPTIVE NOTES: If appropriate, enter the type of report, e.g., interim, progress, summary, annual, or final. Give the inclusive dates when a specific reporting period is covered.

5. AUTHOR(S): Enter the name(s) of author(s) as shown on or in the report. Enter last name, first name, middle initial. If military, show rank and branch of service. The name of the principal author is an absolute minimum requirement.

6. REPORT DATE: Enter the date of the report as day, month, year, or month, year. If more than one date appears on the report, use date of publication.

7a. TOTAL NUMBER OF PAGES. The total page count should follow normal pagination procedures, i.e., enter the number of pages containing information.

7b. NUMBER OF REFERENCES: Enter the total number of references cited in the report.

8a CONTRACT OR GRANT NUMBER: If appropriate, enter the applicable number of the contract or grant under which the report was written.

8b, 8c, & 8d. PROJECT NUMBER: Enter the appropriate military department identification, such as project number, subproject number, system numbers, task number, etc.

9a. ORIGINATOR'S REPORT NUMBER(S): Enter the official report number by which the document will be identified and controlled by the originating activity. This number must be unique to this report.

9b OTHER REPORT NUMBER(S). If the report has been assigned any other report numbers *(either by the originator or by the sponsor)*, also enter this number(s).

10. AVAILABILITY/LIMITATION NOTICES: Enter any limitations on further dissemination of the report, other than those imposed by security classification, using standard statements such as:

(1) "Qualified requesters may obtain copies of this report from DDC."

(2) "Foreign announcement and dissemination of this report by DDC is not authorized."

(3) "U. S. Government agencies may obtain copies of this report directly from DDC. Other qualified DDC users shall request through _____."

(4) "U. S. military agencies may obtain copies of this report directly from DDC. Other qualified users shall request through _____."

(5) "All distribution of this report is controlled. Qualified DDC users shall request through _____."

If the report has been furnished to the Office of Technical Services, Department of Commerce, for sale to the public, indicate this fact and enter the price, if known.

11. SUPPLEMENTARY NOTES: Use for additional explanatory notes.

12. SPONSORING MILITARY ACTIVITY: Enter the name of the departmental project office or laboratory sponsoring *(paying for)* the research and development. Include address.

13. ABSTRACT: Enter an abstract giving a brief and factual summary of the document indicative of the report, even though it may also appear elsewhere in the body of the technical report If additional space is required, a continuation sheet shall be attached.

It is highly desirable that the abstract of classified reports be unclassified. Each paragraph of the abstract shall end with an indication of the military security classification of the information in the paragraph, represented as *(TS), (S), (C), or (U)*

There is no limitation on the length of the abstract. However, the suggested length is from 150 to 225 words.

14 KEY WORDS: Key words are technically meaningful terms or short phrases that characterize a report and may be used as index entries for cataloging the report. Key words must be selected so that no security classification is required. Identifiers, such as equipment model designation, trade name, military project code name, geographic location, may be used as key words but will be followed by an indication of technical context The assignment of links, rules, and weights is optional.

UNCLASSIFIED
Security Classification